GERG Project on Ultrasonic Gas Flow Meters, Phase II

GERG TM 11

edited by

P. Lunde, K.-E. Frøysa and M. Vestrheim

GERG TECHNICAL MONOGRAPH 11 (2000)

GERG Project on Ultrasonic Gas Flow Meters, Phase II

edited by

Per Lunde   Christian Michelsen Research AS, Norway
Kjell-Eivind Frøysa Christian Michelsen Research AS, Norway
Magne Vestrheim   University of Bergen, Norway

on behalf of
the GERG project Group

G. H. Sloet   N.V. Nederlandse Gasunie, The Netherlands, convener
R. Sakariassen   Statoil K-Lab, Norway
M. Sangalli   SNAM SpA, Italy
B. Harbrink   Ruhrgas AG, Germany
J. Boekhoven   NAM, The Netherlands
J. H. Sanchez   ENAGAS SA, Spain
K. Wild   BG Technology, UK
J. van Damme   Distrigaz s.a., Belgium
F. Vulovic   Gaz de France DR, France

and

Programme Committee No. 2
- Transmission and Storage -
GROUPE EUROPEEN DE RECHERCHES GAZIERES

TABLE OF CONTENTS

5. METHODS FOR CHARACTERIZATION AND TESTING OF USM TRANSDUCERS UNDER PRESSURE   41

(by P. Lunde and M. Vestrheim)

6. ULTRASONIC METERS AND NOISE   66

(by K. van Bloemendaal, G. H. Sloet, B. Hosten, P. Brassier and F. Vulovic)

Acknowledgments

Summary

There is an increasing interest in using ultrasonic gas metering technology in gas production and transmission. However, there still remains some hesitation in applying the technology for fiscal and sales gas metering until wider experience has been obtained, and industry standards have been established. This interest is highlighted by the research groups of nine of the leading European gas companies joining together to undertake studies on four specific tasks associated with multi-path ultrasonic meters:

(1) *A numerical investigation into the effect of non-ideal flow on the meter error*, carried out by Ruhrgas AG and the University of Essen, Germany (Task leader: Ruhrgas),

(2) *Uncertainty analysis of multipath ultrasonic transit time gas flow meters*, carried out by Christian Michelsen Research AS, Norway (Task leader: Gasunie),

(3) *The development of methods for characterization and testing of USM transducers under pressure*, carried out by Christian Michelsen Research AS, Norway (Task leader: Statoil),

(4) *An experimental and theoretical investigation into the effect of noise on ultrasonic meters*, carried out by N. V. Nederlandse Gasunie, The Netherlands, Gaz de France and the Universite de Bordeaux, France (Task leader: Gasunie).

In this Technical Monograph, the participants share some of the concerns they have experienced in the use of ultrasonic meters, and the results from this research work which addresses those concerns.

The four tasks summarised in this Technical Monograph have undoubtly increased the general knowledge about certain important aspects and effects attributed to USMs, and pointed out directions to follow to increase the reliability and confidence on the use of USMs.

Chapter 1

Introduction

The European Gas Research Group, GERG (Groupe Européen de Recherches Gazières), has undertaken an R&D project with the aim of increasing the general knowledge about, and advancing the technology on, the concept of multipath ultrasonic transit time flow meters (USM) for fiscal, allocation and sales metering of natural gas. This Technical Monograph is based on the project reports resulting from the project.

Metering of natural gas using USMs has been the focus of considerable research effort over the recent 15-20 years. That effort has opened opportunities for the gas industry to benefit from technology that offers accuracy and repeatability from a device having no moving parts. Other advantages of USM technology include:

- non-intrusive measurement (no obstruction of flow),
- no pressure loss,
- large turn-down ratio (40:1 or larger, reducing the need for a multiplicity of meters to cover a wide flow range),
- possibilities for fast time response (measurement of pulsating flow),
- bi-directional operation (reducing need for pipework),
- short upstream and downstream requirements with respect to bends (10D/5D, typically),
- additional information about flow and gas properties (such as flow velocity profile; sound velocity profile, which might be used for density and calorific value determination),
- possibilities of self-diagnostics (from sound velocity, signal level, etc.),
- potentials of remote operation,
- potentials of reduced dependency on flow calibration.

Disadvantages of the USM technology include:

- relatively complex and complicated metering technology,
- relatively new technology which will benefit from further maturing and extended experience with the use of USMs (with respect to robustness, operational reliability, long-time effects, traceability, etc.),
- uncertain sensitivity to installation conditions (bends, pipe roughness, flow conditioners, etc.),
- sensitivity to ultrasonic noise, such as for installation close to pressure regulation valves,
- lack of industrial standards.

In recent years USM technology has been increasingly taken into use for fiscal metering of natural gas, and is gradually considered as a realistic and competitive alternative to the use of more conventional technologies such as as turbine meters and orifice plates [1.1] - [1.10]. In appropriate applications, multipath ultrasonic meters offer significant cost benefits. Reference documents of importance for the use of USMs in the gas industry today are the GERG TM 8 [1.11], the ISO Technical Report ISO/TR 12765 [1.12], and the AGA-9 report [1.13].

The world market for fiscal gas metering is considerable, and today several hundred gas meters are being delivered each year to the gas industry. At present, three manufacturers offer USMs for fiscal metering of gas: Daniel Flow Products (USA and UK) [1.14], FMC Kongsberg Offshore AS (KOS) (Norway) [1.15] and Instromet International (Belgium) [1.16]. Specifications of interest typically include the pressure and temperature ranges 10 - 200 bar and -25 to +55 ^{o}C [1.13]. The flow rate capacity of a USM is determined by the actual velocity of the gas flowing through the meter, typically from 0.4 m/s (or less) to about 30 m/s (or more). Conventionally, USMs provide a measurement of the average flow velocity and volumetric flow rate in the pipe. The three manufacturers report better than ±0.7 % uncertainty (of measured value), as required for custody transfer in large commercial pipelines [1.13]. A method for measuring gas density using USMs is is also reported [1.17].

As a consequence of the growing interest and the lack of international standards, ISO standardisation work on ultrasonic gas metering was initiated in 1990, resulting in an ISO Technical Report [1.12]. In the USA, a document AGA-9 [1.13] has been prepared, providing guidelines and recommendations for practical use of USM for fiscal gas metering, and is being used more or less as a standard in the USA. The ISO work on ultrasonic gas metering was re-initiated in 1999, and is planned to be integrated with the AGA-9 recommendations and the ISO Technical Report ISO/TR 12765 [1.12]. National regulation authorities are also starting to open up for the use of USM in connection with fiscal metering of gas, cf. e.g. [1.18].

GERG has supported a number of R&D projects on USMs. In 1995, a GERG project group initiated work attempting to define the status of multi-path ultrasonic gas metering at that time, and the non-classified results of the study were published in the GERG Technical Monograph No. 8 [1.11]. A more comprehensive and detailed report of the study was given in a technical report [1.19], which has been available to the companies participating in that GERG project.

This first phase of the GERG Project on Ultrasonic Gas Flow Meters was summarized by P.M.A. van der Kam, Gasunie, at the AGA 1996 Operations Conference [1.20]. This GERG project group also identified topics where additional research effort and/or operational experience would be necessary to extend the knowledge and confidence in increasing the use of these meters for the gas and oil industries.

Some of the key aspects of this additional research effort were addressed in a follow-up Phase II of the GERG Project on Ultrasonic Gas Flow Meters, and the research programme concentrated on four specific tasks:

(1) *A numerical investigation into the effect of non-ideal flow on the meter error*, carried out by Ruhrgas AG and the University of Essen, Germany (Task leader: Ruhrgas),

(2) *Uncertainty analysis of multipath ultrasonic transit time gas flow meters*, carried out by Christian Michelsen Research AS, Norway (Task leader: Gasunie),

(3) *The development of methods for characterization and testing of USM transducers under pressure*, carried out by Christian Michelsen Research AS, Norway (Task leader: Statoil),

(4) *An experimental and theoretical investigation into the effect of noise on ultrasonic meters*, carried out by N. V. Nederlandse Gasunie, The Netherlands, Gaz de France, France, and Universite de Bordeaux, France (Task leader: Gasunie).

The importance of the work is highlighted by the number of European gas industry companies who were prepared to collaborate and share the cost of advancing this work. In all, nine companies participated in this GERG project group, namely BG Technology (UK) (formerly British Gas R&D),

Distrigaz (Belgium), ENAGAS (Spain), Nederlandse Gasunie (Netherlands), Gaz de France (France), NAM (Netherlands), Ruhrgas (Germany), SNAM (Italy) and Statoil (Norway).

Some results from Phase II of the GERG Project on Ultrasonic Gas Flow Meters were presented by G. H. Sloet, Gasunie, at the seminar *Practical Developments in Gas Flow Metering* at the National Engineering Laboratory (NEL) in Glasgow, Scotland, April 1998 [1.21], and by K. Wild, BG Technology, at the *4th International Symposium on Fluid Flow Measurement* in Denver, Colorado, June 1999 [1.22].

The present Technical Monograph summarises Phase II of this GERG project, which started towards the end of 1996 and was completed at the end of 1998. The Monograph has been prepared in the period November 1999 to April 2000, and represents an extract of the non-classified parts of the work which have been more fully documented in the following technical project reports: [1.23] (Task 1), [1.24] (Task 2), [1.25] (Task 3) and [1.26], [1.27] (Task 4). In this Technical Monograph, each Task has been summarised by the persons performing the Task.

The Monograph is organised as follows: In Chapter 2, some definitions are given, for convenience when reading the Monograph. Chapter 3 summarises briefly the measurement principle of USMs, and includes a summary of the functional relationship of USMs, serving as a basis for Chapters 4-7 of the Monograph. Task 1 of the GERG project is described in Chapter 4, addressing numerical investigations into the effect of non-ideal flow on the USM uncertainty (uncertainty due to the integration method) [1.23]; [1.28]. In Chapter 5, methods for characterization and testing of USM transducers under pressure are addressed, summarizing the work made under Task 3 of the project [1.25]. The results of Task 4 are described in Chapter 6, discussing the influence of ultrasonic noise on USMs [1.26], [1.27], [1.29]. Task 2 of the project is described in Chapter 7, giving a summary of the USM uncertainty model developed under the project [1.24]. Some closing remarks on the results of the project are given in Chapter 8. A list of previously issued GERG Technical Monographs is included as an Appendix. References for the various chapters are collected at the end of the report.

There has been little attempt to harmonize the notation of the various contributors, but this should not cause much inconvenience in practice.

For a summary of the project results, including conclusions and perspectives of further work, it is referred to the discussion and closing remarks of Chapter 8.

Chapter 2

Some definitions and abbreviations

In the following, some of the terms and abbreviations used in this report, are defined. References to corresponding definitions given elsewhere are included.

USM	A multipath ultrasonic flow meter for gas based on measurement of transit times, and calculation of transit time differences. The wording USM refers to the composite of the meter body ("spoolpiece"), the ultrasonic transducers, the control electronics, and the CPU unit / flow computer.
Large USM	A USM with (nominal) diameter $\geq$ 12" [2.1].
Small USM	A USM with (nominal) diameter $<$ 12" [2.1].
Line conditions	Gas conditions at actual pipe flow operational conditions.
Standard conditions	Gas conditions at 15 °C and 1 atm.
Normal conditions	Gas conditions at 0 °C and 1 atm.
Ideal conditions	Pipe flow situation where no transversal (non-axial) flow velocity components are present, and where the axial flow velocity profile is turbulent and fully developed.
Deviation	The difference between the volumetric flow rate (or flow velocity) measured by the USM under test and the actual volumetric flow rate (or flow velocity) measured by the reference meter [2.1]. Percentage deviation is given relative to the reference measurement.
Error curve	The deviation as a function of flow velocity over a given flow velocity range, at a specific installation condition, pressure, temperature and gas composition.
Flow calibration	Measurement of the error curve (cf. [2.1], Chapter 6.4).
Dry calibration[1]	(or more precisely, "zero flow verification test"). Measurement of quantities which are needed for the operation of the USM, such as relevant dimensions, angles, transit time delays through transducers, cables and electronics, and possibly Δt-correction [2.1].

---

[1] The wording "dry calibration" has come into common use in the USM community today, and is therefore used also here. However, it should be emphasized that this wording may be misleading. The dry calibration is not a *calibration* of the meter in the normal meaning of the word, but a procedure to determine, usually in the factory, a set of correction factors to be used in the meter software (including correction of transit times, cf. Section 3.8). In [1.13] (Chapter 6.3), this procedure is more correctly referred to as "zero flow verification test".

Dry calibration measurements are made typically in the factory, at one or several specific conditions of pressure, temperature and gas composition (cf. Sections 3.5 and 3.8).

Zero flow reading
The maximum allowable flow meter reading when the gas is at rest, i.e. both axial and non-axial flow velocity components are essentially zero [2.1].

Time averaging period
Period of time over which the displayed measured flow velocities and volume flow rates are averaged.

SNR
Signal-to-noise ratio.

Stacking
A signal processing technique used to reduce the effect of noise in the measurements, by adding signal time traces.

Integration technique
(Or flow profile integration technique). Numerical technique to calculate the average flow velocity in the pipe from knowledge of the average flow velocity along each acoustic path in the USM.

Gauss-Jacobi quadrature
A specific integration technique [2.2].

Estimated value
Estimated value of a quantity, obtained either by measurement, or by other means (such as by calculations) [2.3].

USM functional relationship
The set of mathematical equations describing the USM measurement of either: the axial flow velocity, $\bar{v}_A$, the axial volumetric flow rate at line conditions, q, or the axial volumetric flow rate at standard conditions, Q.

Spoolpiece
The USM meter body

Axial flow velocity, v_A
The component of flow velocity along the pipe axis.

Transversal flow velocity
The non-axial components of flow velocity in the pipe.

Interrogation length, L_i
Length of the portion of the intertransducer centre line lying inside a cylinder formed by the inner pipe bore (for acoustic path no. i).

Chord, D_i
Projection of the interrogation length, L_i, into the pipe's cross-sectional plane (for acoustic path no. i).

Chapter 3

Multipath ultrasonic transit time gas flow meters

Per Lunde[*], Kjell-Eivind Frøysa[*] and Magne Vestrheim[**]

[*] *Christian Michelsen Research AS (CMR), Bergen, Norway*
[**] *University of Bergen, Dept. of Physics, Bergen, Norway*

3.1   Introduction

The present chapter summarises briefly the measurement principle of multipath ultrasonic transit time gas flow meters (USMs), and includes a summary of the usual formulation of the functional relationship for such meters. The chapter provides an introductory framework and basis for the other chapters of this Technical Monograph, in which the individual tasks of the GERG project on USMs are described. The present description of the USM functional relationship is an outline of the description given in [3.1] (including some minor modifications and additions), in which further details can be found.

3.2   Principle of measurement

A multipath ultrasonic transit time gas flow meter is a device consisting basically of a cylindrical meter body ("spoolpiece"), ultrasonic transducers typically located along the spoolpiece wall, an electronics unit with cables and a flow computer [3.2]; [3.3]; [3.4]. The transducers are usually mounted in transducer ports and in direct contact with the gas stream, using gas-tight seals (o-rings) to contain the pressure in the pipe.

USMs derive the gas flow rate by measuring electronically the transit times of high frequency sound pulses. Transit times are measured for sound pulses propagating across the pipe, at an angle with respect to the pipe axis, downstream with the gas flow, and upstream against the gas flow. For each acoustic path, the difference between the upstream and downstream propagating transit times is proportional to the average gas flow velocity along the acoustic path (cf. Section 3.4).

The flow profiles in the pipe may be relatively complex, such as e.g. downstream of pipe bends. As an illustration, Fig. 3.1a shows contour plots of the axial and transversal flow velocity profiles calculated 10 diameters (10D) downstream of a double 90° bend out-of plane using a computational fluid dynamics (CFD) program. Similar results downstream of a single 90° bend are shown in Fig. 3.1b. In the two cases the axial profiles are strongly asymmetric, and very different. The transversal flow profiles exhibit typical swirl and cross-flow regimes, respectively. Such profile characteristics influence on the USM measurement (cf. Chapter 4).

Multiple acoustic paths are used to sample the flow velocity profile in the pipe at a set of discrete chords, to improve the metering accuracy. Typically 4-6 paths are used in commercial USMs for fiscal metering today. Numerical integration techniques are then used to calculate the average axial gas flow velocity and the volumetric flow rate through the meter. Different types of geometrical path configurations and numerical integration methods are employed by the various meter manufacturers. In some instruments the paths are configured with parallel chords [3.5]; [3.6]. In other instruments, reflecting paths are employed, configured in a "star-like" pattern, where the acoustic pulses are re-

flected one or two times off the spoolpiece wall [3.7]. The method used to combine the measurements from the individual paths into an average flow velocity (the integration method) also varies with the specific meter design. The integration method could be e.g. the conventional Gauss-Jacobi quadrature or some other (conventional or specially-designed) method.

Fig. 3.2 shows a simple geometry of a single path in a multipath ultrasonic gas flow meter configured with parallel chords (path no. i, $i = 1, ..., N$, where N is the number of paths in the USM). Here, L_{pi} is the distance between the transducers, ϕ_i is the inclination angle (relative to the pipe axis), y_i is the lateral distance from the pipe center (lateral chord position), and R is the inner radius of the pipe.
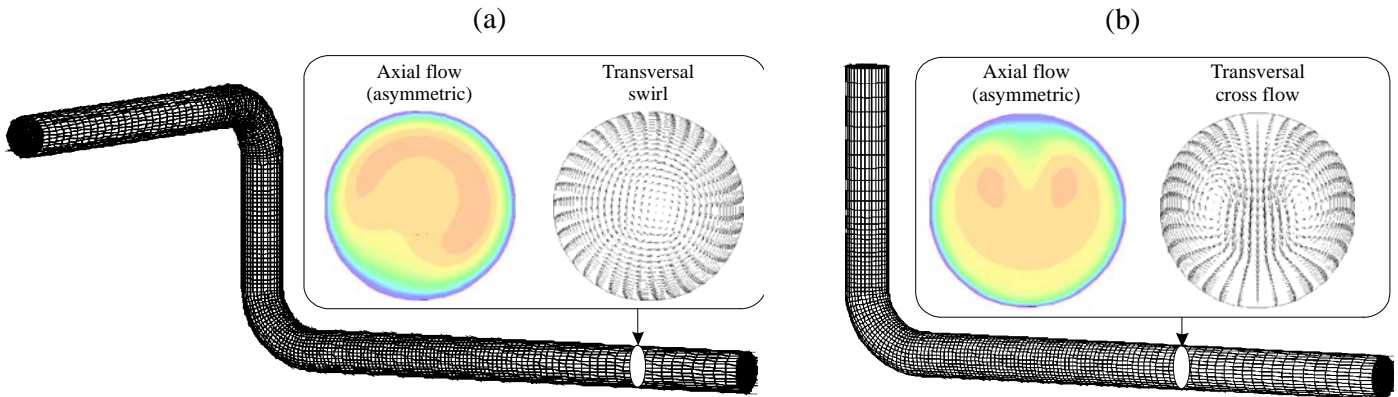
Fig. 3.1   Flow velocity profiles (axial and transversal) calculated 10D downstream a bend using the CFD code *MUSIC* [3.8]. (a) Double 90° bends out of plane, (b) Single 90° bend.
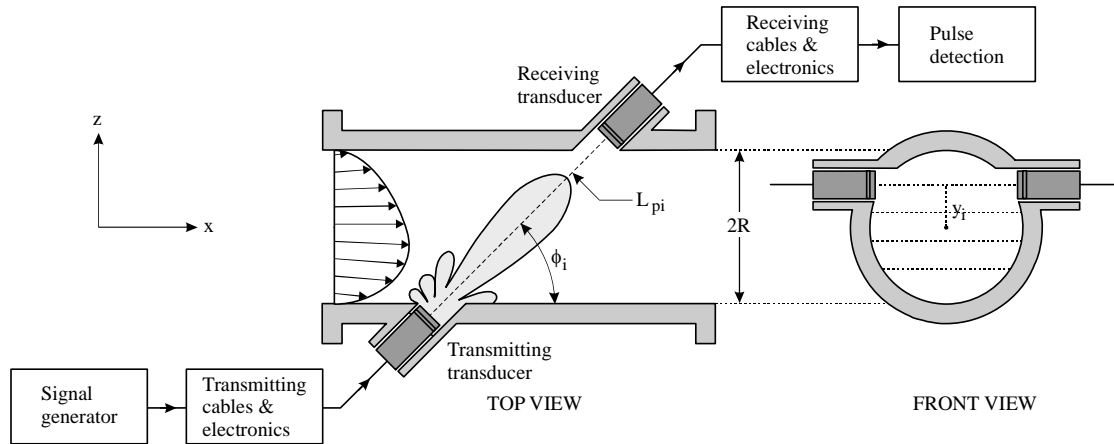
Fig. 3.2   Schematic illustration of a single path in a multipath ultrasonic gas flow meter (for downstream sound propagation). (Left: centre path example ($y_i = 0$); Right: path at lateral chord position y_i.)

3.3   Pipe flow velocity and volumetric flow rate

General expressions for axial flow velocity and volumetric flow rate are discussed in the following, as a basis for the USM measurement, described in Sections 3.4-3.9.

Consider a straight section of a cylindrical gas pipe, as shown in Fig. 3.3. Origo of the Cartesian x-y-z coordinate system is located in the centre of the pipe cross-section, and the x axis is taken along the pipe axis. For a USM configured with parallel chords, the y axis is taken perpendicular to the chords.

Let $\underline{v}(x,y,z,t)$ be the flow velocity vector in the position (x,y,z) at time t, which is decomposed into its axial (x) flow velocity component, $v_A(x,y,z,t)$, and the transversal flow velocity along the chord, $v_T(x,y,z,t)$. The axial and transversal flow velocity profiles are not necessarily axisymmetric, cf. Fig. 3.1. At a fixed cross-sectional plane $x = x_0 =$ constant, and at a fixed time, t_0, the average axial flow velocity (at line conditions), $\bar{v}_A$, the axial volume flow rate (at line conditions), q, and the axial volume flow rate (at standard conditions), Q, are defined as

$$\bar{v}_A = \frac{1}{A}\iint_A v_A(x_0,y,z,t_0)\,dydz \ \text{[m/s]}, \quad q = A\bar{v}_A \ \text{[m}^3\text{/s]}, \quad Q = 3600\frac{PT_0Z_0}{P_0TZ}q \quad \text{[Sm}^3\text{/h]} \quad .$$

(3.1)

Here, $A = \pi R^2$ is the cross-sectional area, P and T are the gas pressure and temperature at line conditions, P_0 and T_0 are the gas pressure and temperature at standard conditions, and Z and Z_0 are the compressibility factors at line and standard conditions, respectively[2]. For a circular cross-section, Eq. (3.1) becomes [3.3]; [3.1]

$$Q = 3600\frac{PT_0Z_0}{P_0TZ}\int_{-R}^{R} D(y)\bar{v}_A(y)\,dy \tag{3.2}$$

where

$$\bar{v}_A(y) = \frac{1}{D(y)}\int_{-\frac{D(y)}{2}}^{\frac{D(y)}{2}} v(x_0,y,z,t_0)\,dz, \qquad D(y) \equiv 2\sqrt{R^2 - y^2} \tag{3.3}$$

are the average axial flow velocity (at line conditions) along the chord D at the lateral position y (the line integral along the chord D), and the chord length, respectively.
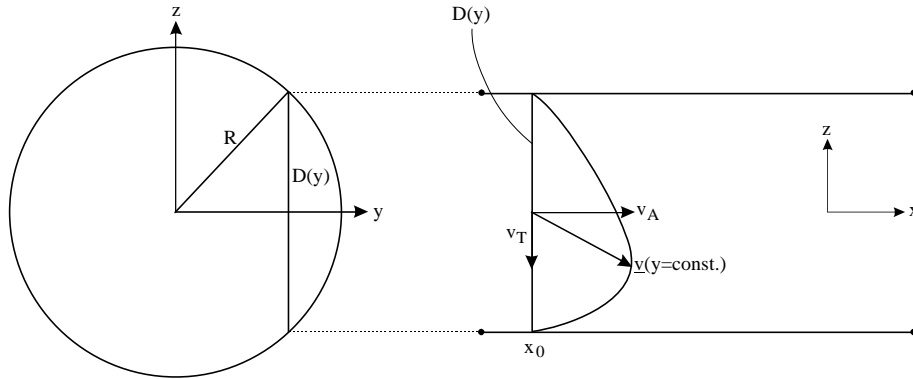
Fig. 3.3   Straight section of cylindrical gas pipe, showing the chord $D(y)$, and an example of a flow profile in the plane $y =$ constant. Also shown is the component of the flow velocity vector in the plane y = constant, $\underline{v}(y{=}const.)$, its axial flow velocity component, v_A, and its transversal flow velocity component along the chord, v_T.

3.4   USM approximations

Eq. (3.2) is an exact expression for Q, which is particularly suitable for USMs with parallel chords that are perpendicular to the y axis. Q as given by Eq. (3.2) is then approximated by a finite sum, in

---

[2]   Here, P_0 and T_0 are defined to represent standard conditions (1 atm., 15 °C). Alternatively, P_0 and T_0 could represent normal conditions (1 atm., 0 °C). In that case, the axial volumetric flow rate at normal conditons, Q, would be given in units of Nm^3/h.

which estimated values for the input quantities are used. This type of approach can formally be divided into two different groups of approximations, as described in the following.

3.4.1 Approximation 1

The first group of approximations concerns the use of

(1) a *finite-sum* approximation of the flow integral appearing in Eq. (3.2) (i.e. the use of a finite number of discrete acoustic paths, $i = 1, ..., N$, cf. Fig. 3.4a);

(2) a *ray tracing approximation* for the sound propagation of each acoustic path in a flowing medium, based on an assumption of a *uniform axial flow velocity profile*, and *no transversal flow velocity components*;

(3) *averaging* over an *axial distance and a small time interval*.
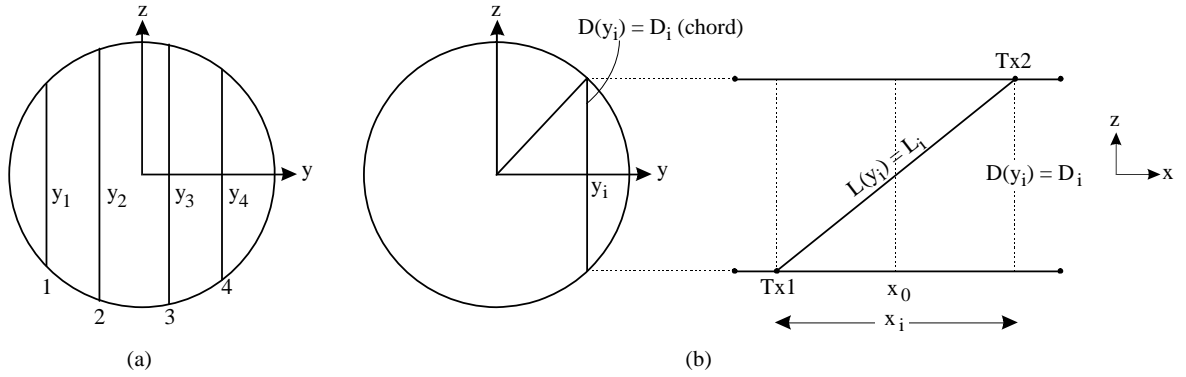
Fig. 3.4   Geometry of a multipath USM configured with parallel chords (4-path example). (a) Chords of multipath configuration, (b) Geometry of path no. *i*.

In the usual theoretical treatment of USMs, a ray tracing approximation is used [3.9]. This approach is essentially a high-frequency approximation of geometrical acoustics, valid only when the acoustic wavelength is small compared with the acoustic beam width, and the beam width is small compared with the pipe diameter [3.10]. In this approach, it has traditionally been assumed that the flow velocity profile is purely axial, v_A, with no transversal flow velocity components ($v_y = v_z = 0$, giving $v_T = 0$) [3.9][3]. It can then be shown that to "first order" in the axial flow velocity profile (i.e., for a uniform axial profile, $v_A =$ constant)[4] [3.9]; [3.1], the upstream and downstream transit times along the interrogation length (L_i), for acoustic path no. *i* at lateral position y_i, are approximately given as

$$t_{1i} \approx \frac{D_i}{|sin\,\phi_i| \left(\sqrt{c_i^2 - \bar{v}_i^2\, sin^2\,\phi_i} - \bar{v}_i\, cos\,\phi_i \right)}$$

(3.4a)

$$t_{2i} \approx \frac{D_i}{|sin\,\phi_i| \left(\sqrt{c_i^2 - \bar{v}_i^2\, sin^2\,\phi_i} + \bar{v}_i\, cos\,\phi_i \right)} \quad ,$$

(3.4b)

---

[3]   Modifications of Eqs. (3.4) and (3.5) to account for the influence of transversal flow velocity components have been proposed and used in e.g. ref. [3.11].

[4]   Assumed that the ray theory holds, the transit time expressions given by Eqs. (3.4) are exact in case of a uniform axial flow velocity profile, $v_A(x_0,y,z,t_0)$.   For other profiles, Eqs. (3.4) represent approximate expressions, cf. [3.1].

respectively. Here, $\bar{v}_i$ is the average axial flow velocity along acoustic path no. i, i.e., $\bar{v}_i = \int v_{A,i} d\ell$ is the line integral along the acoustic path, where $v_{A,i} = v_A(x, y=y_i, z, t)$. c_i is the average sound velocity along the path. L_i is the interrogation length of path no. i (i.e., the length of the portion of the inter-transducer centre line lying inside a cylinder formed by the inner pipe diameter). $D_i \equiv 2\sqrt{R^2 - y_i^2}$ is the chord length of acoustic path no. i (i.e., the length of the projection of the interrogation length L_i of acoustic path no. i in the y-z plane (the pipe cross-sectional plane)).
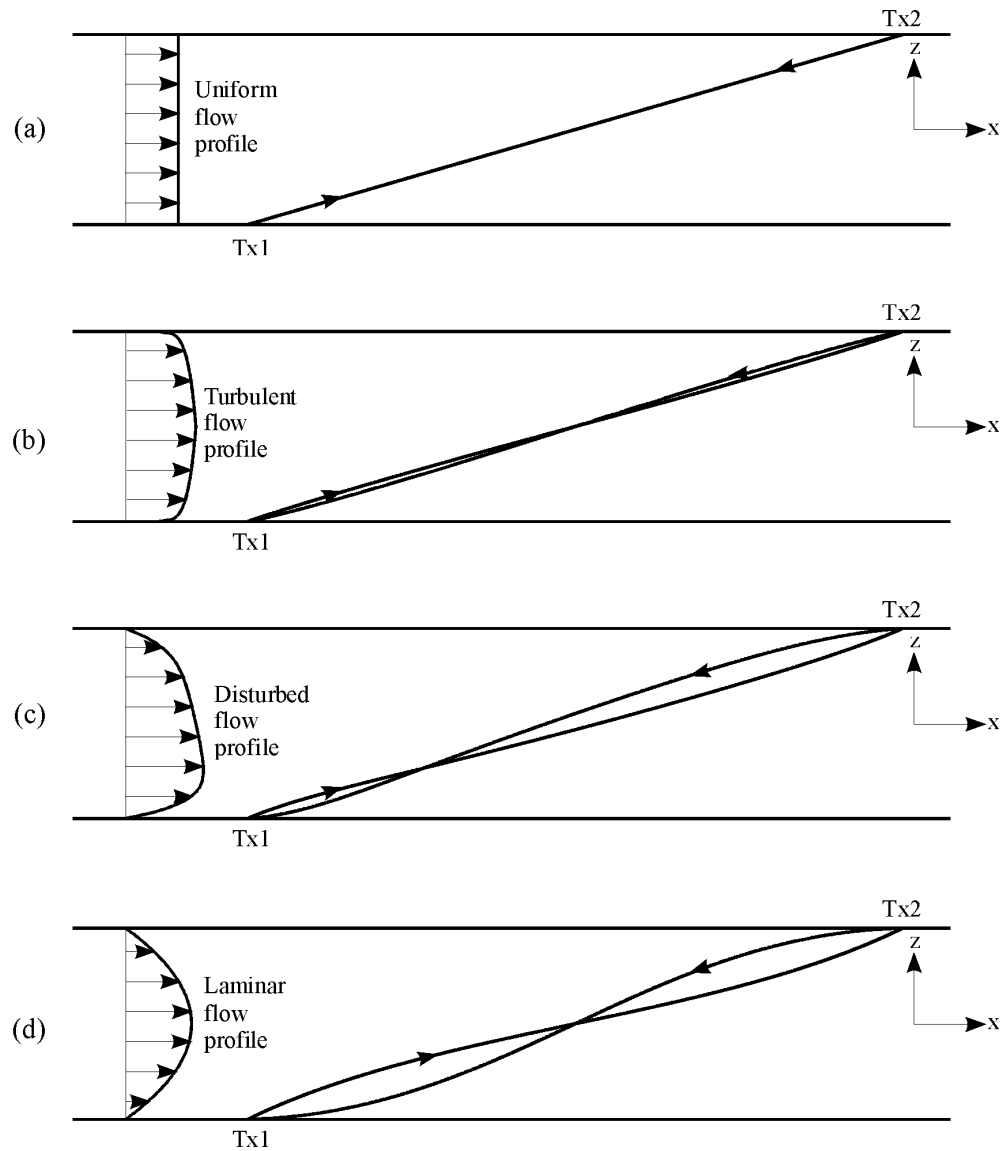
Fig. 3.5   Ray paths of the upstream and downstream sound propagation of an acoustic path (simplified, based on ray tracing theory, - and shown with exaggerated curvatures and an inclination angle of 15° for illustration). The ray paths are calculated for four examples of axial flow velocity profiles: (a) uniform flow profile, (b) fully developed turbulent flow (power-law profile with exponent = 1/9, i.e. Reynolds number ≈ 10^6), (c) an asymmetric, disturbed flow profile, and (d) a laminar flow profile (not so relevant for gas flow). No transversal flow. The same maximum flow velocity is used for all calculations (except for (c), which is 25 % lower).

From the ray-tracing equations, it can be shown that since the flow velocity is not constant over the cross-section of the pipe, the acoustic path will not be a straight line but a curved one. The path an-

gle with respect to the pipe axis will not be a constant, and the upstream path will differ from the downstream one. The curvature of the path will depend both on the flow velocity profile and the Mach number, $\bar{v}_i / c_i$, and it increases with increasing Mach number and with the curvature of the velocity profile. Fig. 3.5 shows simulation examples of upstream and downstream ray paths for four examples of axial flow velocity profiles (with no transversal flow), drawn with exaggerated curvatures and at an inclination angle of 15° for the purpose of illustration. Eqs. (3.4) thus represent approximate expressions, with respect to (1) frequency (the ray tracing approach), (2) low Mach numbers, (3) uniform axial flow velocity profile and (4) no transversal flow[5].

From Eqs. (3.4) one finds (without further approximations) that

$$\bar{v}_i = \frac{L_i(t_{1i} - t_{2i})}{2t_{1i}t_{2i}\cos\phi_i} = \frac{L_i^2(t_{1i} - t_{2i})}{2x_it_{1i}t_{2i}} = \frac{2\sqrt{R^2 - y_i^2}(t_{1i} - t_{2i})}{t_{1i}t_{2i} / \sin 2\phi_i /} \quad . \tag{3.5}$$

In USMs, it is generally assumed that $\bar{v}(y_i)$, the average axial flow velocity over the chord $D(y_i)$ (i.e., at the fixed axial position $x = x_0$ and the fixed time $t = t_0$), given by Eq. (3.3), can be approximated by $\bar{v}_i$, the average axial flow velocity along the acoustic path no. i, given by Eq. (3.5) That means, the approximation

$$\bar{v}(y_i) \approx \bar{v}_i \tag{3.6}$$

is used. In practice, this means that the average axial flow velocity over the chord D_i is averaged over an axial distance x_i (typically of the order of the chord length[6], D_i), and over a small time interval (one complete cycle of "shots" over all paths, typically between 5 and 500 ms, depending on meter size [3.4]). It is thus implicitly assumed that the axial flow velocity profile is constant over the axial distance x_i, and stationary over the small time interval in question.

Under these assumptions, the value of Q given by Eq. (3.2) can be approximated by the finite-sum expression

$$Q \approx 3600\pi R^2 \frac{PT_0Z_0}{P_0TZ} \sum_{i=1}^{N} w_i\bar{v}_i \quad , \tag{3.7}$$

and calculated by applying a suitable numerical integration technique. Here, N is the number of the acoustic paths used in the USM, and w_i is the integration weight factor of path no. i. This method has been implemented in various ways in USMs. The weight factors w_i depend on the the applied inte-

---

[5] The authors have the opinion that, in order to provide a more solid and sound theoretical basis (functional relationship) for such an important fiscal measurement instrument as a USM, the traditional ray tracing theory of USMs which lead to Eqs. (3.4) should be revisited, accounting for the effects of (a) non-uniform flow velocity profiles and (b) transversal flow.

   With respect to (a), recent preliminary investigations by the authors have revealed that for largely curved (disturbed) profiles, Eqs. (3.4) give systematic and significant timing errors for high velocities (20-30 m/s). Hence, axial flow profile effects may lead to systematic and significant errors by using Eq. (3.5), due to the profiles' influence on the transit times.

   With respect to (b), the *ad-hoc* inclusion of transversal flow velocity components proposed and used e.g. in ref. [3.11], should be derived in a more formally correct way.

   With respect to the ray theory approach itself, more comprehensive wave theory descriptions may be used to investigate the influence of the ray approximation and the accompanying inhererent limitations with respect to frequency.

[6] For USMs applying beam reflection, the axial averaging distance is larger.

gration technique. Depending on the method used, the path locations y_i can be chosen so that the weight factors are constants that do not require an assumption of axial flow velocity profile.

3.4.2 Approximation 2

The second group of approximations concerns the use of *estimated values* (measured, or measured/calculated) for the input quantities *P, T, Z, Z_0, R, y_i, ϕ_i, t_{1i}* and t_{2i} ($i = 1, 2, ..., N$) [3.1], giving

$$Q \approx \hat{Q} \equiv 7200\pi\hat{R}^2 \frac{\hat{P}T_0\hat{Z}_0}{P_0\hat{T}\hat{Z}} \sum_{i=1}^{N} w_i \frac{\sqrt{\hat{R}^2 - \hat{y}_i^2}(\hat{t}_{1i} - \hat{t}_{2i})}{\hat{t}_{1i}\hat{t}_{2i}/\sin 2\hat{\phi}_i/} \tag{3.8}$$

where the hat notation "$\hat{x}$" is used to denote the estimate of a quantity "x". The hat notation is useful for the uncertainty analysis of USMs (cf. Chapter 7), but is omitted in the following.

3.5   Pressure and temperature corrections

To correct for the small dimensional changes (expansion/contraction) of the spoolpiece caused by the operational pressure and temperature in the field (cf. Fig. 3.6), some meter manufacturers have implemented correction factors for such dimensional changes[7].
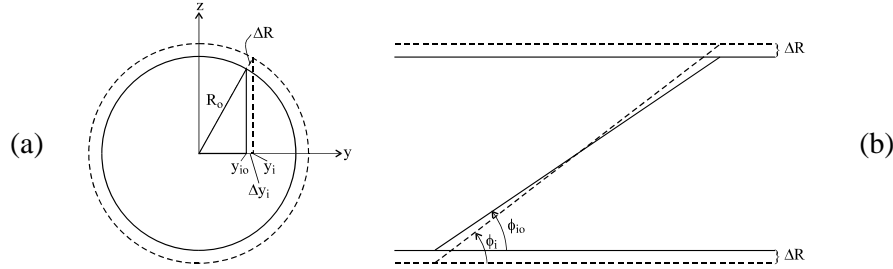
Fig. 3.6   Geometry for acoustic path no. *i* in the USM.   (a) Cross-section showing the lateral (y_i) change with *T* and *P*; (b) Cross-section showing the angular (ϕ_i) change with *P*.

At a temperature *T* and pressure *P*, the pipe radius (*R*), the lateral chord positions (y_i), and the inclination angles (ϕ_i), are [3.1]

$$R \approx K_T K_P R_0$$
$$y_i \approx K_T K_P y_{i0} \tag{3.9}$$
$$\phi_i = \tan^{-1}\left(K_P \tan(\phi_{i0})\right), \quad i = 1, ..., N$$

where subscript zero is used to denote the relevant estimate at $P_0 = 1$ atm. and $T_0 = 20$ °C conditions ("dry calibration" values). The correction factors for temperature and pressure expansion/contraction are given as [3.1]; [3.3]

---

[7]   For each individual USM, AGA-9 recommends measurement and documentation of relevant dimensions of the meter at atmospheric conditions and a temperature 20 °C, as a part of the "dry calibration" of the USM [3.4]. This concerns the average inner diameter of the spoolpiece, the length of each acoustic path between transducer faces, the axial distance between transducer pairs, and inclination angles. Some recommendations for measurements of these quantities in the factory are given in [3.4].

$$K_T \equiv 1 + \alpha \Delta T \ , \qquad\qquad K_P \equiv 1 + \frac{2 R_0 \Delta P}{t_{spool} \rho_{spool} c_{spool}^2} \ , \qquad\qquad (3.10)$$

respectively, where $\Delta T \equiv T\text{-}T_0$ and $\Delta P \equiv P\text{-}P_0$. Here, α, ρ_{spool} and c_{spool} are the coefficient of linear thermal expansion, the density, and the compressional wave velocity, respectively, of the spoolpiece material (usually steel), and t_{spool} is the average wall thickness of the spoolpiece.

3.6 Time averaging

In practice, the transit times t_{1i} and t_{2i} for upstream and downstream sound propagation appearing in Eq. (3.8) are *time averaged* transit times. There are two ways of doing this averaging, either by averaging the *measured* transit times and do the time correction afterwards (cf. Section 3.8), or by averaging the *corrected* transit times. These two methods should be equivalent. In the latter approach, the corrected transit times of each path are averaged over N_{ave} "shots", so that

$$t_{1i} = \frac{1}{N_{ave}} \sum_{n=1}^{N_{ave}} t_{1i}^{(n)} \ , \qquad t_{2i} = \frac{1}{N_{ave}} \sum_{n=1}^{N_{ave}} t_{2i}^{(n)} \ , \qquad i = 1,..,N \qquad\qquad (3.11)$$

for upstream and downstream propagation, respectively. Here, $t_{1i}^{(n)}$ and $t_{2i}^{(n)}$ are the corrected upstream and downstream transit time estimates of "shot" no. n, determined from measurements. In USMs such averaging is used to improve the accuracy of the time detection method with respect to e.g. noise and random time fluctuations of the signal. The number of averagings used in the time averaging interval, N_{ave}, may be different for different USMs. The integer N_{ave} may be in the range one to several hundred.

It is to be noted that t_{1i} and t_{2i} , as given by Eqs. (3.4)-(3.5), originate from the ray tracing theory [3.9], [3.12]. The actual ray theory concerns the propagation of a wave front in a flowing medium, and is not so concerned with the actual acoustic field variable this description should apply to (whether it is sound pressure, or particle velocity, etc.). In practice, however, t_{1i} and t_{2i} are determined from measurements of $t_{1i}^{(n)}$ and $t_{2i}^{(n)}$ using Eq. (3.11), i.e. determined from measurement of physical field variables. Consequently, the actual acoustic field variable has to be specified so that the transit time corrections made in USMs can be expressed precisely, with the correct phase contributions, cf. Section 3.8. That means, to include all relevant time delays to correct for.

To relate $t_{1i}^{(n)}$ and $t_{2i}^{(n)}$ to acoustic wave-theory quantities, it is in the following assumed that they correspond to plane-wave propagation of the sound pressure signal over the interrogation length, L_i, so that

$t_{1i}^{(n)}$, $t_{2i}^{(n)}$: Plane-wave upstream and downstream travel times, respectively, along the interrogation length, L_i, of path no. i ("shot" no. n), at line conditions *[plane-wave sound pressure signal in the gas at the "pipe wall position point" at the transmitting side **-to-** plane-wave sound pressure signal in the gas at the "pipe wall position point" at the receiving side]*.

$t_{1i}^{(n)}$ and $t_{2i}^{(n)}$ are the two transit times of path no. i one wishes to determine. However, in practice, $t_{1i}^{(n)}$ and $t_{2i}^{(n)}$ can not be measured directly in the USM, as discussed in the following (Sections 3.7-3.9) [8].

3.7   Transit time detection

In practice, the transit times in USMs are typically measured by detecting one or several predetermined zero crossings in the received voltage (or current) signal, and using the time difference between corresponding zero crossings in the excitation and received signals as the transit time.
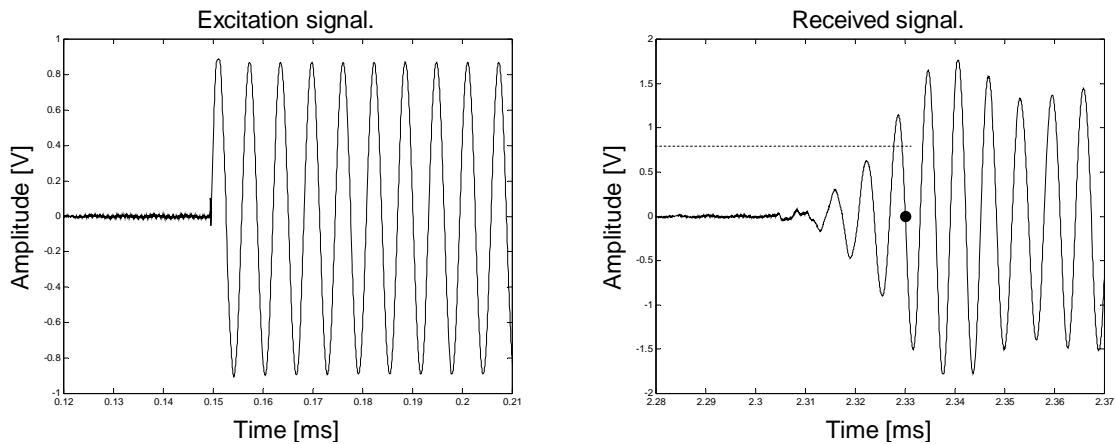
Fig. 3.7.   Transit time detection using a single zero-crossing (marked) in the transient start part of the received voltage signal (usually a short pulse). (Note that here the received voltage is higher than the excitation voltage, since amplifier gain has not been corrected for.)
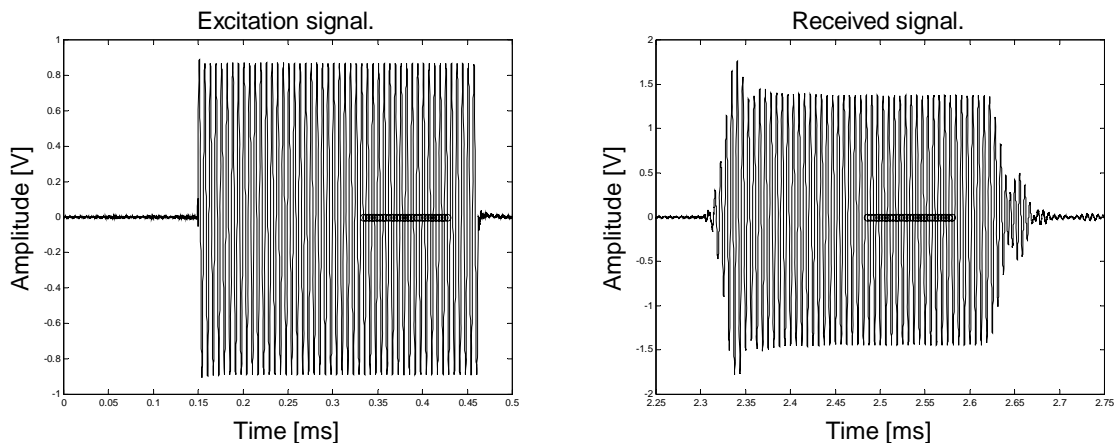
Fig. 3.8.   Time detection using a longer signal (tone burst) and detection of several zero-crossings (marked) in the stationary part of the received voltage signal. (Note that the received voltage is higher than the excitation voltage, since amplifier gain has not been corrected for.)

---

[8]   Up to here, the description is idealized. In practice, one has to correct for time delays of the transducers, cables and electronics, cf. Section 3.8. Moreover, the assumption of plane-wave propagation is an idealized concept, as discussed above, and in practice one has to work with real sound fields. Corrections to account for real sound field effects (diffraction correction) are also considered in Section 3.8.

A simple way, which is widely used [3.3], is to trigger on a predetermined amplitude level in the received signal and then detect the first subsequent zero-crossing, as shown in Fig. 3.7. This technique may be refined using a longer signal and detecting several zero-crossings in the stationary part of the signal, cf. Fig. 3.8. In this way the transient part of the signal where the signal period varies, is avoided[9]. Further, for every signal "shot" the transit time is computed as an average of the individual transit times corresponding to each positive-going (or negative-going) zero-crossing. A more advanced method for period identification is to make use of the relatively fixed amplitude pattern in the transient part of the signal. All methods require that in the received signals, the same predetermined zero-crossings are identified in every "shot", at all conditions of pressure, temperature, flow velocity, noise, etc. ("period identification"). In general, this is not a straigthforward task.

When the acoustic signal becomes significantly corrupted (such as by noise), the signal detection becomes increasingly difficult. Two kinds of error may occur: false period identification or erronous detection of zero-crossing locations. The latter leads to timing errors. In practice, the consequence of erronous zero-crossing locations may be more important than false period identification, since the latter may be rejected based on validity tests and self-checking routines.

In the following, the resulting measured transit times are denoted $t_{1i}^{m,n}$ and $t_{2i}^{m,n}$, where[10]

$t_{1i}^{m,n}$, $t_{2i}^{m,n}$: Measured *time differences* between the excitation signal and the detected signal ("shot" no. *n*), for upstream and downstream propagation of path no. *i*, respectively, at line conditions *[excitation voltage signal -to- voltage signal on which time detection is made]*.

3.8 Transit time corrections

The measured upstream and downstream transit times of "shot" no. *n*, $t_{1i}^{m,n}$ and $t_{2i}^{m,n}$, also contain possible time delays due to the electronics, cables, transducers and diffraction effects, and possible cavities in front of the transducers, cf. Fig. 3.2. To achieve sufficient accuracy of the USM, these additional time delays may have to be corrected for in the USM, as discussed in the following.

Such time corrections have been implemented in different ways by the different USM manufacturers. One possible way of expressing the time corrections is [3.1][11]

$$t_{1i}^{(n)} = t_{1i}^{m,n} - t_{1i,0}^{eltr} - t_i^{cavity}$$

$$t_{2i}^{(n)} = t_{2i}^{m,n} - t_{1i,0}^{eltr} + \Delta t_{i,0}^{corr} - t_i^{cavity}$$

(3.12)

where

---

[9] It should be noted that before transit time corrections (Section 3.8), the transit times measured by these two methods will not in general be equal.

[10] In general, four different combinations of current/voltage signals can be used for time detection: (1) voltage excitation signal and received voltage signal; (2) current excitation signal and received current signal; (3) voltage excitation signal and received current signal; and (4) current excitation signal and received voltage signal. Which combination that is used in a particular meter type, is the choice of the manufacturer, and is normally not communicated to the customer. The particular choice may be based on reciprocity considerations, etc. For simplicity and shortness, the description of Sections 3.7-3.8 accounts only for case (1), voltage excitation signal and received voltage signal. Descriptions of the other cases (2)-(4) can be made similarly.

[11] An alternative way of expressing the time corrections is discussed in [3.1].

$$\Delta t_{i,0}^{corr} \equiv t_{1i,0}^{eltr} - t_{2i,0}^{eltr} \tag{3.13}$$

is the Δt-correction, and t_i^{cavity} has been assumed to be equal in the upstream and downstream directions. Here, the following definitions have been used:

$t_{1i,0}^{eltr}$, $t_{2i,0}^{eltr}$: Upstream and downstream *electronics/cable/transducer/diffraction delays,* respectively, of path no. *i* (transmit and receive), at dry calibration conditions. That means, the sum of: (1) Travel time in the transmitting electronics/cable/transducer *[excitation voltage signal -to- plane-wave sound pressure signal in the gas at the at the centre point of the transmitting transducer front]; plus:* (2) Travel time in the receiving transducer/cable/electronics including diffraction effects at the transducer *[plane-wave sound pressure signal in the gas at the centre point of the receiving transducer front (in absence of the receiving transducer) -to- voltage signal on which time detection is made],*

t_i^{cavity} : *Cavity delay* of path no. *i*, at line conditions. That means, the sum of: (1) Travel time in the cavity in front of the transmitting transducer *[plane-wave sound pressure signal in the gas at the centre point of the transmitting transducer front -to- plane-wave sound pressure signal in the gas at the "pipe wall position point" at the transmitting side]; plus:* (2) Travel time in the cavity in front of the receiving transducer *[plane-wave sound pressure signal in the gas at the "pipe wall position point" at the receiving side -to- plane-wave sound pressure signal in the gas at the centre point of the receiving transducer front (in absence of the receiving transducer)]* (discussed in Section 3.9).

Subscript zero on a quantity indicates that the quantity is specified at dry calibration conditions (with respect to pressure, temperature and gas composition).

The formulation Eq. (3.12) involving the Δt-correction $\Delta t_{i,0}^{corr}$ has been used here for the following reason: If the electronics and the transducers of path no. *i* were reciprocal, and - in addition - the measurement system was *operated* in a reciprocal way, the Δt-correction would be expected to be zero, $\Delta t_{i,0}^{corr} = 0$ (cf. section 5.2). That means, the electronics/cable/transducer/diffraction delays of path no. *i* were then expected to be equal for upwards and downwards propagation, $t_{1i,0}^{eltr} = t_{2i,0}^{eltr}$. This would be valid at all frequencies, temperatures, pressures and flow velocities. Hence, in this case no Δt-correction would be expected to be needed. However, in practice, reciprocity is rarely fulfilled completely[12], and the Δt-correction is not zero in general, $\Delta t_{i,0}^{corr} \neq 0$. The main question is then whether $\Delta t_{i,0}^{corr}$ is so large that it can affect the USM measurement uncertainty.

Typically, estimate values for the quantities $t_{1i,0}^{eltr}$ and $\Delta t_{i,0}^{corr}$ (or equivalent quantities) are found in a "dry calibration" procedure, and used for correction of the measured transit times, e.g. as modelled by Eqs. (3.12)[13]. Dry calibration of transit times is typically carried out at no-flow conditions in a laboratory test cell or the spoolpiece, prior to a possible flow calibration and the field installation of the USM. Dry calibration may be carried out at one or several combination(s) of pressure and tem-

---

[12] Here, the statement "reciprocity not fulfilled" refers to one or both of the two following cases: (1) the electronics or the transducers are not reciprocal by themselves, or (2) the electronics and transducers may be reciprocal, but are not *operated* in a reciprocal way (cf. Section 5.2).

[13] Eqs. (3.12) covers non-reciprocally operated USMs as well as the idealised case of reciprocal operation.

perature. Typically, nitrogen gas may be used for this purpose. The specific dry calibration proce-dure which is used by the various USM manufacturers may differ. Possible dry calibration proce-dures and aspects are discussed on a general basis e.g. in [3.2] and [3.4] (Chapter 6.3). Specific me-ter dependent dry calibration methods are not included in the functional relationship described here. Note that in the present description it is assumed that $\Delta t_{i,0}^{corr}$ is the same with and without flow.

Note also that the parameters determined in the dry calibration procedure (such as $t_{1i,0}^{eltr}$ and $\Delta t_{i,0}^{corr}$) normally vary with the environmenal conditions (P, T, gas composition), so that under operation they may take another value than the value used in the transit time correction of the USM, cf. Section 3.10. It should also be noted that $t_{1i,0}^{eltr}$ changes with the transducer distance (i.e. with path length, or USM size, see below).

Hence, if only the dry calibration values are used for $t_{1i,0}^{eltr}$ and $\Delta t_{i,0}^{corr}$, so that possible changes of these two quantities with P, T, time, transducer distance, etc., are not corrected for, this results in timing errors. The main question in this respect is whether such changes of $t_{1i,0}^{eltr}$ and $\Delta t_{i,0}^{corr}$ are large enough to influence significantly on the USM measurement uncertainty. Such aspect can be analysed using the uncertainty model described in Chapter 7. The variation of $t_{1i,0}^{eltr}$ with P and T and transducer dis-tance is addressed in Chapter 5.

To clarify these aspects, partly for later reference (Chapter 5), and partly since it is relevant in actual meters[14], it may be useful to relate the quantity $t_{1i,0}^{eltr}$ to the transducer delay, $t_{1i,0}^{tr}$, and the diffraction time shift, $t_{1i,0}^{diff}$. This relationship is given as (together with the corresponding relationship for down-stream propagation, with subscript 2)

$$t_{1i,0}^{eltr} = t_{1i,0}^{el,cab} + t_{1i,0}^{tr} + t_{1i,0}^{diff}$$

$$t_{2i,0}^{eltr} = t_{2i,0}^{el,cab} + t_{2i,0}^{tr} + t_{2i,0}^{diff}$$

(3.14)

where

$t_{1i,0}^{el,cab}$, $t_{2i,0}^{el,cab}$: Upstream and downstream *electronics & cable delays,* respectively, of path no. *i* (transmit and receive), at dry calibration conditions. That means, the sum of: (1) Travel time in the transmitting electronics/cable *[excitation voltage signal **-to-** voltage at transmitting transducer input]; **plus**:* (2) Travel time in the receiving electronics/cable *[open-circuit voltage at receiving transducer output **-to-** voltage signal on which time detection is made],*

$t_{1i,0}^{tr}$, $t_{2i,0}^{tr}$: Upstream and downstream *transducer time delay*, respectively, of path no. *i* (transmit and receive), at dry calibration conditions. That means, the sum of: (1) Travel time in the transmitting transducer *[voltage at transmitting transducer input **-to-** plane-wave sound pressure in the gas at the centre point of the transmitting transducer front]; **plus**:* (2) Travel time in the receiving transducer *[free-field sound pressure in the gas, integrated over a circular "measurement area" corresponding to the receiving trans-*

---

14 Some USM manufacturers use quantities corresponding to $t_{1i,0}^{eltr}$ for transit time correction. Other manufacturers use $t_{1i,0}^{el,cab}$, $t_{1i,0}^{tr}$ and $t_{1i,0}^{diff}$.

*ducer front in absence of the receiving transducer) **-to-** open-circuit voltage at the receiving transducer output],*

$t_{1i,0}^{diff}$, $t_{2i,0}^{diff}$: Upstream and downstream d*iffraction time shift*, respectively, of path no. *i*, at dry calibration conditions. That means, the time shift[15] in the gas due to acoustic diffraction at the receiving transducer front *[plane-wave sound pressure in the gas at the centre point of the receiving transducer front (in absence of the receiving transducer) **-to-** free-field sound pressure in the gas, integrated over a circular "measurement area" corresponding to the receiving transducer front (in absence of the receiving transducer)].*

It should be noted that by some manufacturers Eqs. (3.12) (or equivalent formulations) are used for transit time correction, while a combination of Eqs. (3.12) and (3.14) are used by others.

With respect to time detection, different USM manufactures may use different approaches, as discussed in Section 3.7. For instance, time detection can be made in the transient first part of the signal (using e.g. one of the first zero crossings in the signal), or in the middle part of the signal (using e.g. one or several zero crossings in the stationary part), cf. Figs. 3.7 and 3.8. The above description should cover both cases. However, time should always be referred to the same "position" (the same predetermined zero crossing(s)) within the received signal.

3.9   Cavity delay correction

For USMs applying cavity delay correction[16], the measured transit times may be corrected for the travel time in the two transducer cavities of path no. *i* using the cavity delay t_i^{cavity} and Eqs. (3.12). The cavity delay t_i^{cavity} may be estimated under operational conditions (online), as described in the following. Using the simplifying assumptions of (1) no net flow in the cavites along path no. *i*[17], and (2) that the average sound velocity in the two cavities of path no. *i* is equal to the average sound velocity along the whole path, a simplified but still useful expression for this quantity may be [3.1]

$$t_i^{cavity} = K_{TP}^* t_{i0}^{cavity} \tag{3.15a}$$

---

[15] Note that since the phase of a real wave (with diffraction effects) is shifted in the negative direction relative to a plane wave (which is an idealized description), $t_{1i,0}^{diff}$ and $t_{2i,0}^{diff}$ are negative quantities, due to the sign convention used in Eqs. (3.14).

[16] For ultrasonic transducers mounted with their front face *centre point* "flush" with the inner pipe wall (at the "pipe wall position point"), the transducer front edge protrudes into the pipe bore. For such USMs, no cavity delay correction is used (see comments in the text).

    For ultrasonic transducers mounted with the *front edge* "flush" with the inner pipe wall, or for transducers set back from the pipe wall, a cavity is formed in front of the transducers. For the formulation of the USM method given by Eqs. (3.8), a correction for the time delay in the transducer cavities may be needed, as descibed in the text. However, it should be noted that for such mounting, [3.2] has given an alternative formulation of the USM method which does not need cavity delay correction, under the same assumptions of (1) no net flow in the cavites, and (2) that the average sound velocity in the two cavities of path no. *i* is equal to the average sound velocity along the whole path, as used in the text. In this case an alternative formula to Eqs. (3.8) has been obtained, cf. Eq. (A.25) in [3.2], based on a similar approach as used by [3.9].

[17] In general, the assumption of no net flow in the cavities is not true. This topic has been addressed by e.g. [3.13], and the influence of flow in the cavities on the USM measurement (transit times, flow profiles, etc.) should be further investigated in the future.

where

$$K_{TP}^* = K_T K_P \frac{sin(\phi_{i0})}{sin\left(tan^{-1}\left(K_P \, tan(\phi_{i0})\right)\right)} \qquad (3.15b)$$

$$t_{i0}^{cavity} = \frac{L_{ci0}}{c_i} \qquad (3.15c)$$

$$L_{ci0} \equiv L_{pi0} - L_{i0} = L_{pi0} - \frac{2\sqrt{R_0^2 - y_{i0}^2}}{|\,sin\,\phi_{i0}\,|} \qquad (3.15d)$$

$$c_i = \frac{L_i \sqrt{(t_{1i} + t_{2i})^2 \, cos^2\,\phi_i + (t_{1i} - t_{2i})^2 \, sin^2\,\phi_i}}{2t_{1i}t_{2i} \, cos\,\phi_i} \quad . \qquad (3.15e)$$

Here, K_{TP}^* is the temperature and pressure correction factor for the cavity delay correction, and subscript zero is used to denote the relevant estimates at dry calibration conditions (with respect to pressure and temperature). The average sound velocity of path no. i, c_i, is estimated online, at line conditions. L_{pi0} is the distance between the transducers at dry calibration conditions.

In general t_i^{cavity} may also include possible influence of cavity interference on the time detection, caused by signal reflections from the cavity walls. That has not been accounted for in Eqs. (3.15), but may be partly[18] accounted for by the dry calibration (if dry calibration is performed in the meter's spoolpiece).

It is important to be aware that, for USMs using transducers mounted with their front face *centre point* "flush" with the inner pipe wall (i.e., at the "pipe wall position point") ($L_{ci0} = 0$), there will still be uncertainties in the exact location of the transducers (due to uncertainties in the estimates of L_{pi0}, R_0, y_{i0} and ϕ_{i0}, see Eq. (3.15d)). A tiny transducer cavity or protrusion may thus be the result of such uncertainties. Therefore, even if cavity delay correction is not used actively in such meters, the uncertainty related to the cavity delay correction will still be of relevance (cf. Section 7.2.4).

3.10   Ultrasonic transducers

The ultrasonic signals required for the flow measurement are generated and received by ultrasonic transducers. The main purpose of the USM transducers is to convert an electrical signal (e.g. a voltage pulse or tone burst) into an acoustic signal (e.g. a sound pressure pulse or tone burst), and vice versa.

Real transducers have finite sizes in order to generate directive ultrasonic beams at sufficient sound levels. The beamwidths and side lobe levels are determined by the acoustic wavelength, the effective sizes of the transducers, and the vibration patterns over the transducer front. These soundfields may deviate from the idealized models often used in describing the measurement principle and the functional relationship for USMs, cf. Section 3.4.1. The soundfield distributions determines the directions into which the sound is transmitted in the pipe, and also from which directions the sound (and the acoustic noise) is received by the receiving transducers.

---

[18] In this context, "partly" refers e.g. to the fact that flow in the pipe (and thus in the cavity) will most likely alter such interference, so that only partly compensation for the interference may be obtained.

In practice, the mounting of the finite size transducers requires finite sized conduits into the pipe wall ("transducer ports"), with resulting small cavities in front of the mounted transducers. Such cavities may perturb the flow pattern in the measurement section of the pipe to some degree, cf. Footnotes 16 and 17. If such perturbations are significant this may complicate or limit the evaluation and use of the measured transit times and also the evaluation of the resulting measurement uncertainty. The finite transducer sizes and the possible effects of perturbed flow patterns may also affect the integration techniques used to obtain the total pipe flow and the evaluation of the contributions to the measurement uncertainty. These conduits in the pipe wall and the transducer cavities may also result in possible edges, gaps, etc. in the construction, which may act "favorably" towards generating extra flow vortices and possibly interfering acoustic noise.

The transducers will in addition to the spatial filtering of the sound (due to the finite beamwidth and the side lobes), as mentioned above, also result in a significant temporal filtering of the signals (due to the finite frequency bandwidth) and will thus affect the pulse forms and the transit times measured. The usually limited bandwidths available may strongly impact on the transient build-up and ring-down of the acoustic pulses in the pipe, and thus affect strategies used for transit time detection and pulse rate transmissions and pulse sequencing used in the meter, cf. Section 3.7.

For gas flow meters, the ultrasonic transducers are further usually directly exposed to the rather harsh and varying environmental conditions inside the pipe. These units accordingly have to endure corrosive gases, traces of liquids and particles, and the large variations in pressure, temperature and humidity without compromising the acoustic performance of the transducers to a significant degree with respect to the measurements in the meter.

Thus for a real world USM, many aspects concerning the functioning of the ultrasonic transducers need to be taken into account in order to obtain an accurate, reliable, operationally safe and economic metering system. Some aspects of the practical functioning of the ultrasonic transducers in a USM are presently well understood and described, and can be included in the functional relationships for such meters. Other aspects are still not so well investigated and evaluated, and further work remains to be done. The question of testing or measuring important characteristics of the ultrasonic transducers for relevant environmental conditions will be discussed in Chapter 5. Some further more general comments concerning the functioning of such transducers are given below. These comments provide a connection between, on one hand, the discussion of the measurement principle and the functional relationships for USMs given above, and on the other hand, the work on testing/characterization of transducers (Chapter 5) and the work on developing uncertainty models and evaluation of measurement uncertainties for USMs discussed in several later chapters (Chapters 4, 6 and 7).

● *USM transducer technology.* Fig. 3.2 shows schematically a single path in a multipath USM, with the transmitting and receiving ultrasonic transducers, illustrated for downstream propagation. Piezoelectric transducers are typically used in such meters. They employ a piezoelectric crystal or ceramic, which is built into a full transducer construction. A combination of metal and polymer materials (e.g. epoxy and epoxy composites) is often used in USM transducer constructions. Because the acoustic impedance of the gas is much smaller than that of the piezoelectric element, one or several layers of material are typically used between the gas and the piezoelectric element to maximize the acoustic efficiency ("matching layer"). The matching layer material has an acoustic impedance between those for the gas and for the piezoelectric element. In some transducers metal encapsulation is used. The different USM manufacturers use different transducer designs, with different electrical, acoustical and mechanical properties.

The piezoelectric element is set into vibration when an alternating voltage is applied to it. The vibrating element generates sound waves in the transducer construction, and the vibration of the transducer front generates sound waves in the gas. Since the piezoelectric effect is reversible, the piezo-

electric element will produce an alternating voltage related to the mechanical strain when the element is distorted by the action of an incident sound wave.

Usually the surface of the transducer has a plane circular shape. When continuosly transmitting at a single frequency, the sound pressure field in the gas takes the form of an acoustic beam (cf. Fig. 3.2), the width of which depends on the ratio of the the transducer diameter to the acoustic wavelength: the larger this ratio, the more narrow the beam. Because the acoustic beam spreads, the sound pressure level gradually decreases along the beam. Furthermore, the sound is attenuated by the absorption in the gas. A simplified, practical and common approach is to model the transducer sound field by the sound field radiated by a plane circular piston mounted in an infinitely large and rigid baffle [3.14], [3.15]. However, real transducers tend to vibrate and radiate differently from this idealised "plane piston model", - often very differently. In addition the transducer properties may vary with frequency and with environmental conditions, such as temperature and pressure.

• **Transducer characteristics.** In general, a number of "transducer characteristics" are used to describe and test ultrasonic transducers. With respect to ultrasonic flow metering, certain characteristics are already used actively for correction of transit times in USMs available on the market, like the transducer time delay, $t_{1i,0}^{tr}$, the diffraction time shift, $t_{1i,0}^{diff}$, the Δt-correction, $\Delta t_{i,0}^{corr}$, and reciprocity conditions, cf. Eqs. (3.12)-(3.14).

There are also other transducer characteristics which are not used directly today for correction of transit times, but which are still very important for the functionality and performance of the meter, including correction of transit times. Characteristics like the electrical input impedance/admittance, directivity, voltage source sensitivity, transmit-receive voltage-voltage transfer function, etc., are very useful in the transducer design phase, also to evaluate the transducer performance rel. to "expected normal behaviour" (see below and Section 5.2), and also for quality control of the transducer after some period of operation. However, it is expected that in the future, advances in description of ultrasonic transducers may be used to relate also such "other characteristics" more closely to the USM functional relationship, - for example correction of transit times. Such developments may provide possibilities for using modelling tools as a valuable aid e.g. in the correction of transit times, in addition to the purely empirical approach used today.

Moreover, in the future, as USM technology is further developed and matured, and as USMs become more accepted for fiscal metering of gas, it is likely that the need and requirements for doing characterization measurements of the USM transducers at (or close to) operational conditions (with respect to pressure, temperature and gas composition) will be stronger.

• **Desired characteristics of USM transducers.** There are many concerns regarding the desired properties of the transducer, as discussed in the following.

Basically, from the underlaying theory of USMs (Section 3.4.1), the *ideal* transducer should preferably not be materialized at all at the pipe wall, but in spite of that deliver a plane wave signal from a point at the pipe wall, and the same signal should be delivered independent of environmental conditions (pressure, temperature, gas composition). This is of course impossible, and in reality, a number of compromises have to be accepted.

Firstly, real transducers should preferably "deliver" a signal which, as far as possible, is not significantly changed over the environmental conditions specified for the meter (with respect to pressure, temperature and gas composition), at different transducer distances (path lengths), and over time. Signals should be "delivered" with a sufficient signal-to-noise ratio (SNR) for the accuracy required by the time detection method (which depends on the actual time detection method implemented in the USM at hand), and with a directivity (beamwidth, side lobe level) giving sufficient acoustic effi-

ciency of the USM. The signals should not be significantly different for the two directions of the path, or between paths, and should not be significantly changed by changing a transducer in the path. It is frequently a wish or even a requirement that the ultrasonic transducers can be exchanged without requiring a flow recalibration of the USM. Moreover, the transducer signals should not be significantly affected by the mounting and acoustic coupling to the spoolpiece, or by noise generation in the gas or the pipework.

In the context of USMs, no "significant change of the signal" means that the transit times $t_{1i}^{(n)}$ and $t_{2i}^{(n)}$ are not significantly changed (all corrections having been made, cf. Eqs. (3.12)).

Secondly, the transducers should also exhibit "expected normal behaviour" with changing environmental conditions (pressure, temperature and gas composition). A transducer built up according to a certain design should have properties as expected for that design, also under changing conditions of pressure, temperature and gas. However, "expected normal behaviour" does of course allow for changes of properties with pressure, temperature and gas composition, see below.

"Abnormal behaviour" relative to expected normal behaviour for the transducer type at hand can be monitored from measured properties like directivity, sensitivity responses, transfer function response, impedance/admittance response, time delay, diffraction time shift, linearity, reciprocity, etc. Abnormal behaviour can be due to the manufacturing process, like procedures, materials used, material failures, bad design/construction, etc. Abnormal transducer behaviour can also develop under operation of the meter, either gradually over time, or suddenly, with a consequent change of the electrical and acoustical behaviour of the transducer. One possible mechanical cause of abnormal behaviour may be bonding defect at a surface between two materials (e.g. metal and epoxy), as a result of pressure and/or temperature changes, or vibration. There are examples where "abnormal" behaviour seems to be more normal than the expected normal behaviour, which means that one is "asking for trouble". Abnormal transducer behaviour can result in individual transducer behaviour that is so much off that the use of such a transducer will compromise the performance of the meter. It is not always easy to detect abnormal transducer behaviour under flow calibration or field operation of the USM. Moreover, it may happen that the transducer appears to be "normal" at the test conditions used, but shows abnormal behaviour at some operational conditions. Consequently, it is imperative to understand both the "expected normal behaviour" and the actual behaviour of the transducer at hand, mechanicaly, electrically and acoustically, over the complete operational pressure and temperature range specified for the meter, and over time.

● *Change of transducer characteristics with gas parameters and path length.* As mentioned above, "expected normal behaviour" does allow for changes of transducer properties with pressure, P, temperature, T, and gas composition. For example, epoxy materials are strongly temperature dependent, and the use of such materials will affect the temperature characteristics of the transducer (with respect to transit time and amplitude), and in some cases also the pressure characteristics.

In such cases the transducer delay, $t_{1i,0}^{tr}$, will change with T and P (cf. Fig. 5.4). The diffraction correction, $t_{1i,0}^{diff}$, may also change somewhat with P and T (cf. Fig. 5.5). In addition, $t_{1i,0}^{diff}$ changes with transducer distance (i.e., with path length and USM dimension) (cf. Fig. 5.5). $t_{1i,0}^{tr}$ and $t_{1i,0}^{diff}$ may also change over time ("drift"), due to changes in material properties or construction over time.

Such changes with P, T, transducer distance and time, may have consequences for the USM uncertainty. Changes in $t_{1i,0}^{tr}$ and $t_{1i,0}^{diff}$ consequently results in changes in $t_{1i,0}^{eltr}$ and $\Delta t_{i,0}^{corr}$, cf. Eqs. (3.14), so that these may be changed relative to their dry calibration values. If such changes are not corrected for in the meter, they may influence on the uncertainty of the USM measurement, cf. Eq. (3.12) and

Chapter 7. The main question is whether the changes are large enough to influence on the USM uncertainty to a significant degree for the transducer at hand. This topic is discussed in Chapter 5

3.11   Relationship to GERG project on USMs, Phase II

The above brief description of the measurement principle and the set of equations constituting the USM functional relationship, Eqs. (3.8)-(3.15), may serve as an introductory framework and basis for the description of the four tasks in Phase II of the GERG project, given in Chapters 4-7.

Chapter 4 addresses numerical investigations of USM integration methods, and effects of non-ideal flow on the meter error. That means, the uncertainty of the flow rate Q due to numerical discretisation of the axial volume flow rate integral, Eq. (3.2), i.e. the use of a finite number of discrete acoustic paths. In the context of the uncertainty model described in Chapter 7, this concerns the "integration uncertainty" contribution, E_I, to the total USM uncertainty, cf. Eq. (7.1). Two of the five contributions to E_I have been addressed in Chapter 4, namely the contributions E_{Ida} and E_{Ids}, defined in Section 7.2.5. For these two contributions, the effects of installation conditions (bends), and effects of orientation of the meter relative to the flow profile, are considered.

In Chapter 5, methods for characterization and testing of USM transducers under pressure are addressed. The work considers two groups of transducer characteristics: (1) characteristics which are used for correction of transit times (dry calibration parameters, cf. Eqs. (3.12)-(3.14)), and (2) characteristics which are not used directly for correction of transit times, but which are still very important for the functionality and performance of the meter, including correction of transit times.   The former group includes transducer time delay, diffraction time shift, etc. The latter group includes characteristics to ensure that the transducers operate according to "expected normal behaviour" under operational conditions, such as the electrical impedance/admittance, directivity, linearity, and others. Measurements are made up to 100 bar, at 15 and 50/60 $^{\circ}$C, for three types of transducers made available for the project by two USM manufacturers.

Chapter 6 describes an experimental and theoretical investigation into the effects of ultrasonic noise on ultrasonic flow meters. In particular, effects of incoherent (non-synchronous) ultrasonic noise produced by pressure regulation valves (PRVs) are addressed, as well as propagation of noise along the pipe (structure borne noise). Noise suppression technology from six USM manufacturers are investigated in flow tests. This topic concerns one of the contributions to the uncertainty of the detected transit times, $t_{1i}^{m,n}$ and $t_{2i}^{m,n}$, cf. Eqs. (3.8), (3.11) and (3.12).

In Chapter 7 an uncertainty model for multipath ultrasonic transit time gas flow meters is described. The model is based on the USM functional relationship given in the present chapter, Eqs. (3.8)-(3.15). The uncertainty model is developed in conformity with recommended ISO procedures for expression of uncertainty in measurement (the *Guide*) [3.16], and the proposed revision of ISO 5168 [3.17]. The model has been implemented in a PC program, *GARUSO* (Version 1.0). The propagation of input uncertainties of gas parameters, geometry parameters, transit time parameters and the integration method is accounted for. Description of the correlated and un-correlated contributions to the USM measurement uncertainty is essential in this context.

Chapter 4

Prediction of measurement errors of ultrasonic flowmeters in disturbed flow conditions

Achim Hilgenstock[*)], Thomas Hüwener[**)] and B. Nath[***)]

[*)] *Ruhrgas AG, Dorsten, Germany*
[**)] *University of Essen, Essen, Germany*
[***)] *Elster Produktion GmbH, Mainz-Kastel, Germany*

Abstract

The Kalibra® program developed by Ruhrgas AG is a numerical tool for predicting measurement uncertainties of ultrasonic flowmeters in disturbed flows. Inputs required include a reference flow field (normally the ideal flow field in which a meter is calibrated), a disturbed flow condition (e.g. behind bends, valves, etc.) and the meter's sound path configuration. Based on these inputs, "measurement" errors of ultrasonic flowmeters caused by flow disturbances can be predicted numerically. This paper investigates the results of different disturbances generated in a double bend out of plane for four different ultrasonic flowmeters. Artificial flow conditions are used to determine the impact of swirl, profile deformation and decay on meter accuracy in separate steps. The effects of changing the meter's angle of installation in the pipe are also examined.

4.1   Introduction

In many industrial applications, the precise measurement of volumetric flow rates is of crucial importance. The gas industry employs various kinds of flow metering principles such as turbine flowmeters, orifice plates and ultrasonic flowmeters. All these devices are more or less sensitive to upstream flow disturbances. This paper focuses on the behavior of ultrasonic flowmeters in the presence of flow disturbances.

For flowmeter manufacturers and customers it is extremely interesting to know how a meter will respond to a specific flow disturbance before the meter is actually installed. It is well known that e.g. simple bends in pipes generate flow disturbances such as swirl and profile deformation. These disturbances can be reduced by installing long straight pipes or flow conditioners upstream of the meter, but this increases installation costs and may cause an additional pressure loss.

In the past, flow disturbances were mainly investigated by experimental profile measurements performed using pressure probes, laser doppler anemometry or other techniques. Yet these experimental investigations are time-consuming and, especially under high-pressure flow conditions, very expensive. Knowledge about the flow profiles was in most cases restricted to several measurement traverses or measurement planes. A complete set of three-dimensional flow field data in a pipe was very difficult to obtain.

With the improving performance of workstations and decreasing prices for hardware, the use of CFD (Computational Fluid Dynamics) has become more and more interesting. Ruhrgas AG has obtained a license for a commercially available CFD program known as *Fluent* [4.1], to help reduce its experi-

mental costs by complementing or replacing experimental work. The advantage of CFD over experiments is that simulation is usually much cheaper and faster to perform than comparable experiments. CFD also provides information on the complete flow field in the area of interest as opposed to discrete measurement points.

The results of the numerical simulation of disturbed flow in pipe systems are used as input data for a program developed by Ruhrgas AG. This program, known as Kalibra®, computes the "measurement" errors for given ultrasonic flowmeters under disturbed flow conditions.

4.2   Flow simulation inside a typical pipe configuration

As part of this paper the flow inside a double bend out of plane was investigated as an example of a typical pipe configuration at a gas metering station, using computational fluid dynamics. The numerical result was validated by experimental data measured with a two-component laser doppler system by PTB in Germany [4.2]. Good agreement of experimental and numerical data was found [4.3].

Fig. 4.1 is the result of a numerical simulation with Fluent based on the RNG turbulence model: Parts of the pipe are cut out to allow an inside view. At three different cross sections, the velocity profiles are shown as "envelopes" over the arrow heads of the local velocity vectors, visualizing the process of profile deformation caused by this double bend out of plane.
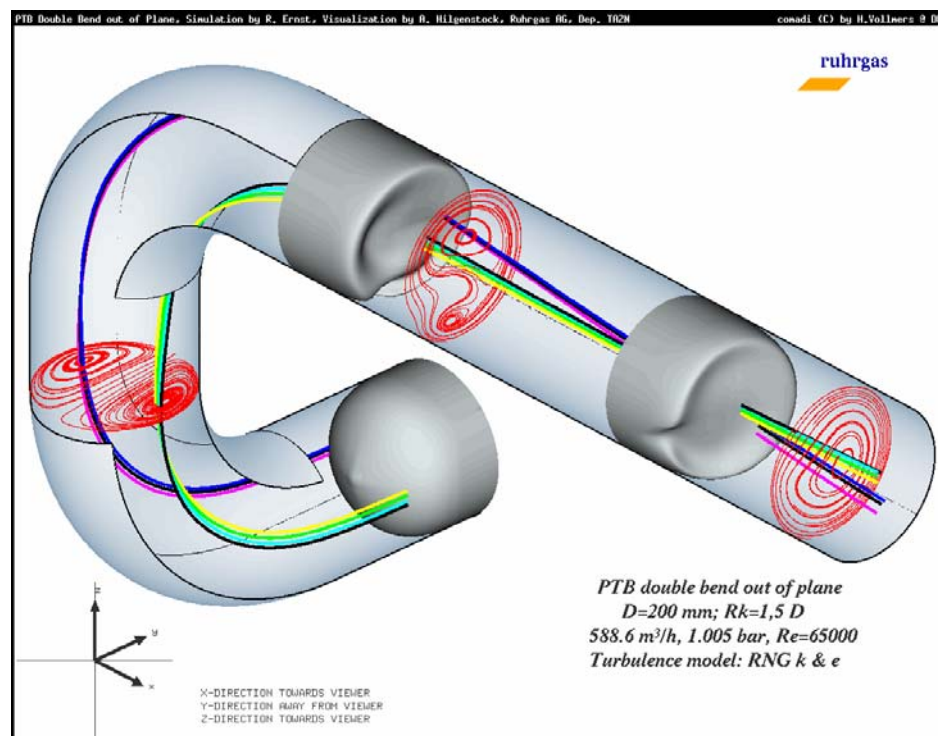
Fig. 4.1   Flow visualization inside double bend out of plane based on CFD simulation. (An animation of the flow simulation is available on the Internet: http://www.ptb.de/deutsch/org/1/13/131/131d3.htm#Install.)

Downstream of the first bend, two-dimensional streamlines in a cross plane indicate the typical vortical flow behind a single 90° bend, i.e. a pair of counter-rotating vortices. A few selected three-dimensional streamlines passing through the centers of these vortices have also been drawn into the figure.

While passing through the second bend, this double vortex system starts to form the typical single swirl type flow behind a double bend. Downstream of the second bend it changes into a centered single vortex.

The figure clearly shows the deformation of the velocity profiles in the straight pipe section downstream of the second bend. The small velocity plateau in the center of the pipe is caused by the very low axial flow velocity on the inside of this pipe configuration behind the first bend, while the dips in the profiles at 0.5D and 3D behind the second bend are due to flow deceleration behind the second bend (for details of the profile development refer to the animation available in the Internet).

The numerical data of the disturbed flow condition is used as input data for the Kalibra$^®$ program to predict uncertainties of ultrasonic flowmeters in the following chapter.

4.3   Kalibra$^®$ - a numerical tool for investigating the performance of ultrasonic flowmeters

The principle of ultrasonic flow metering is well known and briefly explained for a simple meter featuring two transducers mounted at a distance, L, of each other and at an angle, φ, to the direction of flow. By measuring the transit time of a sound wave from the emitting transducer to the receiving one (t_- in the downstream direction and t_+ in the upstream direction), the mean velocity can be derived along the ultrasonic path, $\overline{u}_{ultra}$, detected by the ultrasonic meter by solving Eq. (4.1) [4.4]:

$$\overline{u}_{ultra} = \frac{L}{2cos(\varphi)} \frac{t_+ - t_-}{t_+ \cdot t_-} . \tag{4.1}$$

In Eq. (4.1), the distance, L, and the angle, φ, are known from the meter's geometry, while the time is measured in the ultrasonic meter itself. To determine the volumetric flow rate, Q, the velocity, $\overline{u}_{ultra}$, in Eq. (4.1) has to be multiplied by the cross sectional area, A, of the meter and a calibration factor, k. This factor relates the velocity, $\overline{u}_{ultra}$, measured in the meter, to the mean axial velocity in the meter cross section:

$$Q = kA\overline{u}_{ultra} . \tag{4.2}$$

The calibration factor, k, is dependent on the sound path configuration realized in the meter, while the local velocity distribution depends on the upstream flow disturbances and the Reynolds number.

The basic idea underlying Kalibra$^®$ was already presented at the FLOMEKO'96 conference in Beijing, 1996 [4.4]: Unlike measurements, numerical simulation can draw on the complete data of the flow field in the pipe, hence, the velocity, $\overline{u}_{ultra}$ can be calculated from the data by numerical integration of the local velocity vectors, $u(l)$, along the ultrasonic path, L:

$$\overline{u}_{ultra} = \frac{1}{cos(\varphi)L} \int_0^L u(l)dl . \tag{4.3}$$

Combining Eqs. (4.2) and (4.3) allows a numerical determination of the calibration factor, k, because the volumetric flow rate is known in the numerical solution:

$$k = \frac{QL\cos(\varphi)}{A\int\limits_{0}^{L} u(l)dl}. \tag{4.4}$$

Eq. (4.4) can be solved numerically for undisturbed flow conditions to determine calibration factor k_{undis}, and for disturbed flow conditions to also determine calibration factor k_{dis}.

In practice, meters are calibrated under undisturbed (ideal) flow conditions, but they are often used in more or less disturbed flow situations. The calibration factor, k_{undis}, for ideal flow conditions is known from the calibration procedure. Using the same calibration factor under disturbed flow conditions results in a volumetric flow rate, Q_{dis}, which is not equal to the real volumetric flow rate, Q, because flow conditions inside the meter are not ideal:

$$Q \neq Q_{dis} = k_{undis} A \bar{u}_{ultra,dis} \ . \tag{4.5}$$

Based on that, the measurement error, ΔQ, in % due to the disturbed flow conditions can be calculated by Eq. (4.6):

$$\Delta Q = 100\%(Q - Q_{dis})/Q \ . \tag{4.6}$$
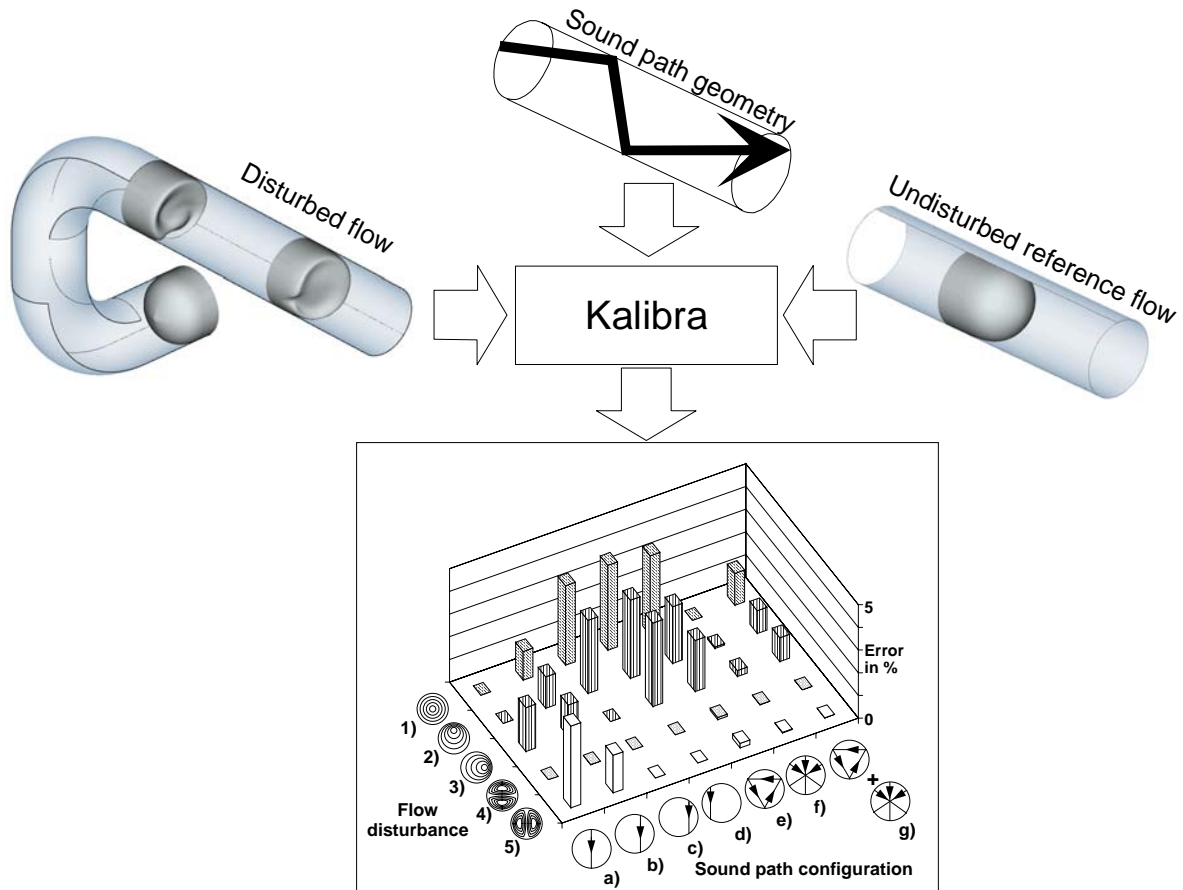
Fig. 4.2   Input and output of Kalibra[®].

From the above discussion it is now clear that Kalibra[®] requires three different inputs, as visualized in Fig. 4.2:

1. The disturbed flow field to determine the calibration factors for non-uniform velocity fields due to complex pipe configurations ahead of the meter.

2. The sound path configuration of the meter itself.

3. The reference flow field to determine the calibration factors for each sound path under ideal flow conditions.

Based on these inputs, Kalibra® determines the information necessary for predicting "measurement" errors due to flow disturbance. This allows

- manufacturers to find the optimum sound path configuration for the flowmeter which is least sensitive to the different flow disturbances,

- customers to re-calibrate meters even under disturbed flow conditions, customers to optimize the position of an ultrasonic flowmeter in a given installation,

- customers to optimize flow conditioners upstream of ultrasonic flowmeters to condition the flow for an optimum use of ultrasonic flowmeters.

4.3.1   Kalibra® validation

Since Kalibra® is based on a numerical method, it is necessary to validate the results by comparing the numerical output with an analytical solution, if possible. To validate the method, fully developed velocity profiles for laminar and turbulent flows in a circular pipe are used as reference flows. For these types of flow and different sound path configurations, the calibration factor, k, can be derived analytically [4.5], and compared with the program's numerical output:

- For laminar flows and a centric path configuration, the calibration factor is $k_{lam,cent} = 0.75$,

- For turbulent flows and a centric path configuration, the calibration factor is $k_{turb} = 2n/(2n+1)$; n is the Nikuradse exponent which is a function of the Reynolds number,

- For laminar flows and an eccentric path configuration, the calibration factor is $k_{lam,ecc} = 0.75(1-h^2/R^2)^{-1}$, with h being the eccentricity of the sound path towards the pipe axis, and R the pipe radius.

Depending on the numerical grid used for the discretisation of the computational domain, the difference between the calculated calibration factors and the ones determined analytically was relatively small. For a cross-sectional grid with a resolution of 41*41 node points, the error was less than 0.32 %. Hence, the method was validated successfully.

4.4   Examples of practical Kalibra® applications

In the tests described in this chapter, Kalibra® was tested on real flow disturbances and realistic ultrasonic flowmeters. The aim was to investigate the influence of swirl, velocity profile deformation and decay of flow disturbances on the accuracy of four different ultrasonic meters installed at different angles of rotation with respect to the pipe configuration. The discussion is focused on typical flow disturbances generated in double bends out of plane.

4.4.1   Sound path configurations

Figs. 4.3 to 4.5 show three different sound path configurations in the so-called 0° position. To check the 0° position of the coordinate system for the double bend out of plane, refer to the coordinate system in these figures and to Fig. 4.1.
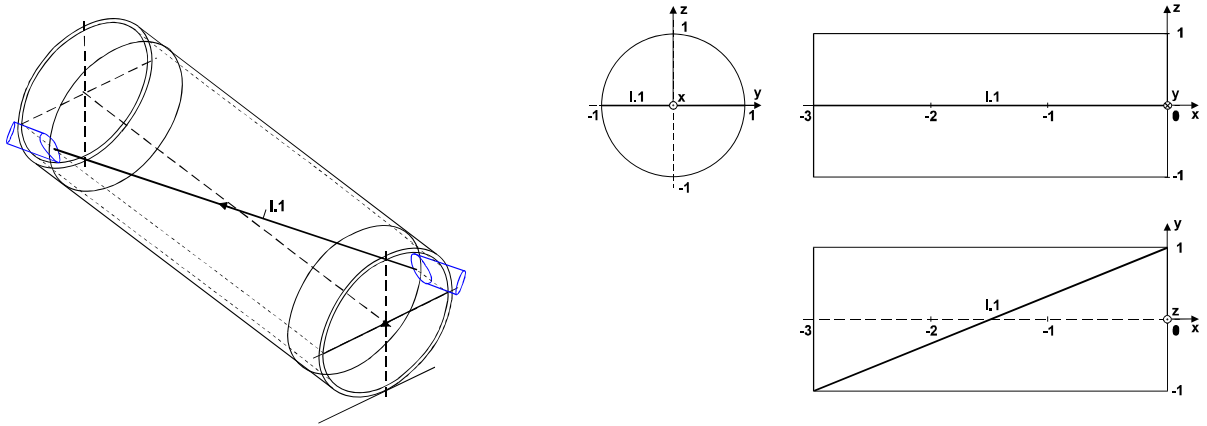
Fig. 4.3   Sound path configuration I. One single centric sound path.
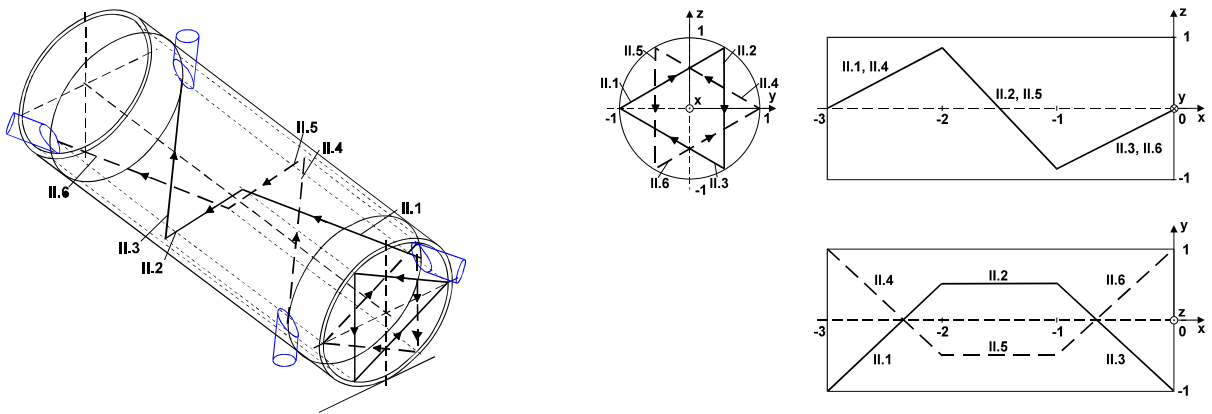
Fig. 4.4   Sound path configuration II. Two-path system.
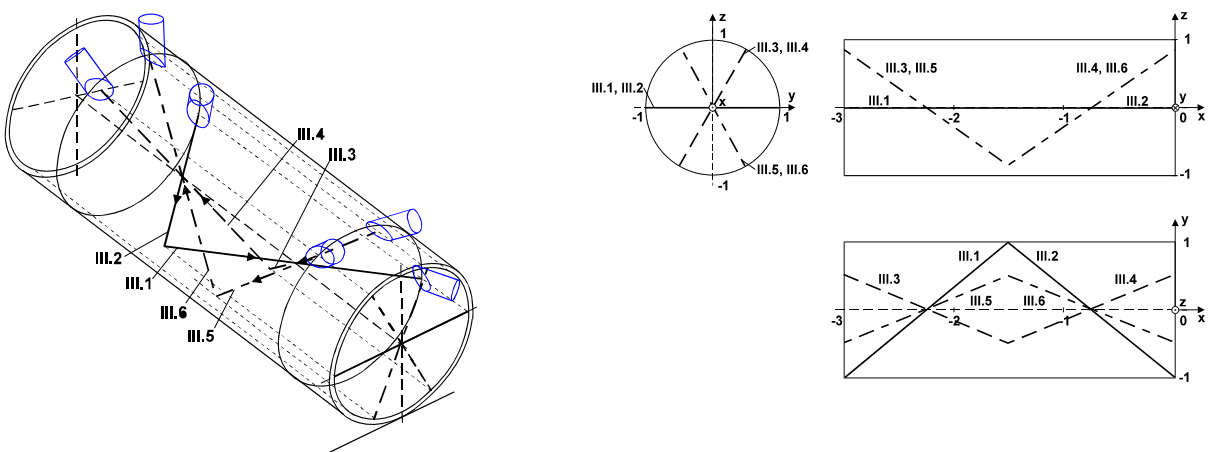
Fig. 4.5   Sound path configuration III. Three-path system.

The path configurations described below are artificial and not exactly the same as those realized in real flowmeters, but they are similar to what is available on the market. Figs. 4.3 to 4.5 show a 3-

dimensional plot of the sound path and three different planar views, (front, side and top view). The Roman numbers in these figures denote the sound path configuration, while the Arabian numbers indicate the number of the sound path in that configuration.

Configuration I, shown in Fig. 4.3, is the most simple path configuration in this investigation. It consists of only one path, passing the pipe axis without any reflection on pipe walls.

The second sound path configuration is shown in Fig. 4.4. The meter consists of two sound paths, each forming a triangle in the direction of flow. Each sound path is reflected twice on the pipe wall.

The third configuration is shown in Fig. 4.5. The meter consists of three centric sound paths with one reflection on the pipe wall for each path. In the axial direction the paths are arranged to form a star, as can be seen in the middle of Fig. 4.5.

The fourth path configuration investigated was a combination of configurations II and III. It is not shown here because it would not provide any new geometrical information. Path configuration IV is very similar to a real ultrasonic flowmeter.

4.4.2   Flow disturbances

As can be seen from Fig. 4.1, real flow disturbances consist of: axial velocity profile deformations, swirl, the decay of swirl and velocity profile deformation due to friction effects in the downstream direction. Each of the disturbances has a different impact on the performance of ultrasonic flowmeters. In order to investigate the effect of swirl, profile deformation and decay separately, three "artificial" flow disturbances are generated:

An <u>undisturbed axial velocity profile with swirl</u> in order to test meter sensitivity to swirl. The velocity profiles do not change in the axial direction, so the decay process is neglected as well. This disturbance is characterized by the symbol

and called disturbance 1.
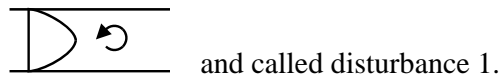
A <u>disturbed axial velocity profile without swirl</u> in order to test meter sensitivity to axial velocity profile deformation. The velocity profiles again do not change in the axial direction. This disturbance is characterized by the symbol

and called disturbance 2.
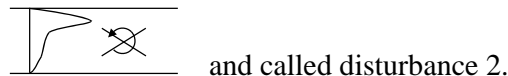
A <u>disturbed velocity profile with swirl</u> which is almost a real profile, but again change in the axial direction is not taken into account. This disturbance is characterized by the symbol

and called disturbance 3.
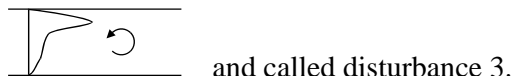
The artificial profiles are based on the calculated velocity distribution at a distinct axial position downstream of the double bend out of plane and obtained by "manually" setting the velocity component as required.

In addition to these three "artificial" velocity distributions, the real velocity profile is used as the fourth disturbance taking all physical flow phenomena into account. This disturbance is marked "real profile" in the following figures.

4.4.3   Meter sensitivity 3.3 D downstream of double bend out of plane

In each of the following simulations, the inlet planes of the ultrasonic flowmeters are positioned 3.3 pipe diameters (D) downstream of the second bend of the pipe configuration shown in Fig. 4.1 in the so-called zero degree position. Meter rotation around the pipe axis and its influence on meter performance are discussed below. At the 3.3D position in the pipe (see Fig. 4.1 for flow details), the swirl is relatively centered in the pipe axis and the cross flow components are about 10 % of the axial velocities. The profile deformation shows a relatively uniform axial velocity distribution with slightly higher values close to the pipe wall and a small area of low velocities in the 9 o'clock position.

The following figure visualizes the predicted measurement errors of the volumetric flow rates versus the flow disturbances and sound path configurations.
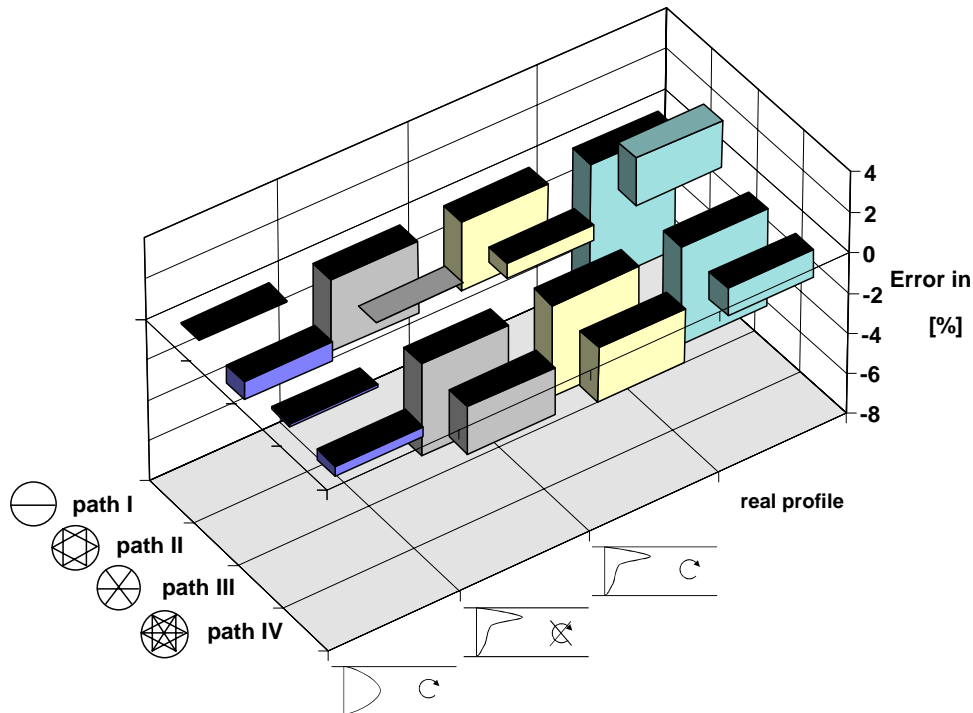
Fig. 4.6   Predicted measurement errors of the volumetric flow rate 3.3 D downstream of double bend out of plane.

Fig. 4.6 shows that all path configurations are relatively non-sensitive to a single swirl in the flow (disturbance 1). The detected error is between almost zero and one percent. Path configuration II shows the highest sensitivity. Note that the "real" meter (path IV) has not even the smallest of an error for that type of artificial flow.

In the case of axial velocity profile deformation without swirl (disturbance 2), the least sensitive meter is that with path configuration II, which is just the inverse result of what was described above. All

other configurations show errors due to profile deformation that are generally higher than those expected under swirling flow conditions (configurations I, III and IV). This shows that ultrasonic flow-meter performance is affected much more by profile deformation than by swirling flows.

The result obtained when taking profile deformation and swirl into account (disturbance 3) is similar to that discussed above.

In the real profile case (disturbance 4), not only the decay process (which should normally result in a decreasing error) plays an important role. Measurement results are also affected by the rotation of the axial profile deformation with the axial position due to the overlaid swirl. Fig. 4.6 shows that real profile path configurations I, II and III have a far higher sensitivity for that velocity distribution than any other disturbance discussed so far. The highest errors occur for path configurations I and III. The smallest error is predicted for meter IV which is close to a real flowmeter. For that configuration, the error is about 1.5 % when installed close to the bend, which is a good result given the high disturbance.

4.4.4 Dependency on angle of meter rotation relative to the pipe configuration ahead

Normally, meters are installed at a well defined axial position, but the installation angle is selected irrespective of the piping ahead. The following observations demonstrate that the angle of meter installation with respect to the piping is of crucial importance. Fig. 4.7 shows the predicted measurement error of the volumetric flow rate, ΔQ, versus the angle of rotation, with the meter installed in the same axial position as in the previous chapter (i.e. at 3.3D). For this configuration, the real velocity distribution with swirl, profile deformation and decay is taken into account.
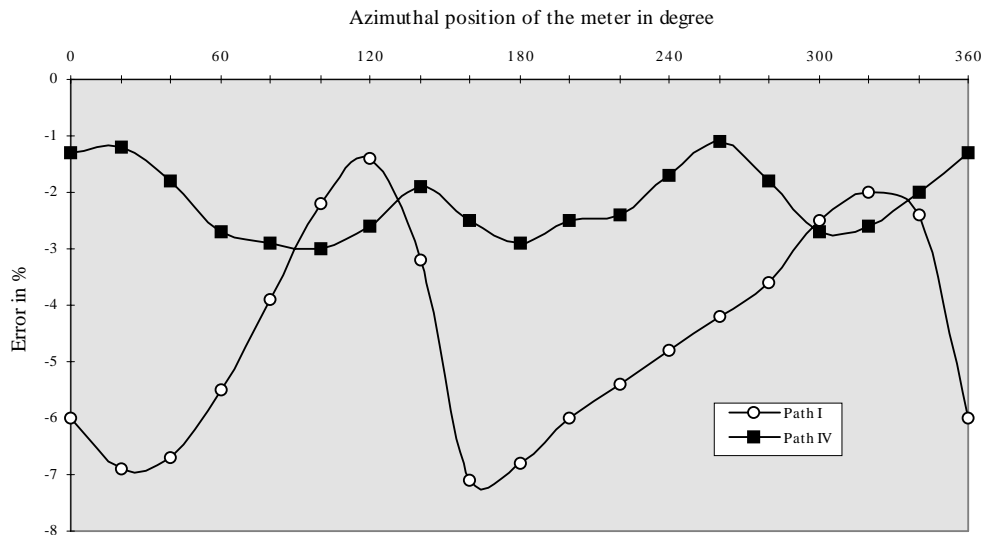
Fig. 4.7   Predicted measurement error of the volumetric flow rate versus angle of rotation for disturbed velocity profile 3.3 D downstream of double bend out of plane.

The diagram clearly shows that path configuration I (single path) is - as expected - very sensitive to the angle of installation. The error varies between -1.4 % and -7.1 %. The error curves are not symmetrical for the rotation because the real velocity distribution in the pipe is also non-symmetrical.

Path configuration IV is far less sensitive than the previous one. Yet, the error is still between -1.1 % and -3.0 %, depending on the position of the device. From the discussion above, it is obvious that the angle of rotation of the meters has a major impact on measurement accuracy and has to be taken into account when installing ultrasonic flowmeters.

4.5 Summary and conclusions

Kalibra®, a numerical program for predicting the measurement errors of ultrasonic flowmeters was proven by using flow conditions that can be described analytically. For these conditions the calibration factors were derived analytically and compared with the numerical result. The accuracy of the method was shown to be better than 0.3 % for a computational mesh of 41*41 node points in a pipe cross section.
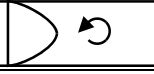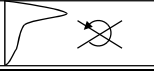
Based on the method developed, the performance of different ultrasonic flowmeters was tested for different sources of flow disturbance, typically found in double bends out of plane. By generating "artificial" flow conditions it was possible to show that swirl only has a minor impact on meter accuracy. Profile deformation on the other hand turned out to have a much greater influence on the performance of the ultrasonic flowmeters investigated.

With the real velocity distribution taken into account, sound path configuration IV, which is similar to a real flowmeter, was found to be least sensitive to the disturbances investigated.

All meters are more or less sensitive to the angle of rotation of the meter with respect to the pipe configuration. Again, the "real" flowmeter showed to be least sensitive in the performed comparison.

The main results of the sensitivity tests are summarized in the following table:

Table 1. Sensitivity of the investigated sound path configurations I-IV to swirl, velocity profile deformation and the real profile (axial decay of disturbances).

Disturbance:				real profile with decay	rotational position
path I	++	--	--	--	--
path II	+	++	++	+	not tested here
path III	++	--	--	--	not tested here
path IV	+	-	-	++	+

++ = no sensitivity, -- = very sensitive

Unlike turbine flowmeters, ultrasonic flowmeters are less affected by swirl but highly sensitive to velocity profile deformation. This may be helpful in selecting the optimum flow conditioner upstream of ultrasonic flowmeters.

Generating artificial flows helps to optimize ultrasonic flowmeters with respect to their sensitivity to flow disturbances.

Kalibra® can provide results within seconds, making improvements much cheaper than by experimental work.

4.6 ACKNOWLEDGMENTS

Chapter 5

Methods for characterization and testing of USM transducers under pressure

Per Lunde[*)] and Magne Vestrheim[**)]

[*)] *Christian Michelsen Research AS (CMR), Bergen, Norway*
[**)] *University of Bergen, Dept. of Physics, Bergen, Norway*

Abstract

Methods for characterization and testing of USM transducers under pressure are addressed. The work considers two groups of transducer characteristics: (1) characteristics which are used for correction of transit times (dry calibration parameters, cf. Eqs. (3.12)-(3.14)), and (2) characteristics which are not used directly for correction of transit times, but which are still very important for the functionality and performance of the meter, including correction of transit times. The former group includes transducer time delay, diffraction time shift, etc. The latter group includes characteristics to ensure that the transducers operate according to "expected normal behaviour" under operational conditions, such as the electrical impedance/admittance, directivity, linearity, and others. Measurements are made up to 100 bar, at 15 and 50/60 $^{\circ}$C, for three types of transducers made available for the project by two USM manufacturers.

5.1   Introduction

5.1.1   Background

Fig. 3.2 shows schematically a single path in a multipath USM, with the transmitting and receiving ultrasonic transducers, illustrated for downstream propagation. As described in Section 3.10, the ultrasonic transducers are critical components of an ultrasonic gas flow meter. Changes in the transducer characteristics with changing pressure, temperature, gas conditions, transducer distance and time, may influence on the USM performance not evident during a normal flow calibration.

Transducer characteristics of importance in this connection include:

(1) Characteristics which are used for correction of transit times. This includes dry calibration transit time parameters like the electronics/cable/transducer/diffraction time delay, t^{eltr}, and the Δt-correction, Δt^{corr}, cf. Eqs. (3.12). Note that t^{eltr} may be been decomposed into the electronics/cable time delay, $t^{el,cab}$, the transducer time delay, t^{tr}, and the diffraction time shift, t^{diff}, cf. Eqs. (3.14)[19].

---

[19] For simplicity, and without loss of generality, the quantities $t^{eltr}_{1i,0}$, $\Delta t^{corr}_{i,0}$, $t^{el,cab}_{1i,0}$, $t^{tr}_{1i,0}$, and $t^{diff}_{1i,0}$ used in Chapter 3, are here denoted t^{eltr}, Δt^{corr}, $t^{el,cab}$, t^{tr} and t^{diff}, respectively.

(2) Characteristics which are not used directly for correction of transit times today, but which are still very important for the functionality and performance of the meter, including correction of transit times. These may be used to ensure that the transducers operate according to "expected normal behaviour" under operational conditions, and for quality control of the transducers after some period of operation. Such characteristics are typically the electrical impedance/admittance, directivity, linearity, sensitivity, transmit-receive transfer function, and others.

There are several reasons for measuring these transducer characteristics under pressure, and at different temperatures:

(1) To determine the "expected normal behaviour" at operational conditions for the transducer type at hand. The "expected normal behaviour" may change significantly with pressure and temperature [5.1], and measurements over the P and T ranges gives useful information about whether the "expected normal behaviour" is actually "good acoustic behaviour" over the ranges in question.

(2) To ensure that individual transducers actually function according to "expected normal behaviour" at operational conditions (within actual limits), over the pressure and temperature range specified for the USM, and over time.

(3) To determine the changes of the transit time corrections t^{eltr} and Δt^{corr} with P, T and transducer distance, so that, if necessary, compensation for the changes can be made. If compensation is *not* made, the changes of t^{eltr} and Δt^{corr} will act as uncertainties contributing to the total USM uncertainty (cf. Chapter 7). The main question is then whether the changes are large enough to influence significantly on the USM uncertainty.

5.1.2   Scope of work

The scope of work for Task 3 of the GERG project was three-fold [5.1]:

1. Develop methods for measurement of transducer characteristics in gas at elevated pressures, at different temperatures (in a pressure chamber, using nitrogen up to 100 bar). The transducer characteristics to be addressed in the work were:

   - The directivity of the transducer, $|D(\theta)|$, at selected frequencies in the 100 - 200 kHz band (covering the operational frequency frequency band of the transducer),
   - The time delay of the transducer, t^{tr}, at its operational frequency,
   - Linearity check of the transducer and the gas medium (in combination), at its operational frequency.

2. Carry out characterization measurements, up to 100 bar at 15 and 50/60 ^{o}C, for transducers made available for the project by USM manufacturers[20].

3. Work out proposed methods and procedures to do severity level testing of the transducers (methods to check that the transducer performance is preserved after the transducer has undergone a "severe treatment").

The first two of these three objectives are described here.

---

[20] One of the USM transducer types was characterised at 50 ^{o}C; the other two types were characterised at 60 ^{o}C.

This scope of work represents a limited investigation of transducer characteristics under pressure, as discussed further in Section 5.5. It has been selected from a proposed broader scope of work [5.2], including (in addition to the above mentioned characteristics) characterization under pressure of the electrical input impedance / admittance, Z_T, Y_T, the voltage source sensitivity, $|S_V|$, the transmit-receive voltage-voltage transfer function, $|H_{VV}|$ (cf. Section 5.2 for definitions).

In fact, some of these other transducer characteristics have been included and measured here, such as the electrical input impedance / admittance response, Z_T, Y_T (under pressure), the voltage source sensitivity, $|S_V|$ (at 1 atm. only), the diffraction time shift, t^{diff} (under pressure), the transmit-receive voltage-voltage transfer function, $|H_{VV}|$ (at 1 atm. only), and the bandwidth BW and the Q-factor (at 1 atm. only), cf. Sections 5.3.2 and 5.4.

5.1.3   Outline of work

As a background for understanding the importance of the various transducer characteristics and their implications for the USM measurement, an overview and discussion of such characteristics is given in Section 5.2, in addition to the discussion given in Section 3.10. These discussions may provide a basis for understanding the role of the transducer in the USM, including the influence of changing transducer characteristics with P, T, time, transducer distance, etc.; and also a basis for possible further improvements of USM technology. Measurement methods which have been developed and demonstrated for characterization and testing of USM transducers under pressure, at different temperatures, are described in Section 5.3. Some examples of non-classified measurement results are given in Section 5.4. A summary and discussion is given in Section 5.5.

Some of the transducer characteristics which are being used for correction of transit times are investigated experimentally over a range of pressures (P), temperatures (T) and transducer distances. This includes the transducer time delay t^{tr} and the diffraction time shift, t^{diff}. It is shown that the variations of these characteristics over the P, T and transducer distance ranges are large enough to significantly affect the USM measurement uncertainty, if they are not corrected for in the USM, cf. Section 5.4.

In addition, a number of other characteristics (which are not used directly for correction of transit times) are evaluated experimentally (either at 1 atm. or under pressure), like the impedance/admittance, directivity, source sensitivity, and the transmit-receive voltage-voltage transfer function, cf. Section 5.4.

The description given here is a condensed outline of ref. [5.1]. Note that due to confidentiality concerns, only some selected non-classified measurement results are given here, in addition to a discussion of the main general results from the work.

5.2   Important transducer characteristics and their relevance to USMs

In general, electrical and acoustical transducer characteristics of relevance for USM operation include:

- the electrical input impedance, $Z_T(f)$, or admittance, $Y_T(f)$, response,
- the linearity of the transducer and the gas medium[21],
- the voltage source sensitivity response (magnitude), $|S_V(f)|$,
- the directivity (or beam pattern) (magnitude), $|D(\theta)|$,
- the electromechanical efficiency of the transducer,
- the transducer time delay, t^{tr},
- the diffraction time shift[22] of the transducer, t^{diff},
- the transmit-receive voltage-voltage transfer function response (magnitude), $|H_{VV}(f)|$,
- the bandwidth, BW, and Q-factor, Q,
- reciprocity,
- the Δt-correction, Δt^{corr}.

In addition there are other transducer properties of considerable importance, such as

- the level of acoustic "cross-talk" in the spoolpiece (i.e., the direct noise generated by the transmitting transducer, coupled to and propagated through the spoolpiece, and acting as coherent (synchronous) noise, which can not be averaged out),
- the reproducibility of the transducer production series (electrical / acoustical characteristics),
- pressure and temperature stability of the transducers (electrical / acoustical characteristics),
- the lifetime stability and performance of the transducer (electrical / acoustical characteristics),
- robustness (with respect to vibration, etc.),
- the chemical resistence to relevant natural gas components.

Definitions of some of these transducer characteristics are given in the following, together with a brief discussion of their relevance to USMs and accurate gas metering.

- ***Electrical impedance*** and ***admittance***. The electrical input impedance and admittance of the transducer at the frequency f, $Z_T(f)$ and $Y_T(f)$, are defined as (using complex notation)

$$Z_T(f) \equiv \frac{V_{in}(f)}{I_{in}(f)} = R_T(f) + iX_T(f), \tag{5.1a}$$

$$Y_T(f) \equiv \frac{I_{in}(f)}{V_{in}(f)} = \frac{1}{Z_T(f)} = G_T(f) + iB_T(f), \tag{5.1b}$$

respectively. Here, R_T and X_T are the electrical input resistance and reactance, and G_T and B_T are the electrical input conductance and susceptance. V_{in} and I_{in} are the input voltage and current to the transmitting transducer, respectively.

---

[21] Large mechanical displacements in the transducer may cause non-linear effects *in the transducer* (saturation, distortion, generation of higher harmonics, etc.). High sound pressure levels in the gas may may cause similar non-linear effects *in the gas*. These two types of non-linearity may occur independently.

[22] The classification of t^{diff} as a transducer characteristic is discussed later in this section.

Z_T (or alternatively, Y_T) provides important information about the transducer, needed to operate the meter in an optimum way. Firstly, knowledge of Z_T is essential for matching of the USM electronics to the transducers. Unless the transducer is both reciprocal *and* operated in a reciprocal way (see below), Z_T influences on the Δt-correction, Δt^{corr}, which is used in the transit time correction, cf. Eq. (3.12). For relevant USM transducers, Z_T is likely to change significantly with gas temperature T (due to e.g. temperature dependent material properties), and to some extent also with pressure P (at least at "high" pressures, for which the coupling to the gas becomes more influent, and also at lower pressures for some transducer constructions) [5.1]. It may also change over time (drift, ageing). That means, in such cases, if Z_T varies with T, P and time, Δt^{corr} may also vary with P, T and time.

Secondly, Z_T influences on the time delay of the transducer cables, i.e. on $\Delta t^{el,cab}$ (cf. [5.1]), which is a part of the transit time correction, cf. Eqs. (3.12)-(3.14). Hence, knowledge of Z_T as a function of pressure and temperature is useful to enable more precise correction for the cable time delay in the measurement of transducer time delay.

Thirdly, the electrical admittance (or impedance) response is a useful function for transducer diagnostics (monitoring of possible changes in the transducer performance or construction, cf. [5.1]). It has also shown to be useful for testing of lifetime stability properties of the transducers, as well as testing of transducer reproducibility (cf. e.g. Section 5.4).

- *Linearity.* In general, non-linearity effects in the transducer or in the gas medium should be avoided for operation of USMs. Such effects may be introduced by driving the transducer with "high" voltages[23], giving either too large displacements in the transducer (transducer non-linearity), or too high sound pressure levels (SPL) in the gas (gas non-linearity).

The operation of the transducers *and* the gas medium in their linear regions is important, for several reasons. Firstly, linearity is a condition for reciprocity. Reciprocal or close-to-reciprocal operation of the electronics/tranducers system is preferred, to keep Δt^{corr} as small as possible. In such cases the change of Δt^{corr} with P and T will be less than in non-reciprocal systems, which may have consequences for the measurement uncertainty of the USM, if these changes of Δt^{corr} are not corrected for.

Secondly, non-linarity distorts the signal form and influences on the zero crossings by introducing asymmetry in the signal, giving timing errors.

Thirdly, non-linearity in the gas may influence on the directivity (broadening the main lobe, increasing the side lobe level), and thus may influence on the diffraction time shift, t^{diff}, which again influences on the electronics/cable/transducer/diffraction time delay, t^{eltr}, which is used for transit time correction, cf. Eqs. (3.12)-(3.14).

- *Voltage source sensitivity.* The magnitude of the voltage source sensitivity at the frequency f, $|S_V(f)|$, is defined as

$$\left| S_V(f) \right| \equiv \left| \frac{P_{1m}(f)}{V_{in}(f)} \right|, \tag{5.2}$$

---

[23] Whether a given excitation voltage is "high" or not, depends on the transducer at hand.

where $P_{1m}(f)$ is the axial sound pressure at a reference distance of 1 m from the transducer, and $V_{in}(f)$ is the input voltage to the transducer. $|S_V(f)|$ determines the sound pressure level (SPL) radiated by the transducer in the gas at a given axial distance and frequency, for a given voltage input, and how SPL varies with the frequency at a constant axial distance.

In general one wishes to operate the USM with a high SPL relative to the noise level *in the gas*, so that a high signal-to-noise ratio (SNR) is achieved for *gas borne noise*. Noise sources in this context are e.g.:

- Pressure regulation valves (radiating incoherent (non-synchronous) noise, which can be re-duced e.g. by signal averaging ("stacking")),

- Turbulent flow velocity fluctuations (at high flow velocities).

On the other hand, one does not wish to operate the USM with such a high SPL that nonlinearity in the gas or the transducer (as transmitter) is introduced (see above). To control the SPL radiated by the transducer, the voltage source sensitivity is a common transducer characteristic. For relevant USM transducers, $|S_V(f)|$ is likely to change with pressure, temperature and gas composition.

Measurement of $|S_V(f)|$ is also very useful for testing of lifetime stability properties of the transducers, as well as testing of transducer reproducibility (cf. e.g. Section 5.4).

● *Directivity.* For a transducer radiating an axisymmetric sound field, the magnitude of the trans-ducer directivity function at the frequency f, $|D(\theta)|$, is defined as

$$|D(\theta)| \equiv \left| \frac{P(\theta)}{P_{axis}} \right|,\tag{5.3}$$

where θ is the angle relative to the acoustical axis of the transducer, $P(\theta)$ is the sound pressure in the observation point (r,θ) (where r is the distance from the centre of the transducer front), and P_{axis} is the axial ($\theta = 0$) sound pressure at the distance r.

From $|D(\theta)|$ the beam width of the main lobe radiated by the transducer, and the angular position and the level of the side lobes (relative to the main lobe) can be determined. It is usually assumed that the transmitting and receiving directivity of a transducer are equal. $|D(\theta)|$ therefore determines / in-fluences on:

- The acoustic *beam width* at the opposite transducer and transducer cavity. Usually the -3 dB (half power) beamwidth is specified. In general, a narrow main lobe (high directivity, narrow beamwidth) is of interest. That will contribute to reduce possible phase shift in the received signal due to unwanted interference effects in the transducer cavity (acting as coherent noise). A phase shift causes timing error. On the other hand, the main lobe should be sufficiently broad to avoid beam drift effects at high velocities.

- The *side lobe level* (relative to the main lobe) and the acoustic *reverberation* in the pipe. High sidelobes and reverberation may potentially cause phase shift (and thus timing error) in the re-ceived signal, due to interference of the measurement signal with unwanted echoes from the pipe wall and transducer cavity (acting as coherent noise). Such interference is very difficult to detect or observe under operation. A low side lobe level is thus desired.

- The sensitivity to *pressure regulation valve noise*, influencing through the main lobe and the side lobes (angular position and level). A narrow main lobe and low side lobe level (relative to the main lobe) is thus desired.

- The *received signal level.* High directivity (narrow beamwidth, low side lobe level) gives a stronger signal, a more efficient transducer, and a better signal-to-noise ratio (SNR).

- The *diffraction time shift*, t^{diff}, is closely related to the transducer directivity, and thus change if the directivity changes (such as with pressure, temperature, gas composition or time).

- Whether the *mechanical axis* (often used as a basis for mounting the transducer) is the same as the acoustical axis (which is the desired property).

To control such factors, the directivity $|D(\theta)|$ is an important characteristic. For relevant USM transducers, the directivity (beam width and side lobe level) is likely to change with gas composition and temperature, and to some extent also with pressure [5.1].

Measurement of $|D(\theta)|$ is also very useful for testing of lifetime stability properties of the transducers, as well as testing of transducer reproducibility (cf. e.g. Section 5.4).

• **Transducer time delay**. The transducer time delay, t^{tr}, is defined in Section 3.8[24], and accounts for the time used for the signal to propagate in the transducer. t^{tr} is a parameter involved in the correction of measured transit times of current USMs (cf. Eqs. (3.12)-(3.14)), to achieve high accuracy of the USM measurement. t^{tr} will depend on whether time detection is made in the transient start part of the signal or in the stationary part, cf. Sections 3.7-3.8.

In practice, t^{tr} tends to change with temperature, T (due to temperature dependent materials used in the transducer), and may also for some transducer constructions change with pressure, P, cf. Fig. 5.4. In addition, t^{tr} depends on transducer type, and may change over time. These changes make the transit time correction $t_{1i,0}^{eltr}$ dependent on P, T and time, relative to the dry calibration value, cf. Eqs. (3.12)-(3.14).

The main questions are then: (1) whether the effects of changes in $t_{1i,0}^{eltr}$ with P, T and time are large enough to influence on the USM measurement uncertainty to a significant degree; and if they are: (2) whether such changes of $t_{1i,0}^{eltr}$ with P, T and time are accounted (corrected) for or not, in the time corrections of the USM. The influence of deviation in $t_{1i,0}^{eltr}$ from the dry calibration value used in the USM can be analysed using the uncertainty model described in Chapter 7. The influence of measured systematic changes in t^{tr} with P and T is discussed in Section 5.4.

• **Diffraction time shift**. The diffraction time shift, t^{diff}, is defined in Section 3.8[25], and accounts for the time shift due to diffraction effects. t^{diff} is introduced as a direct consequence of the plane-wave description of sound propagation in the gas, which is used in the basic theory of USMs, cf. Section 3.7, but which is not a correct description. t^{diff} represents a correction to the plane-wave description.

---

[24] In Section 3.8 t^{tr} is denoted $t_{1i,0}^{tr}$ for upstream propagation (or $t_{2i,0}^{tr}$, for downstream propagation).

[25] In Section 3.8, t^{diff} is denoted $t_{1i,0}^{diff}$ for upstream propagation (or $t_{2i,0}^{diff}$, for downstream propagation).

Consequently, t^{diff} is closely related to the directivity of the transmitting transducer, $|D(\theta)|$, and it may be considered as a property of the transmitting transducer[26]. t^{diff} is a parameter involved in the correction of measured transit times of current USMs (cf. Eqs. (3.12)-(3.14)), to achieve high accuracy of the USM measurement. t^{diff} will depend on whether time detection is made in the transient start part of the signal or in the stationary part, cf. Sections 3.7-3.8.

In practice, t^{diff} tends to change somewhat with temperature, T, and pressure, P, cf. Fig. 5.5, such as e.g. due to changes of the directivity $|D(\theta)|$ with P and T. In addition, t^{diff} depends on transducer type, and may change over time. Equally or more important is the systematic change of t^{diff} with distance between the transducers (i.e. with path length, or USM size), cf. Fig. 5.5. These changes make the transit time correction $t_{1i,0}^{eltr}$ dependent on P, T, time and especially on transducer distance, relative to the dry calibration value, cf. Eqs. (3.12)-(3.14).

Since t^{diff} varies systematically with transducer distance (cf. Fig. 5.5), this parameter is important e.g. in connection with exchange of transducers in the USM (individual transducers, or pair of transducers). If for instance a pair of transducers to be mounted in the USM is not dry calibrated at the same distance as the "old" pair of transducers to be replaced, and the difference in t^{diff} for the two distances is not corrected for, a systematic timing error will result for the acoustic path in question.

The main questions are then: (1) whether the effects of changes in $t_{1i,0}^{eltr}$ with P, T, time and transducer distance are large enough to influence in the USM measurement uncertainty to a significant degree; and if they are: (2) whether such changes of $t_{1i,0}^{eltr}$ with P, T time and transducer distance are accounted (corrected) for or not, in the time corrections of the USM. The influence of deviation in $t_{1i,0}^{eltr}$ from the dry calibration value used in the USM can be analysed using the uncertainty model described in Chapter 7. The influence of measured systematic changes in t^{diff} with P and T is discussed in Section 5.4.

● *Transmit-receive voltage-voltage transfer function[27].* The magnitude of the transmit-receive voltage-voltage transfer function at the frequency f is defined as

---

[26] It may possibly seem a bit odd that the "diffraction time shift" t^{diff}, is classified as a characteristic of the transmitting transducer, especially since t^{diff} varies with the transducer distance. The reason for this classification is that t^{diff} is closely related to the directivity $|D(\theta)|$ of the transmitting transducer. It is not a property of the gas medium, although it depends on the gas sound velocity, and it is not a property of the receiving transducer, although it depends on the area of the front face of the receiving transducer. In particular, for a given transducer distance, frequency and transducer radius, t^{diff} is determined by the vibration pattern of the transmitting transducer's front surface, and not by the receiving transducer. Hence, it is natural to associate t^{diff} with the transmitting transducer, in accordance with normal practice in acoustics.

[27] As described in Section 3.7, another transfer function than H_{VV} may possibly be of interest for specific meters (depending on whether current or voltage signals are used for time detection). These may be the current-current transfer function H_{II}, the current-voltage transfer function H_{IV}, or the voltage-current transfer function H_{VI}. However, by knowing the electrical output impedance of the transmitting electronics, and the electrical input impedance of the receiving electronics, $|H_{II}|$, $|H_{IV}|$ and $|H_{VI}|$ can in principle all be calculated from $|H_{VV}|$ (not described here). Therefore, to simplify and limit the discussion, only $|H_{VV}|$ is discussed here.

$$|H_{VV}(f)| \equiv \left| \frac{V_{out}^{1m}(f)}{V_{in}(f)} \right| , \tag{5.4}$$

where $V_{out}^{1m}(f)$ is the open-circuit output voltage at the receiving transducer located at a reference axial distance of 1 m from the transducer, and $V_{in}(f)$ is the input voltage to the transmitting transducer. $|H_{VV}(f)|$ determines the actual output voltage at the receiving transducer at a given distance and frequency, for a given input voltage to the transmitting transducer.

In general one wishes to operate the USM with a high output voltage relative to the level of structure (pipe) borne and electromagnetic noise, so that a high signal-to-noise ratio (SNR) is achieved. Noise sources in this context are e.g.

  - Electromagnetic noise from the electrical network and the electronics unit (incoherent (non-synchronous) noise, which can be reduced e.g. by signal averaging ("stacking")),

  - Structure (pipe) borne noise from pressure regulation valves, etc. (acting as incoherent (non-synchronous) noise, which can be reduced e.g. by signal averaging ("stacking")),

  - Acoustic cross-talk in the spoolpiece (i.e., the direct noise generated by the transmitting transducer, coupled to and propagated through the spoolpiece, and acting as coherent (synchronous) noise, which can not be averaged out).

On the other hand, one does not wish to operate the USM with such high voltages that nonlinearity in the gas or transducer (as transmitter and receiver) is introduced (see above). To control such factors, the transfer function $|H_{VV}(f)|$ and its frequency response are common and useful transducer characteristics. For relevant USM transducers, the transfer function is likely to change with pressure, temperature and gas composition [5.1].

Measurement of $|H_{VV}(f)|$ is also very useful for testing of lifetime stability properties of the transducers, as well as testing of transducer reproducibility.

● **Bandwidth** and **Q-factor**. The bandwidth *(BW)* and the Q-factor *(Q)* of the transducer are measures of the frequency response of the transducer. There are several ways to define those, depending on which transducer function that is used as the basis for the definitions (electrical impedance, source sensitivity or transmit-receive transfer function). For USM operation, a useful approach may be to define these quantities from the magnitude of the transmit-receive voltage-voltage transfer function $|H_{VV}(\omega)|$, giving

$$BW \equiv f_{+3dB} - f_{-3dB} , \qquad Q \equiv \frac{f_{max}}{f_{+3dB} - f_{-3dB}} , \tag{5.5}$$

respectively, where f_{max} is the frequency of the maximum of the transfer function $|H_{VV}(\omega)|$, and f_{+3dB} and f_{-3dB} are the two frequencies at which $|H_{VV}(\omega)|$ has decreased 3 dB relative to the maximum value at f_{max}, and where $f_{+3dB} > f_{-3dB}$. In this definition, *BW* and *Q* are defined for combined transmit and receive operation (such as e.g. for a transducer pair, or for a single transducer used in transmit-receive mode, applying a reflector).

The *BW* and *Q* of the USM transducers influence strongly on the

  - Noise robustness of the USM, such as with respect to pressure regulation valves (by frequency filtering),

50

- Signal form (rise time and "ringing"), which influences on the the signal detection (period identification) and the transit time determination. For such purposes, a low Q-factor is in general of interest.

- **Reciprocity.** For an acoustic path of the USM to be reciprocal, two conditions have to be fulfilled:

  - Firstly, the transducer and the electronics are to be reciprocal by *themselves*.

  - Secondly, the combined transducer and electronics *system* (transmit and receive) has to be reciprocal (at zero flow conditions). That is, the electronics and transducers are to be *operated* in a reciprocal manner [5.3].

Whether the combined transducer and electronics system is operated in a reciprocal manner or not, concerns the relationships between the electrical impedance of the transducer, Z_T, and the electrical impedance of the electronics. That is, the ratio of the output impedance of the transmiting electronics to the input impedance of the transducer, and the ratio of the output impedance of the transducer to the input impedance of the receiving electronics. Certain impedance ratios have to be fulfilled (not described here).

Reciprocal or close-to-reciprocal operation of the tranducers is definitely to be preferred, to keep Δt^{corr} and its variation with pressure P and temperature T as small as possible. If the electronics and the transducers of acoustic path no. i were reciprocal, and - in addition - the measurement system was *operated* in a reciprocal way, the Δt-correction would be expected to be zero, $\Delta t^{corr} = 0$. That means, the electronics/cable/transducer/diffraction delays of path no. i were then expected to be equal for upwards and downwards propagation, $t_{1i,0}^{eltr} = t_{2i,0}^{eltr}$. This would be valid at all frequencies, temperatures, pressures and flow velocities (including zero flow reading at zero flow). Hence, in this case no Δt-correction would be expected to be needed.

In practice, however, reciprocity is rarely fulfilled completely under all conditions of operation, and the Δt-correction is not zero in general, $\Delta t^{corr} \neq 0$. Compromises may have to be made in the electronics design and the electrical matching to the transducers. Very important in this context is also the variation of the electrical impedance Z_T of the transducer with temperature T (and possibly pressure P) one often finds in practice (cf. Section 5.4). Consequently, even though close-to-reciprocal operation may be achieved at certain conditions, such variation of Z_T with P and T may lead to violation of reciprocity in certain ranges of P and T. The main question is then whether Δt^{corr} becomes so large that it affects the USM measurement uncertainty (see below).

- **Δt-correction.** The Δt-correction, Δt^{corr}, is defined in Section 3.8[28], and accounts for the difference between the upstream and downstream electronics/cable/transducer/diffraction time delays, cf. Eq. (3.13). It is usually measured in a dry calibration procedure. Δt^{corr} is an important parameter used in current USMs for correction of the measured transit times (cf. Eq. (3.12)), to achieve as-close-to-zero flow reading at no-flow conditions as possible. This parameter becomes increasingly important at low flow velocities.

As discussed in connection with the electrical impedance and reciprocity above, Δt^{corr} mauy change with P, T and time if the transducer impedance Z_T changes with with P, T and time. The main ques-

---

[28] In Section 3.8, Δt^{corr} is denoted $\Delta t_{i,0}^{corr}$.

tions are then: (1) whether the effects of changes in Δt^{corr} with *P*, *T* and time are large enough to influence in the USM measurement uncertainty to a significant degree; and if they are: (2) whether such changes of Δt^{corr} with *P*, *T* and time are accounted (corrected) for or not, in the time corrections of the USM. The influence of deviation in Δt^{corr} from the dry calibration value used in the USM can be analysed using the uncertainty model described in Chapter 7.

5.3   Characterization and testing methods under pressure

At atmospheric conditions, well defined methods and procedures are available for characterising transducers. In the present work some measurement methods and procedures have been developed and demonstrated for transducer characterization and testing in a 200 bar pressure chamber, for characeristics like the electrical impedance/admittance, linearity, directivity, transducer time delay and diffraction time shift.

5.3.1   Measurement facilities

To carry out ultrasonic measurements under relatively controlled temperature and pressure conditions, a 200 bar pressure chamber has been acquired by Christian Michelsen Research (CMR), suitable for non hazardous gases. A photograph and a principle sketch of the chamber is shown in Fig. 5.1. The 220 litre pressure chamber is basically made of a 24" pipe with wall thickness of about 34 mm, and is certified for pressures up to 200 bar. The inner diameter is 53 cm, and the maximum inner length is 130 cm. The inner walls of the tank have been covered with an acoustic damping material to reduce the acoustic reflections from the wall and thus improve the signal to noise ratio (SNR) related to coherent noise. The pressure tank is located in a water bath for temperature stabilisation. A 6 kW heater and a circulation pump provide a uniform heating of the water.

The pressure and temperature are measured with specified (and calibratied) uncertainty of ±0.3 bar and ±0.025 K, respectively. With respect to pressure and temperature stabilization, far better precision is achieved. For a given temperature, for instance, the pressure may be kept constant to within 0.1 bar over a period of several hours. With respect to temperature, the variation of *T* over a measurment cycle (15-20 s) was typically 0.002 K or less, for the measurement of transducer delay.

The chamber is equipped with a precision electrically controlled rotary and linear positioning system (Ealing Electro-optics) for setting transducer angle and distance, with stepper motors and remote operation control. The rotary stage is used for directivity measurements. The linear stage is used for the time delay and linearity measurements. A photograph of the system mounted in the pressure chamber is shown in Fig. 5.2.

For measurement of transducer characteristics in air at 1 atm., and for admittance measurements in the pressure chamber, a PC-based logging and analysis software system developed at CMR, *TransLog* and *TransDoc,* is used [5.4], [5.5].

For measurement of the transducer directivity, $|D(\theta)|$, in the pressure chamber, a PC program *BeamPatt* has been developed. This Windows program enables the user to interactively set up the measurement system, and then start an automatic measurement cycle. Measurement data are logged to a data file for later processing. Directivity measurements are made using a 3 mm diameter microphone,
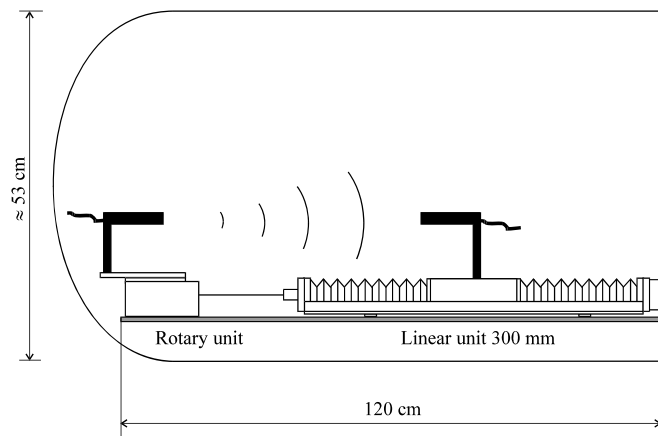
Fig. 5.1   Photograph and principle sketch of the 200 bar pressure chamber, with ultrasonic transducers and the Ealing positioning system. The dimensions given are inner dimensions.
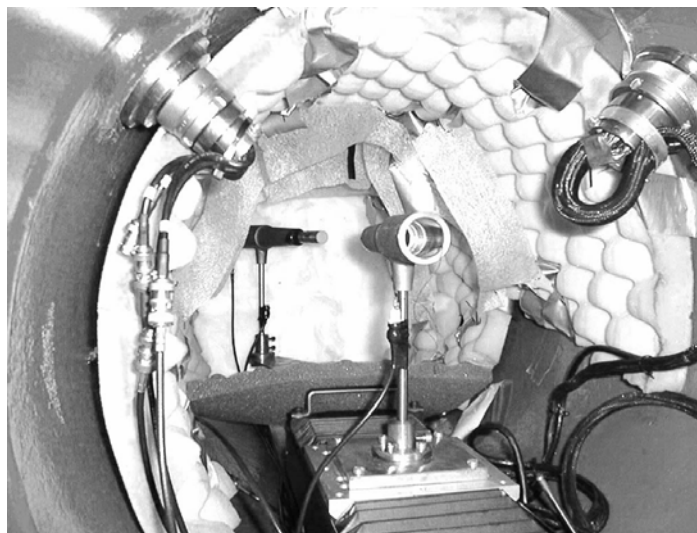
Fig. 5.2   Photograph of the Ealing positioning system mounted in the 200 bar pressure chamber, with ultrasonic transducers.

designed for use at elevated pressures. Calibration data of the microphone response were available for atmospheric conditions, but not for elevated pressures (however that is not important for the directivity measurements).

5.3.2   Measurement methods and procedures

The following transducer characteristics have been measured [5.1]:

- The input electrical impedance response, $Z_T(f)$, and admittance response, $Y_T(f)$, in air at 1 atm. and room temperature, and in N_2 at 3-100 bar and 15 and 50/60 °C,
- Linearity check of the transducer and the gas medium (in combination), at its operational frequency, in N_2 at 3-100 bar and 15 and 50/60 °C
- The voltage source sensitivity response, $|S_V(f)|$, in air at 1 atm. and room temperature,
- The directivity of the transducer, $|D(\theta)|$, at selected frequencies in the frequency band around its operational frequency, in N_2 at 3-100 bar and 15 and 50/60 °C,
- The delay time of the transducer, t^{tr}, at its operational frequency, in N_2 at 3-100 bar and 15 and 50/60 °C,
- The diffraction time shift of the transducer, t^{diff}, at its operational frequency, in N_2 at 3-100 bar and 15 and 50/60 °C,
- The transmit-receive voltage-voltage transfer function response, $|H_{VV}(f)|$, in air at 1 atm. and room temperature,
- The bandwidth, BW, and Q-factor, Q, in air at 1 atm. and room temperature.

The methods used for measurement of the various transducer characteristics are briefly described in the following. Uncertainty considerations have been given for those characterization functions which were specified in the scope of work (cf. Section 5.1.2), i.e., the directivity, transducer time delay and the linearity measurements [5.1].

- ***Electrical impedance*** and ***admittance***. The electrical input impedance response, $Z_T(f)$, and admittance response, $Y_T(f)$, have been measured in the pressure chamber using the *TransLog / TransDoc* system. The measurements are made in N_2 over the pressure range 3-100 bar[29], at two temperatures, 15 and 50/60 °C, over a frequency band which covers well the operational signal frequency specified for each transducer.

The transducer is located in the chamber, and coupled to a Hewlett Packard 4192A Impedance Analyzer via a 6 m coaxial cable, including a coaxial connector for penetrating the chamber wall. The Impedance Analyzer is controlled by the *TransLog* program. The measurements setup is the same as used for the directivity measurements (see below), with the microphone still present (for practical reasons), but not active.

The effective inductance and capacitance of the cable and connector have been measured to be about 300 nH/m and 102 pF/m, respectively. The influence of the cable/connector on the admittance measurements has been checked by measuring the transducer admittance of a transducer with and without the cable/connector. A small but nearly negligible influence of the cable/connector has been found.

- ***Linearity check***. With respect to instrumentation, signal frequency, etc., the measurement set-up for the amplitude linearity check is the same as used for the transducer time delay measurements (see

---

[29] $Z_T(f)$ and $Y_T(f)$ have also been measured in air at 1 atm and room temperature conditions, for check purposes.

below). The measurements should be made with a representative relevant electrical loading of the transducers, or the effects of a loading should be checked.

For each *P-T* point, the pressure is kept constant to within 0.1 bar over the linearity measurement cycle (10 excitation voltages). The temperature *T* is measured 2 times for each excitation voltage (resulting in one data file). The variation of *T* over this period (15-20 s) is typically 0.002 K or less. The variation of *T* over the linearity measurement cycle (10 excitation voltages) is typically 0.004 – 0.02 K or less.

For a given *P-T* point, the linearity measurements is taken in connection with (after) the time delay measurements. The linearity measurement (see above) is started at the highest driving voltage investigated, V_{max} (which is either equal to or slightly lower than the maximum driving voltage specified by the manufacturer). The driving voltage is then reduced successively from $0.9 \cdot V_{max}$ to $0.1 \cdot V_{max}$ (20 dB down)[30], with averaging over 50 "shots" for each voltage setting.

An uncertainty analysis suggest that the relative expanded uncertainty of the linearity measurement may be about 2 % (0.2 dB) (at a 95 % confidence level), as a tentative and preliminary estimate (on lack of reliable data for some of the input uncertainties).

• ***Voltage source sensitivity.*** The magnitude of the voltage source sensitivity response, $|S_V(\omega)|$, has been measured only in air at 1 atm. and room temperature. These measurements were made outside the pressure chamber using a separate measurement setup, the *TransLog / TransDoc* system, used for testing of transducers in air.

The measurements were made using a transducer and a microphone, mounted at a distance of typically 30 cm, which for all transducers investigated here should be well in the far field. The transducer is excited with long voltage bursts at a given repetition rate and amplitude, and the received output voltage amplitude is measured by an analog peak detector in the stationary part of the signal. Measurements were made over a relatively wide frequency band around the operational frequency of the transducers. The measurements are (in software) corrected for the amplifier gain used, corrected for the response of the B&K 4138 microphone used, corrected for absorption in air at the relevant environmental conditions, and extrapolated spherically to the reference distance 1 m from the transducer (cf. Eq. (5.2)).

Similar source sensitivity measurements at elevated pressures would require use of a standard microphone which has been calibrated at such pressures and temperatures, and over the required frequency band. Such measurements have not been performed yet.

• ***Directivity.*** The measurement setup used for the directivity measurements in the pressure chamber consists of the Ealing positioning system (cf. Figs. 5.1 and 5.2) with the transducer mounted on the rotary stage at one end, and the 3 mm. diam. microphone mounted on the linear stage, where the distance between the transducer and the microphone can be varied. For the directivity measurements a transducer-microphone distance of typically 30 cm has been used, which for all transducers investigated here should be well into the far field. The transducer and the microphone are connected to the transmitting and receiving equipment via two 6 m coaxial cables and coaxial connectors. The correct alignment of the transducers and microphone on the transducer's acoustic axis is important.

The transducer is excited using a relatively long voltage burst delivered by a function generator via a transmitting amplifier. A digital oscilloscope is used to measure the output voltage signal received

---

[30] It is realised that a larger dynamic range should have been used, such as e.g. 30 or 40 dB.

by the microphone. The signal generator, oscilloscope and Ealing rotary stage are controlled by the *BeamPatt* program. The receiver signal is led to the oscilloscope via a signal conditioner, a measuring amplifier and a filter. For each frequency, a sufficiently low excitation voltage V_{in} is used to reduce apparent non-linear effects on the signal (such as distorted, asymmetric signals). This point turned out to be important. For this reason, the use of different $|V_{in}|$ at different frequencies was required for certain transducers.

The measurements of $|D(\theta)|$ are taken for a few (5 or 6) frequencies in a frequency band $\pm$(15-30 kHz) around the operational signal frequency specified for each transducer. For a given *P-T* point, $|D(\theta)|$ is measured from -25° to +25°, at an angular resolution[31] of 0.5°. The pressure and temperature in the gas is measured for each directivity measurement. $|D(\theta)|$ is measured in a single plane, which will not be sufficient for transducers showing strongly non-axisymmetric radiation.

The uncertainty of the directivity measurements is difficult to estimate precisely due to an unknown level of coherent (synchronous) acoustic reverberation in the pressure chamber (due to side lobe radiation, etc.), which may interfere with the measurement signal. An uncertainty analysis combined with comparisons with free-field directivity measurements made outside the chamber, suggest that the expanded uncertainty of the directivity measurements in the pressure chamber may tentatively be of the order of 0.1 dB around the top of the main lobe, and less than 1-2 dB at the -15 dB level (rel. to the main lobe).

- **Transducer time delay**. The measurement set-up used for measurement of the transducer time delay t^{tr} in the pressure chamber consists of (transmit and receive) electronics and cables, a transducer mounted in its holder, and an acoustic reflector. The use of a reflector is chosen to enable characterization of individual transducers (not pairs). With the electronics and measurement set-up developed under this project, the goal is to measure the transducer time delay t^{tr} itself, essentially without the delay of the electronics (transmit and receive), the 6 m coaxial cable, the coaxial connector used for pressure chamber penetration, and the diffraction time shift, t^{diff}. The basic measurement is illustrated schematically in Fig. 5.3, and may be briefly explained as follows.
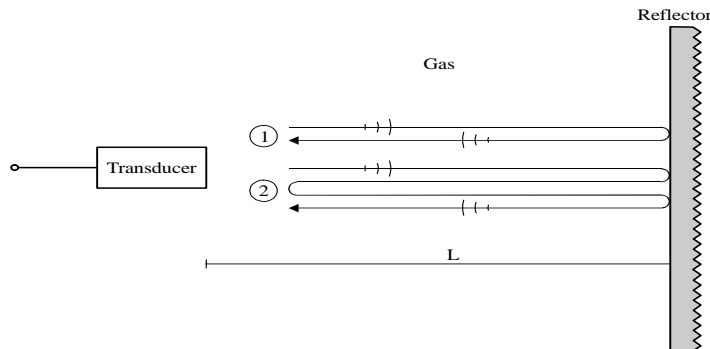
Fig. 5.3. Sketch of the measurement principle used for transducer time delay measurements in the 200 bar pressure chamber.

A signal generator emits 60 (or 70, for some transducers) periods of a voltage sine burst at the chosen carrier frequency of the transducer under test. This voltage signal is led via a power amplifier to the transducer. An electronic switch is being used to disconnect the transmitting electronics during signal reception. The transmitted sound pressure pulse is reflected at the reflector at a distance from the

---

[31] With the present set-up, better angular resolution could easily have been used, down to 0.01°.

transducer. Both the first and the second reflected signals are used to derive an estimate of the transducer delay. The reflector is large so that the diffraction correction at the reflector is neglected here.

The transducer-reflector distances are chosen as a compromise between (1) transducer "ringdown" (to improve the SNR related to coherent "ringdown" noise), (2) the diffraction correction (one wants to work on a smooth part of the diffraction time shift curve, cf. Fig. 5.5), and (3) the diameter of the reflector to function as an ideal and infinitely large reflector (to a good approximation). Different measurement distances L_1, L_2 and L_3 have been used to enable a check of the consistency of the results obtained for the transducer time delay.

The transducer time delay measurements are taken for the operational signal frequency specified for each transducer. The signal traces are sampled using a Le Croy 9310CL digital oscilloscope, usually at a sampling rate of 20 MHz (50 ns time resolution), and with 8 bit amplitude resolution. For each signal trace measurement, the gain was adjusted so that the main measurement signal (reflection no. 1) occupied about 75 % of the oscilloscopes's dynamic range, or more. With this method, both the excitation voltage signal fed to the transducer and the two signals returned from the reflector are recorded on the same signal trace.

The two time differences between (1) the excitation signal and reflection no. 1, t_1^{meas}, and (2) the excitation signal and reflection no. 2, t_2^{meas}, are measured.   From these two time measurements, and an estimate of the time delay of the coaxial cable/connector, t^{cable}, the transducer time delay t^{tr} was determined as

$$t^{tr} = 2t_1^{meas} - t_2^{meas} - t^{cable} \quad . \tag{5.7}$$

Estimation of the cable time delay, t^{cable}, is made on basis of measurements of Z_T, the electrical input impedance of the transducer, and a distributed-elements transmission-line model for the coaxial cable. Estimated cable time delays are in the range 20-210 ns for the 6 m cable (depends essentially on transducer type and temperature).

The simplifications and assumptions used to derive Eq. (5.7) are discussed in Ref. [5.1]. Among others, it is assumed that on reflection at the transducer (which is relatively small compared to the acoustic beamwidth), the transducer acts essentially as a new source of sound. The simplification is thus used that the diffraction time shift for reflection no. 2 is approximately equal to the diffraction time shift for reflection no. 1.

The uncertainty of the transducer time delay measurements as given by Eq. (5.7) is difficult to estimate precisely, mainly due to the above mentioned assumption related to the diffraction correction on reflection at the transducer which is incorporated in the present method. The uncertainty of this assumption is not known at present, and determination of that will require accurate experimental determination of the diffraction correction effects of the transducers. A detailed uncertainty analysis of the measurement method has been made, but the lack of reliable input uncertainty for this assumption (which is expected to dominate the measurement uncertainty) prohibits a reliable estimate for the uncertainty of the t^{tr} measurement. As a tentative and preliminary figure, it is expected that t^{tr} is determined here with an expanded uncertainty of a few hundred ns. However, further work is required to determine the uncertainty of the above mentioned assumption.

It should be noted that in the present work, a transducer time delay t^{tr} is measured which corresponds to the *phase* of the appropriate *transducer transfer function*[32]. t^{tr} is then measured by using the transit time detected in the stationary ("continuous wave", or CW) part of the signal, and may be referred to as the "CW transducer time delay"[33].

- ***Diffraction time shift***. An estimate of the diffraction time shift t^{diff} has been obtained here as follows, for each pressure-temperature point over the range 3-100 bar and 15 to 50/60 ^{o}C.

From the measured transducer directivity $|D(\theta)|$ in the pressure chamber, an "effective radius", a_{eff}, of the transducer was estimated by an adaptation of the "plane piston model" for transducer radiation [5.6] to the main lobe of the measured directivity, $|D(\theta)|$[34]. The estimated "effective radius" a_{eff} of the transducer was then used as input to a numerical calculation of the diffraction correction (H^{diff}) and the diffraction time delay (t^{diff}) of a transducer vibrating as a plane piston vibrating in an infinitely large and rigid baffle (the "plane piston model"). These were calculated by [5.7] (using complex notation)

$$H^{diff} \equiv \frac{<p>}{p^{plane}} = 1 - \frac{4}{\pi} \int_0^{\pi/2} e^{\left[ikz\left(1-\sqrt{1+\frac{4a_{eff}^2}{z^2}cos^2\theta}\right)\right]} sin^2\theta\, d\theta\,, \qquad t^{diff} \equiv -\frac{1}{2\pi f} tan^{-1}\left[\frac{Im(H^{diff})}{Re(H^{diff})}\right], \quad (5.8)$$

respectively, where z is the transducer distance, $k = 2\pi f/c$ is the acoustic wavenumber, *f* is the frequency, *c* is the sound velocity in the gas, and $Re(\cdot)$ and $Im(\cdot)$ are the real and imaginary parts of $(\cdot)$. θ is an integration variable. Here, $<p>$ is the free-field sound pressure in the gas, integrated (averaged) over a circular "measurement area" corresponding to the receiving piston transducer front (in absence of the receiving transducer). p^{plane} is the plane wave sound pressure in the gas at the centre point of the receiving transducer (in absence of the receiving transducer).

It should be noted that since none of the transducers actually vibrate as a plane piston mounted in a rigid and infinitely large baffle, the present method is expected to give only a rough estimate of t^{diff}. A more accurate estimate of t^{diff} would involve a direct measurement of the phase of the diffraction

---

[32] Here, the "transducer transfer function" refers to a combined transmitting and receiving transducer transfer function, defined as the product of two transfer functions: (1) the voltage at the transmitting transducer input **-to-** the plane-wave sound pressure in the gas at the centre point of the transmitting transducer front; and (2) the free-field sound pressure in the gas, integrated over a circular "measurement area" corresponding to the receiving transducer front (in absence of the receiving transducer) **-to-** the open-circuit voltage at the receiving transducer output, cf. the definition of t^{tr} in Section 3.8.

[33] One could alternatively measure a transducer time delay t^{tr} associated with a zero crossing in the transient start of the signal, cf. section 3.7. The "CW transducer time delay" and the "transient start transducer time delay" are not necessarily equal, and may show different pressure and temperature characteristics.

[34] Note that the use of the "plane piston model" represents a simplification. The measured directivity results discussed in Section 5.4 show that none of the transducers actually vibrate as a plane piston mounted in an infinitely large and rigid baffle, which is also to be expected, since this model is a relatively idealised one (although very useful and extensively applied). In practice, in the estimation of a_{eff} (i.e. the adaptation of the "plane piston model" to the measured directivity), a relatively good match could be obtained for the main lobe (not shown here). For the side lobes, however, the agreement is in general not so good, and for some transducers the match is very poor.

correction H^{diff}, which is a more complicated measurement than the directivity measurement made here. Such an improved measurement of t^{diff} should be considered in the future.

Note that the estimate of the diffraction time shift t^{diff} obtained by Eq. (5.8) corresponds to the *phase* of the diffraction correction H^{diff}. This estimate of t^{diff} is therefore to be associated with the stationary ("continuous wave", or CW) part of the signal, and may be referred to as the "CW diffraction time shift" [35].

● ***Transmit-receive voltage-voltage transfer function***. The magnitude of the voltage-voltage transfer function response, $|H_{VV}(f)|$, has been measured only in air at 1 atm. and room temperature. The measurements were made using the *TransLog / TransDoc* system, used for testing of transducers in air.

Two transducers of the same type are used for these measurements. The transducers are mounted at a distance of typically 30 cm, which for all transducers investigated here should be well in the far field. The measurements were made over a relatively wide frequency band around the operational frequency of the transducers. The transmitting transducer is excited with long voltage bursts at a given repetition rate and amplitude. The output voltage amplitude received by the receiving transducer is measured by an analog peak detector in the stationary part of the signal. The measurements are (in software) corrected for the amplifier gain used, corrected for non-open-circuit electrical termination of the receiving transducer, corrected for absorption in air at the relevant environmental conditions, and extrapolated spherically to the reference distance 1 m from the transmitting transducer.

Similar transfer function measurements in the pressure chamber and under elevated pressures and different temperatures can be made, either by using a reflector (for individual transducers), or for a pair of transducers. Such measurements have not been performed yet.

● ***Bandwidth*** and ***Q-factor***. The bandwidth, *BW*, and Q-factor, *Q*, are measured from the magnitude of the voltage-voltage transfer function response, $|H_{VV}(f)|$, according to Eqs. (5.5).

5.4   Examples of measurement results

Characterization measurements have been carried out in air at 1 atm. and room temperature (outside the pressure chamber), and in the pressure chamber with nitrogen, up to 100 bar at 15 and 50/60 ^{o}C. Measurements have been made for a limited amount of transducer samples, kindly made available for the project by two USM manufacturers, Daniel Flow Products, UK/USA, and Kongsberg Offshore AS (KOS), Norway. Three different transducer types and two samples of each type were characterised and tested; in total six transducers. The transducer characteristics which were measured are listed in Section 5.3.2.

The measurement results given in [5.1] are all classified, so the discussion of results has to be kept very limited and on a relatively general level. Only a couple of plots showing anonymized measurement results are included here, as examples. However, comments can be given on a general level. The main findings of the work are summarized in the following.

---

[35] One could alternatively estimate a diffraction time shift t^{diff} associated with a zero crossing in the transient start of the signal, cf. section 3.7. The "CW diffraction time shift" and the "transient start diffraction time shift" are not necessarily equal, and may show different pressure, temperature and transducer distance characteristics.

- *Electrical impedance* and **admittance**. The electrical input impedance and admittance responses $Z_T(f)$ and $Y_T(f)$ have been measured in the pressure chamber, with nitrogen up to 100 bar at 15 and 50/60 °C. For all transducers, the responses $Z_T(f)$ and $Y_T(f)$ have been found to be largely affected by temperature. This includes significant variations with temperature at the operational frequencies of the transducers. Such variation may influence on the reciprocity of the USM, and thus on Δt^{corr}.

For some transducers a significant variation of $Z_T(f)$ and $Y_T(f)$ with pressure has also been found, even at relatively low pressures. Other transducers were relatively invariant to pressure changes up to 100 bar. Normally, at such moderate pressures, the impedance and admittance responses do not change significantly with pressure unless the pressure influences on the vibrational characteristics of the transducer, i.e. on the transducer construction itself.

- **Linearity.** Linearity checks have been made in the pressure chamber, with nitrogen up to 100 bar at 15 and 50/60 °C.

Non-linearity (in the transducer or the gas) has been found for the majority of the transducers investigated, indicating that the maximum allowed driving voltage specified by the manufacturer should be lowered for those transducers, so that the they are driven in their linear region. For some transducers, non-linearity has been found also far below the specified maximum driving voltage. Some pressure and temperature dependence of the non-linearity has been found.

- **Voltage source sensitivity.** The frequency response of the source sensitivity $|S_V|$ was measured only in air at 1 atm and room temperature. The frequency response "shapes" were very different for the three types. Such a result may be expected, since the three types are different designs. At the specified operational frequencies of the respective transducers, the source sensitivities of the three types were found to be within about 10 dB.

The level of $|S_V|$ will increase by increasing gas pressure (proportional to the gas density, unless non-linear effects are influent). The "shape" of the frequency response is not expected to be much affected by increasing pressure, at least at "low" and "moderate" pressures. At higher pressures, the coupling to the gas becomes more influent.

$|S_V|$ is expected to change with changing temperature, both with respect to level (for a given frequency), and the "shape" of the frequency response. However, pressure and temperature aspects have not been investigated here.

- **Directivity.** The directivity $|D(\theta)|$ has been measured in the pressure chamber, with nitrogen up to 100 bar at 15 and 50/60 °C. In general, very different directivities have been found for the three transducer types. Such a result is to be expected, since the three types are different designs.

For all three types, the directivity was found to be temperature dependent, especially with respect to the side lobes. Some temperature dependence is always to be expected for transducers constructed with epoxy materials. For one type, the side lobe level is significantly increased at 15 °C relative to the higher temperature, which may possibly increase the level of reverberation in the pipe (unwanted echoes acting as coherent noise, and potentially causing systematic errors in the measured transit times), and also increase the sensitivity to control valve noise.

A change of directivity with frequency was found for all transducers in the frequency band around their operational signal frequency. Some frequency dependence of the directivity is to be expected, since different vibration modes of the transducer normally exhibit different vibration patterns. In some cases relatively dramatic changes were found. This indicates that the directivity in the transient

start part of the signal may be different from the directivity in the stationary part of the signal, which may have consequences for the diffraction time shift t^{diff} if transit times are measured in the transient start part (cf. Section 3.7).

Significant pressure dependence of the directivity is not "expected normal behaviour" at the relatively moderate pressures investigated here (less than 100 bar), apart from some influence of the change of sound velocity in the gas with pressure. However, a significant pressure dependence of the directivity is observed for one transducer type. The directivity of the other two types depend on pressure as well, but to a smaller extent. Two of the transducer types show a large broadening of the beam width with increasing pressure, in the frequency band around their operational frequencies, which may cause unwanted echo/interference/diffraction time shift effects (also with potential influence on the measured transit times).

For two of the three transducer types, high side lobe levels were found in the frequency band around their operational frequencies, esceecially at 15 °C. High side lobe levels may cause acoustic reverberation in (unwanted echoes) the pipe, which is very difficult to detect or observe under operation, but which may interfere with the measurement (direct wave) signal and cause systematic timing errors.

For two of the three transducer types, the acoustical axis was found to deviate from the mechanical axis, by up to $2°$ for the measurement plane investigated. A distinct assymmetric (non-axisymmetric) radiation was found. The degree of asymmetry was observed to vary with pressure and temperature (up to $3°$), and with frequency. In most measurements, the side lobe level was not symmetric for these two transducer types.

Other "abnormal effects" which were discovered for some transducers when measuring the directivity $|D(\theta)|$ are discussed below, under "Other effects". These include (1) change of $|D(\theta)|$ with transducer driving voltage, $|V_{in}|$, and (2) change of $|D(\theta)|$ over time when driving the transducer at the maximum $|V_{in}|$ specified for the transducer.

The directivity $|D(\theta)|$ has also been used to estimate the diffraction time shift t^{diff} (see below).

• **_Transducer time delay_**. The transducer time delay t^{tr} has been measured in the pressure chamber, with nitrogen up to 100 bar at 15 and 50/60 °C.

Transducer time delays ranging from about 3.5 to more than 9 µs have been measured. Some variation of the transducer delays with pressure have been found for all transducer types; for one type the variation is nearly 1 µs over the 20-100 bar range, at 15 °C. For all transducers the transducer delay increases from 15 to 50/60 °C, by about 1 to 2 µs (depends on transducer type).

Fig. 5.4 shows an example of measured transducer time delay, t^{tr}. In this example the change of t^{tr} is nearly 1 µs over the 20-100 bar range, at 15 °C, and in the range 1.5-1.8 µs over the 15-50 °C range.

Such pressure and temperature variations of the transducer delay may give significant errors in the USM measurement, if not accounted for in the transit time corrections of the USM, cf. Eq. (3.12). For a 6" meter, for example, an error in the transit times of 1 µs (corresponds approximately to the change of t^{tr} over the pressure range 20 -100 bar at 15 °C in Fig. 5.4), gives directly a measurement error of the order of 0.4 %. Similarly, a transit time error of 1.5 µs (corresponds approximately to the

change of t^{tr} over the temperature range 15-50 ^{o}C in Fig. 5.4), gives a measurement error of the order of 0.6 %.

On basis of a flow calibration, such systematic errors can be corrected by applying a meter factor. However, in possible future USM calibration scenarios based on a reduced dependence on flow calibration, the control and correction of such systematic changes of the time delays with pressure and temperature become critical and extremely important.
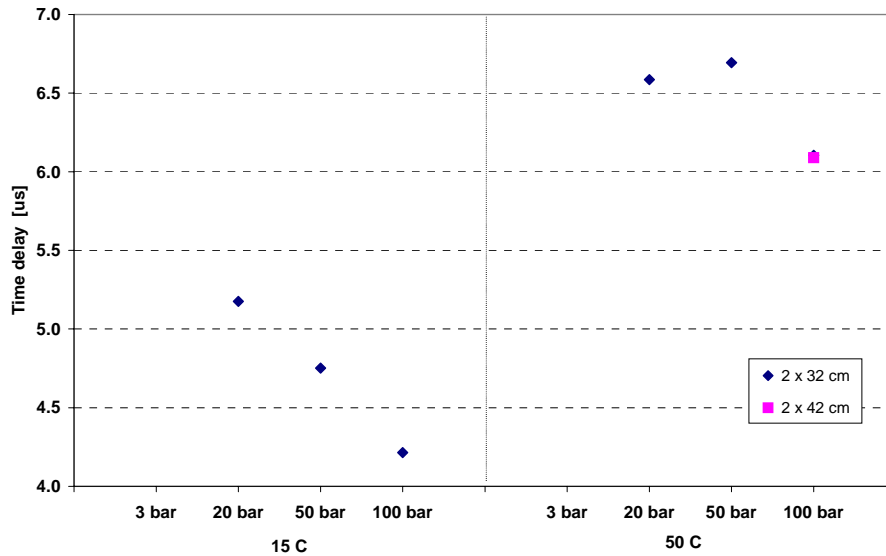
Fig. 5.4. Example of transducer time delay, t^{tr}, measured at pressures 20, 50 and 100 bara, and temperatures 15 and 50 ^{o}C, in the 200 bar pressure chamber.

• **_Diffraction time shift_**. The diffraction time shift t^{diff} has been estimated in the pressure chamber, with nitrogen up to 100 bar at 15 and 50/60 ^{o}C. (Note that t^{diff} is a negative quantity, cf. Section 3.8.)

Fig. 5.5 shows a representative example of the estimated diffraction time shift, $-t^{diff}$, for one of the transducers investigated in the study. In this example the change of t^{diff} is about 0.2 µs over the 20-100 bar / 15-50 ^{o}C ranges, at the transducer distance 20 cm. In addition, t^{diff} varies significantly with the distance between the transducers, so that acoustic diffraction effects makes the effective transducer delay dependent on the path length (or USM size). For this example, a change of t^{diff} in the range 0.5-0.7 µs (dependent on P and T) is observed over the distance range 20-100 cm.

Such pressure, temperature and distance variations of t^{diff} may give significant systematic errors in the USM measurement, if not accounted for in the transit time corrections of the USM, cf. Eq. (3.12). For example, diffraction alone may cause a change of the effective transducer time delay of the order of 0.4 - 0.55 µs from a 6" USM to a 16" USM, cf. Fig. 5.5. If a dry calibration value for t^{eltr} which is correct for a 16" meter at a given pressure and temperature is used in a 6" meter (at the same pressure and temperature), that gives directly a measurement error of the order of 0.2 % if the distance dependence of t^{diff} is not accounted for in the transit time corrections of the USM.

Note that since t^{diff} varies systematically with transducer distance, this parameter becomes important in connection with exchange of transducers in the USM. This point has been discussed in Section 5.2.

With respect to dry calibration and flow calibration aspects, the same comments apply to t^{diff} as for t^{tr}, see above.
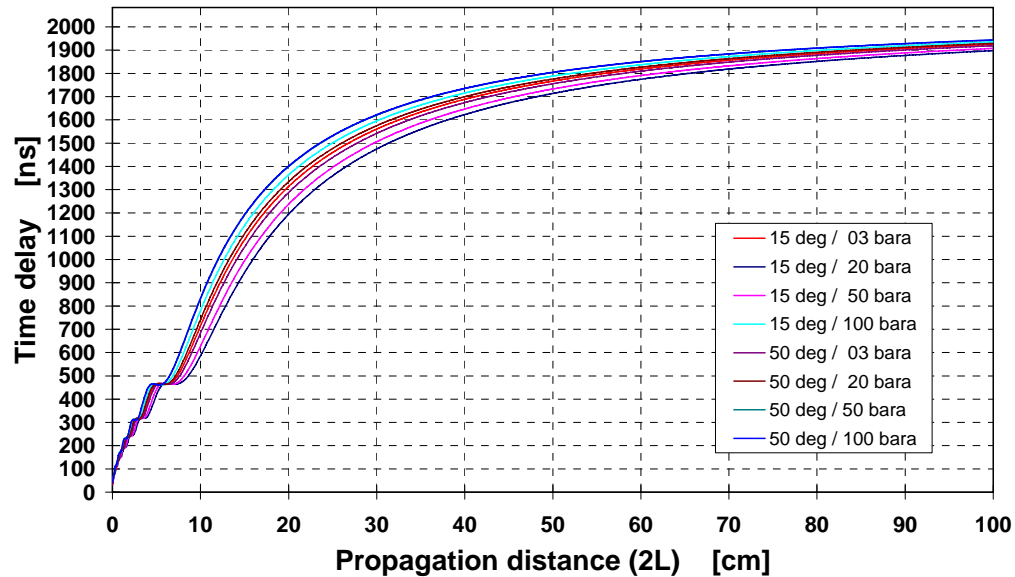
Fig. 5.5. Example of transducer diffraction time shift, $-t^{diff}$, estimated at pressures 3, 20, 50 and 100 bara, and at temperatures 15 and 50 °C.

• **Transmit-receive voltage-voltage transfer function**. The frequency response of the transfer function $|H_{VV}|$ was measured only in air at 1 atm and room temperature. Two of the three transducer types were investigated (one type from each manufacturer). The frequency response "shapes" were very different for the two types (which is to be expected, since they are different designs), but at the specified operational frequencies of the respective transducers, the magnitudes of the transfer function were found to be nearly equal (within 1-2 dB).

The level of $|H_{VV}|$ will increase by increasing gas pressure (proportional to the gas density, unless nonlinear effects are influent). The "shape" of the frequency response is not expected to be much affected by increasing pressure, at least at "low" and "moderate" pressures. At higher pressures, the coupling to the gas becomes more influent.

$|H_{VV}|$ is expected to change with changing temperature, both with respect to level (for a given frequency), and the "shape" of the frequency response. However, pressure and temperature aspects have not been investigated here.

• **Bandwidth** and **Q-factor**. The bandwidth, *BW,* and Q-factor, *Q,* were measured only in air at 1 atm and room temperature. Two of the three transducer types were investigated (one type from each manufacturer). Q-factors in the range 7-11 were measured.

BW and *Q* are not expected to be much affected by increasing pressure, at least at "low" and "moderate" pressures. At higher pressures, the coupling to the gas becomes more influent. On the other hand, *BW* and *Q* may be expected to change with changing temperature. However, pressure and temperature aspects have not been investigated here.

- ***Transducer reproducibility.*** Investigation of transducer reproducibility has not been a part of this work, since only two transducers of each type were investigated, and the basis for evaluation transducer reproducibility is poor. However, for some transducer types, significant differences between the two transducers of the same type were found, such as with respect to the electrical input impedance/admittance responses, $Z_T(f)$, $Y_T(f)$, the voltage source sensitivity, $|S_V(f)|$, the directivity $D(\theta)$, and the transducer time delay, t^{tr}. Evaluation of possible causes of these devations has not been made here.

- ***Lifetime stability aspects.*** Check measurements (of $|S_V(f)|$ and $Z_T(f)$) have been made (in air at 1 atm.) for all transducers, before and after the pressure chamber measurements series, over a period of 6-7 months. The check measurements revealed that four out of six transducers changed significantly over this period, larger than "expected normal behaviour". At least for two of the four transducers, this was visually identified to be caused by mechanical bonding defects, probably caused by the pressure / temperature combinations used for the measurements in the pressure chamber. Only moderate pressurizing / depressurizing rates were used in the work, which transducers normally should withstand.

- ***Other effects.*** During the work, unexpected and undesired acoustic effects ("abnormal" behaviour) were discovered for some transducers.

For one of the transducers, the sound pressure level of the main lobe increased systematically and significantly (several dB) over time when driving the transducer at the maximum excitation voltage specified by the manufacturer. The side lobe level remained unaffected by transducer "duty time". No such effect was observed when driving the transducer at one tenth of the specified maximum excitation voltage. A possible explanation for the effect may be heating effects in the epoxy layer (causing a reduction of the sound velocity in the epoxy), but this has not been investigated further here.

For another transducer, it was observed that by increasing the driving voltage to the transducer, $|V_{in}|$, there was a systematic increase of the the side lobe level at one side of the main lobe (up to about 6-7 dB), and a systematic decrease of the side lobe level at the other side (1-2 dB). The results show that the transducer vibration depends strongly on the excitation voltage, i.e. that the front face vibrates with different "shape" at different driving voltages. No explanation for this "abnormal" behaviour has been found.

- ***General comments:*** The consequences of the observations summarized above, for the accuracy, stability and robustness of the USMs in which these transducers are to be used, will depend on factors such as *how* the transducers are actually operated by the manufacturer, the procedures and the signal processing used, etc. The discussion of such aspects has not been an issue in the present work.

5.5   Summary and discussion

In the present limited study on measurement methods for characterizing USM transducers under pressure, the following characteristics have been investigated experimentally:

1. Transducer characteristics which are used for correction of transit times in USMs today: transducer time delay, t^{tr}, and diffraction time shift, t^{diff} (cf. Section 5.2).

2. Transducer characteristics which are not used directly for correction of transit times, but which are still very important for the functionality and performance of the meter, including correction of transit times (cf. Section 5.2): the electrical input impedance/admittance responses, $Z_T(f)$, $Y_T(f)$, the voltage source sensitivity (at 1 atm. only), $|S_V(f)|$, the directivity, $|D(\theta)|$, the transmit-receive voltage-voltage transfer function (at 1 atm. only), $|H_{VV}(f)|$, the bandwidth BW and Q-factor, Q (at 1 atm. only), and a linearity check.

From these measurements, one has found that:

1. The variations of t^{tr} and t^{diff} over the actual pressure, temperature and transducer distance ranges are so large that they provide significant systematic errors in the USM reading if these variations are not corrected for in the USM. Examples are given in Section 5.4. Such systematic effects can be corrected either through the use of a meter factor (resulting from a flow calibration), or by dry calibration. For possible future USM calibration scenarios based on a reduced dependence on flow calibration, the control and correction of the changes of such systematic effects with pressure, temperature and transducer distance become critical and extremely important, involving traceability and measurement uncertainty aspects of the dry calibration method used.

2. The measurements of $Y_T(f)$, $|S_V(f)|$, $|D(\theta)|$, $|H_{VV}(f)|$ and the linearity check have revealed that, for some of the transducers investigated, deviations relative to "expected normal behaviour" for the transducer types in question have been observed. Some of the effects observed can be fairly well understood and controlled, while other effects of P and T in the measured transducer responses show more surprising and less systematic behaviour. In some cases so strong "abnormal" behaviour has been identified under pressure that it is expected to influence significantly on the USM functionality and performance. Some of this "abnormal" behaviour may possibly be explained by bonding defects in the transducer construction.

In general, it is a reasonable requirement for USM manufacturers that they can document that their transducers and meters are functioning according to "expected normal behaviour". By using such measurements as described in the present work (with more results given in [5.1]), and possible additional measurements (see below), the manufacturers can ensure that their transducers are functioning in a well controlled manner also at elevated pressure and at varying temperatures over the operational range of the flowmeter. This will accordingly contribute to ensure that the flowmeter also will operate in a well controlled manner with respect to the transducer characteristics, and that flowmeter performance is not significantly compromised due to irregular and uncontrolled high-pressure and temperature variations in transducer characteristics.

The work has demonstrated that the measurements of the particular transducers characteristics as mentioned above, can be carried out within a limited effort for transducers used in present-day USMs.

Within the limitations of the project only a limited variation in parameters has been possible. Further work can easily extend these measurements and also include a more extensive documentation and improvement on the obtained measurement uncertainty. In particular, the determination of transducer time delays has been done under a simplifying assumption which limits the expected accuracy. A significantly reduced measurement uncertainty for this quantity is definitely of interest, but will require accurate experimental determination of the diffraction correction effects of the transducers.

Better control with the transducer time delay and the diffraction correction effects, and their variation with pressure, temperature, gas composition and transducer distance, may give perspectives for a reduction of the need for doing dry calibration in the future.

Through the present work, the characterization of USM transducers under operational conditions is considered to have been brought a step forward. However, the work undertaken here is far from complete, and there is clearly more to be done in this field. The most important issues for further work are considered to be:

- To establish traceability and quantify the measurement uncertainty of the transit time parameters measured in the dry calibration and used for transit time correction, such as t^{eltr} and Δt^{corr} (which have here been decomposed into the parameters $t^{el,cab}$, t^{tr}, t^{diff} and Δt^{corr}, cf. Eqs. (3.12)-(3.14)). This issue will be extremely important and critical in possible future USM calibration scenarios with a reduced dependence on flow calibration, and increased dependence on dry calibration. Very little seems to have been done in this field up to now, and this issue will need to be addressed in future development of USM technology for fiscal metering of natural gas.

- To achieve more accurate measurements of the diffraction time shift, t^{diff}, and its change with P, T and transducer distance. These measurements should not be based on the directivity, $|D(\theta)|$ (as done here), but on a more direct measurement of t^{diff}.

- To extend these measurements of dry calibration transit time parameters to the complete range of operational conditions: -25 to +55 $^{\circ}$C [5.8], 10-200 bar.

- To extend the measurement of the other transducer characteristics investigated here in the pressure chamber (such as the impedance/admittance responses, $Z_T(f)$ and $Y_T(f)$, the directivity, $|D(\theta)|$, and the linearity check) to the complete range of operational conditions: -25 to +55 $^{\circ}$C [5.8], 10-200 bar. The results found here strongly indicate that the transducer behaviour will change significantly over this range. The purpose will be to establish the "expected normal behaviour" for the transducer types over this operational range, and to check for possible "abnormal" behaviour (which may compromise the functionality and performance of the meter).

Further, the determination of some additional characteristics under pressure may be of interest for a more complete characterization of ultrasonic transducers for USMs, such as:

- The Δt-correction, Δt^{corr},
- The voltage source sensitivity, $|S_V(f)|$,
- The receiving senstitivity, $|M(f)|$,
- The transmit-reveive voltage-voltage transfer function, $|H_{VV}(f)|$,
- The bandwidh, BW, and Q-factor, Q.

Improved knowledge on the parameters that influence on the USM accuracy (cf. Section 5.2) is essential to exploit and reach the full accuracy potentials of such meters.

Chapter 6

Ultrasonic meters and noise[36]

Part A: **Karen van Bloemendaal**[*] **and Gert H. Sloet**[*]
Part B: **Bernard Hosten**[**]**, Pascale Brassier**[**] **and Frédéric Vulovic**[***]

[*] *N. V. Nederlandse Gasunie, Groeningen, The Netherlands*
[**] *Universite de Bordeaux I, Laboratoire de Mecanique Physique, Talence, France*
[***] *Gaz de France DR, Alfortville, France*

Part A: Ultrasonic meters and noise; An experimental approach

6.1   Introduction

6.1.1   Background

In 1995, the status of multi-path ultrasonic gas flow metering was investigated by a GERG project group. This study not only established the state-of-the-art at that moment, but also identified gaps in the knowledge of such meters, which could be identified as topics for future research. The results were published in GERG Technical Monograph no. 8 [6.1].

The most relevant of these "knowledge-gaps" were taken up in a second GERG project on ultrasonic gas flow meters (USM's). One of these items, the effects of (ultrasonic) noise on USM's, was investigated experimentally by Gasunie, and some results are presented in this paper. The other subjects of the GERG project, the effects of non-ideal flow, the development of a general uncertainty model, the development of procedures to evaluate transducers, and attenuation and propagation of noise in pipelines were or will be reported elsewhere [6.2], [6.3], [6.4], [6.5]. This GERG project ran in 1997 and 1998, and the project group involved 9 European gas companies: BG Technology, UK; Distrigaz, Belgium; ENAGAS, Spain; Gasunie, the Netherlands; Gaz de France, France; NAM, the Netherlands; Ruhrgas, Germany; SNAM, Italy, and Statoil, Norway.

6.1.2   Previous work on USMs and noise

The research of (ultrasonic) noise and the effects of it on USM's is induced by problems with USM's in the neighbourhood of valves and regulators encountered by users of these meters. A few times these problems in field locations were published (for example [6.6], [6.7], [6.8]), but more often the problems are tackled in a practical way. Solutions to the problems are often sought in replacing the (silent) regulator with one of a different type, usually a non-silent one, or by increasing the distance between the regulator and the USM. The 1996 AGA Technical Note on USM's [6.9] also advises not to install USM's in close proximity to throttling devices, and suggests manufacturers to improve signal handling by techniques as for example stacking, and to increase the transducer power in order to

---

[36] This chapter is a "reprint" of the paper [6.18] (Part A), integrated with the paper from Université de Bordeaux and Gaz de France (Part B). These two parts are based on the technical reports of Task 4 [6.19], [6.5].

increase the signal to noise ratio. In [6.8] it was possible to increase the transmission output to the sensors, but this is not usually the case. [6.10] presents a noise suppression algorithm for a USM.

In field situations, varying of flow and pressure difference is often difficult, and noise, if measured at all, can only be measured at one or two locations. In some publications [6.11], [6.12] an attempt is made to investigate the effect of noise on a given meter more systematically. However, the scheduled tests in these cases were curtailed, because the USM's would not operate correctly with substantial pressure reduction, and no noise measurements were performed. In [6.13] many sound spectra were recorded and compared with the signal level of a USM, but this investigation was performed at low pressures. [6.14] presents sound measurements of one regulator and signal to noise ratios of a USM .

6.1.3   Aim of the present work

The aim of the present work is to investigate whether it is, in principle, possible to measure gas flows with USM's in the vicinity of ultrasonic noise sources such as regulators, and if so, how reliable the USM output is. This is done by observation of the performance of as much as possible USM's of different makes in the vicinity of a pressure reducer and simultaneous registration of the noise disturbance in a more systematic way than has been done up till now. It has not been the intention to perform a competitive test, in other words to identify "the best meter".

6.2   Experimental set-up

6.2.1   Test facility

The experiments described in this paper were performed in a test section at the Gasunie laboratory in Groningen. The gas flows first through the test section and then through the reference meters, before it is delivered into the distribution network of Groningen city. Pressure is reduced near the inlet from the supply pressure of 40 bar(a) to the desired test pressure and in case the test pressure is higher than 9 bar(a), between the test section and the reference meters, who always operate at the outlet pressure of 9 bar(a). Flow rate is controlled at the outlet of the facility, and it is limited by the gas demand of the city.

6.2.2   Pipe configurations

The test section was about 18 m long. A large part of this section was of 200 mm diameter pipe. The inlet and the outlet of the test section are defined by 150 mm plug valves, which are a fixed part of the test facility. In the following figures, gas flow is from left to right.
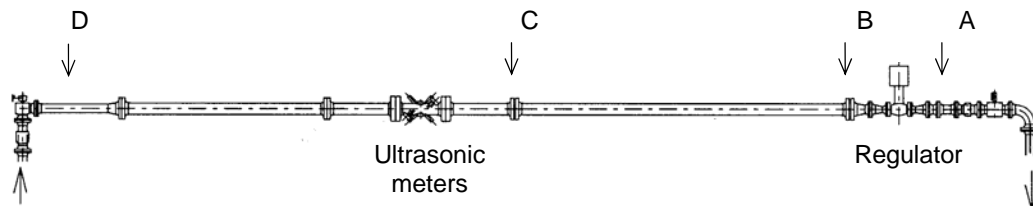

Fig. 6.1   Test Set-up with regulator downstream (DN).

section (DN). Downstream of the 150 mm angular plug valve, the piping expands to 200 mm. Ca. 1.5 m upstream of the end of the test section, the pipe diameter is reduced back to 150 mm. The 100 mm

regulator is mounted between two 100-150 mm reducers and is located about 1 m upstream of the outlet valve. The USM's spool piece (see 2.5) is located about 6 m downstream of the inlet valve; the distance between the USM's and the regulator is about 9 m. Sound measurement sensors (see 2.4) are located upstream (D), close to the middle of the test section (C), further downstream (B) and downstream of the regulator (A).
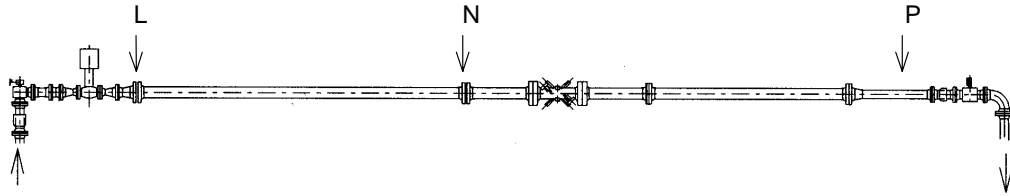
Fig. 6.2   Test Set-up with regulator upstream and USM's in middle of test section (UP-M).
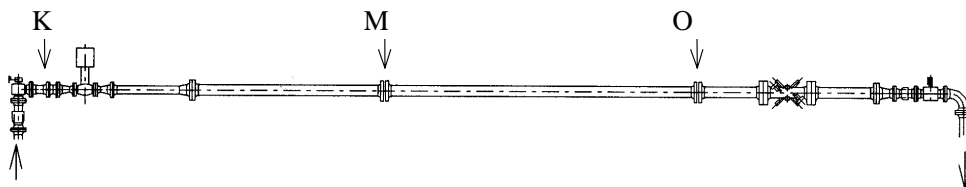
Fig. 6.3   Test set-up with regulator upstream and USM's at long distance (UP-L).

Figs. 6.2 and 6.3 show the set-up with the regulator close to the upstream end of the test section, and the USM's spool piece located respectively near the middle of the test section (UP-M), or at longer distance, about 13 m, from the regulator (UP-L). In the UP-M case, the distance between regulator and USM's was about 9 m, the same as in the DN case. Sound measurement sensors were located at 3 positions downstream of the regulator: close to the regulator (L), near the middle of the test section (N) and near the end of the test section (P). In the UP-L case sound measurement sensors were located upstream of the regulator (K), between locations L and N (M), and between locations N and P (O).

6.2.3   Regulator

The regulator, a 4" axial flow valve see Fig. 6.4, is a product of and made available to the project by Mokveld Valves [6.15]. Bodies of such regulators are standard, the internal cages, the parts where actual pressure reduction takes place, are sized on specification. For this project the maximum pressure difference was set at 27 bar, and maximum flow rate at 30000 m^3/h(s). The regulator was equipped with a pneumatic actuator so that it could be moved into position from the control room. Its position output could be read by the data acquisition system. The regulator was mounted both on the downstream and upstream ends of the test section.

Two cage designs were selected in order to investigate the influence of these constructions on the spectrum, see figure 5. The RVX cage is a "standard" cage with 7 slots, which produces a lot of audible noise. Noise levels of more than 100 dB(A) were recorded in the test room. The RQX cage is a low noise design with 228 holes, producing considerably less audible noise.

Fig. 6.4   Mokveld Regulator   Fig. 6.5   RVX (left) and RQX Cages

6.2.4   Sound measurements

Under all test conditions, the noise levels and spectra were measured inside the pipe at several locations, both upstream and downstream of the regulator (see Figs. 6.1 to 6.3 in Section 6.2.2). For the sound measurements, PCB sensors type 132 A 41 [6.16] were selected. These piezoelectric sensors are very small, 3 mm diameter, and may be used in high pressure surroundings. Response is claimed to be accurate within ½ dB in the range up to 500 kHz. Calibration results of the sensitivity, in the order of 3000 mV/psi, are supplied with each sensor.

The signal of the sensor was recorded on a digital storage oscilloscope. Every sound measurement consists of 60000 data points, sampled at 1 μs, which were stored on file and processed off-line in a Matlab-environment. Every measurement was transformed into a spectrum by a FFT procedure, from which sound pressures in 1/3 -octave frequency bands were calculated. Mean sound pressure values over the frequency range of 50-500 kHz were calculated from these.

6.2.5   Ultrasonic meters

Six major ultrasonic gas flow meter manufacturers were all willing to make available their equipment for the measurements. These were: Daniel; Instromet Ultrasonics; Kongsberg Offshore; Krohne Altometer; Panametrics and Ultraflux. Each manufacturer supplied one set of transducers and the necessary cabling, electronics and flow computers, to complete a 1-path meter. A pulse output frequency could be read by the data acquisition system of the installation for the calibrations (see Section 6.4).

These 6 USM's were all to be exposed to the same test conditions and disturbances such as gas pressure, gas velocity, noise levels and distance to the source of the noise. For this purpose, a special spool piece was designed in which each manufacturer could install one pair of transducers. This spool piece basically consists of a 200 mm ANSI 1500 pipe of 1 m length (see Figs. 6.6 and 6.7). Each meter is (part of) a commercially available product of the manufacturer, each with its own transducer holder design.

The transducer holders are located in the planes B-B, C-C, D-D and E-E. The planes B-B and E-E each contain one straight path (i.e. no reflection on the pipe wall). The path in B-B makes an angle of 55° to the centre line, and is located at half- radius; the path in E-E crosses the centre line at an angle of 60°.Plane C-C contains two straight paths, both through the centre line at an angle of 45°. Plane D-D contains two reflection paths (both transducers of one path are located at the same side of the

pipe, and the ultrasonic beam reflects on the opposite pipe wall). Both paths have angles of 60°. Using this spool piece, and operating the ultrasonic meters one by one, the results of the meters and the effects of the noise could be compared.
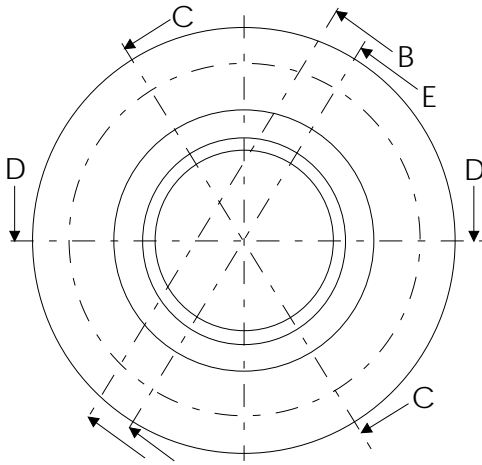
Fig. 6.5. Spool piece cross section
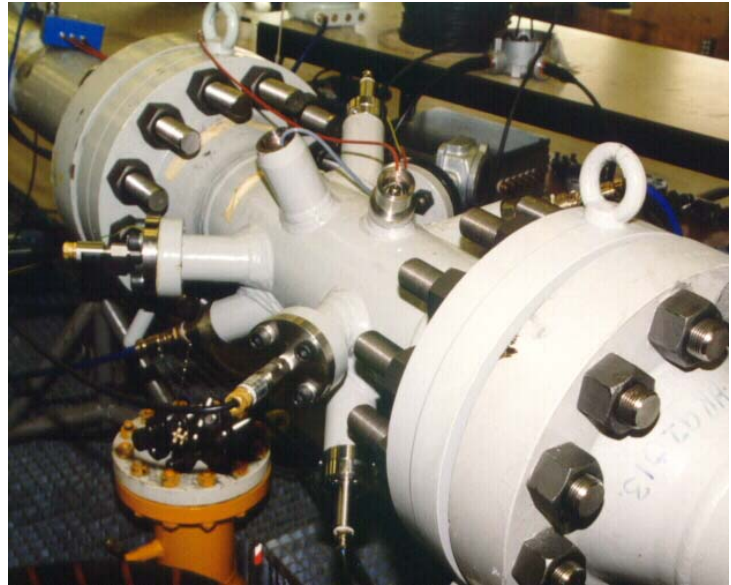
Fig. 6.6 USM spool piece

6.2.6   Test procedure

For each test set-up at three fixed upstream pressures, 15, 24 and 36 bar(a), the flow rate was varied; and at two fixed flow rates, 6800 and 17000 m^3/h(s), the pressure difference was varied. At every test condition sound measurements were performed and all USM's calibrated. During the sound measurements all USM's were switched OFF. The USM's were tested one by one, i.e. when one meter is switched ON, all other meters are switched OFF. This way, the meters are never influenced by (reflections of) signals from other meters. As flow rates are given in standard cubic meters per hour, the actual gas velocity at the USM's is dependent on the local pressure, which is different when the meter is upstream or downstream of the regulator. Appendix A gives an indication of gas velocities at each flow rate.

6.3   Results sound measurements

The sound measurements consist of sampling the signals from the piezoelectric sensors (see 2.4). The calculated mean sound pressures in 1/3-octave frequency bands are plotted against the central frequencies in every band in the range of 30 to 500 kHz. The y-axis is given in the sound pressure unit Pa, on a logarithmical scale, ranging from 1.e-1 to 1.e+4 Pa [37].

In every situation the mean sound pressure in the frequency range 50-500 kHz was calculated also, and plotted against three main variables: the valve position in percentage of maximum valve opening, the product of flow rate and pressure difference and the distance to the regulator.

---

[37] For readers who prefer decibel scales: this scale is equivalent to a linear scale ranging from 74 to 174 dB, relative to the internationally accepted value for reference pressure of 20 µPa [6.17].

6.3.1 Non-silent regulator RVX

Fig. 6.8 shows some results with the non-silent regulator RVX. The regulator was mounted at the downstream end of the test section, and the sensors (B, C and D) were located upstream of the regulator. The pressure upstream of the regulator was 36 bar(a), downstream 9 bar(a), the flow rate was 12000 m³/h(s). The valve position was 41 % open. Fig. 6.9 shows similar results, obtained in similar conditions, from sensor L, N and P, located downstream of the RVX regulator which was mounted at the upstream end of the test section. These figures show clearly more noise downstream of the regulator than upstream, and also relatively more low frequency noise. With distance the noise decays, and this decay is stronger for higher frequencies.
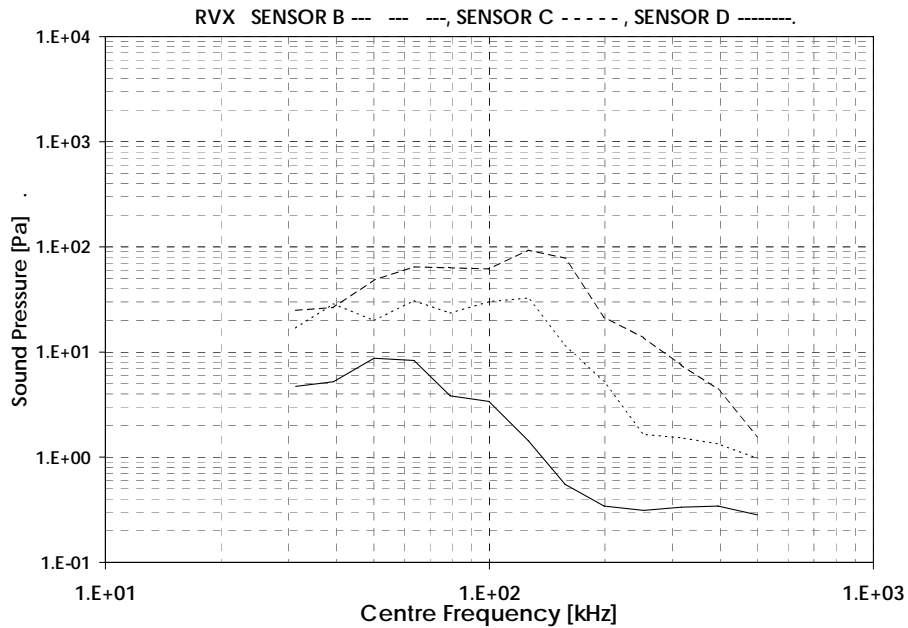
Fig. 6.8.   Results, sound measurements upstream of non-silent regulator RVX
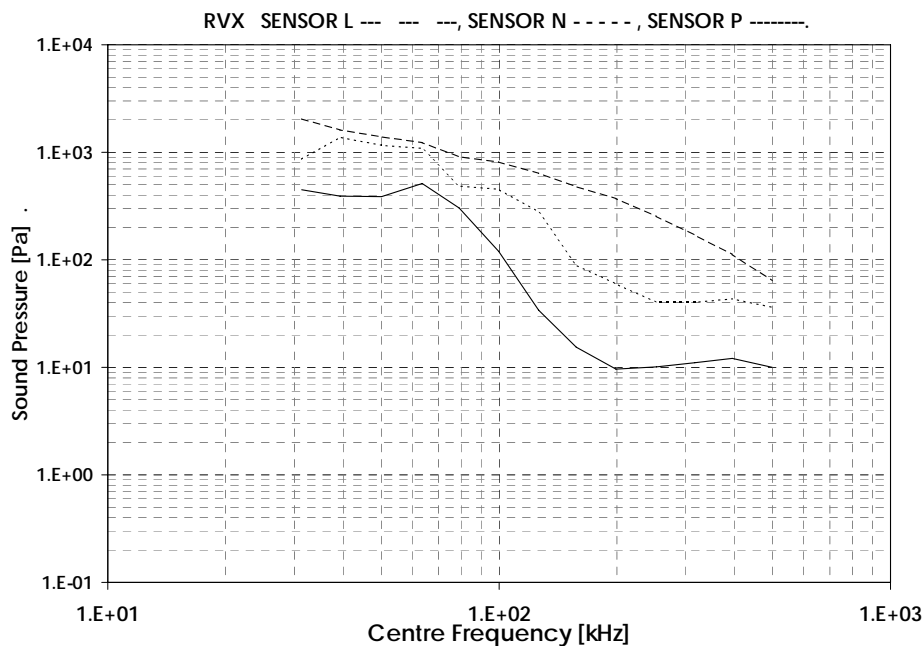
Fig. 6.9.   Results, sound measurements downstream of non-silent regulator RVX

6.3.2   Silent regulator RQX

Figs. 6.10 and 6.11 show results of the silent regulator RQX, under test conditions corresponding to those of Figs. 6.8 and 6.9. Although this regulator is a low-noise one, designed for low noise in the audible range and outside the pipe, this regulator produces more noise inside the pipe in the frequency range of interest 30-500 kHz.
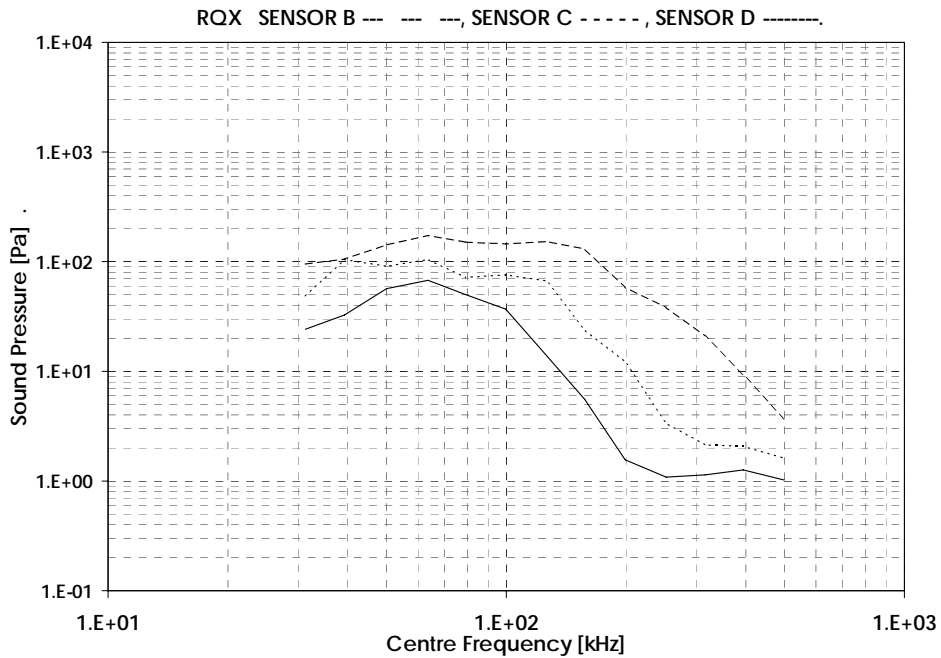
Fig. 6.10. Results, sound measurements upstream of non-silent regulator RQX.
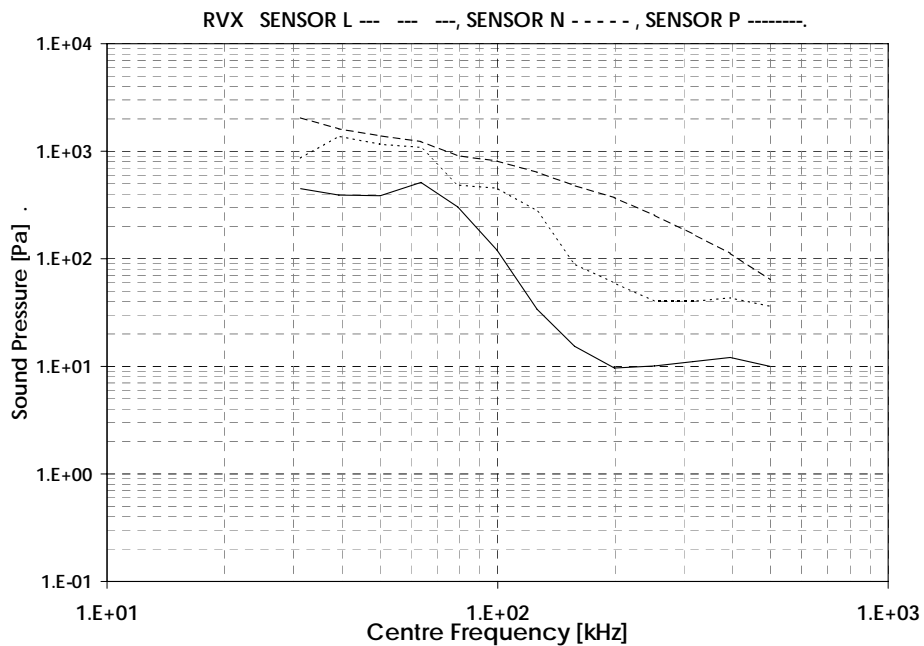
Fig. 6.11. Results, sound measurements downstream of non-silent regulator RQX.

6.3.3 Mean sound pressure in relation to Q*dP, valve position and distance

Analysis of all (more than 500) obtained spectra revealed that the spectrum depends on regulator type, pressure difference across the regulator and flow rate, valve position, and distance to the regulator. In order to show these dependencies, the mean sound pressure (MSP) in the frequency range from 50 to 500 kHz is calculated for every test condition. Similar calculations were performed with two or more smaller ranges, to see the effect of frequency range.

Presented here is MSP(50-500 kHz) as a function of the valve position V, as a function of the product of flow and pressure difference Q*dP which are important parameters in the generation of noise inside the regulator, and as a function of distance to the regulator x as noise is known to decay with distance. Because of the large similarity, only results of non-silent regulator RVX are presented graphically.

RVX MSP(V) SENSOR B.
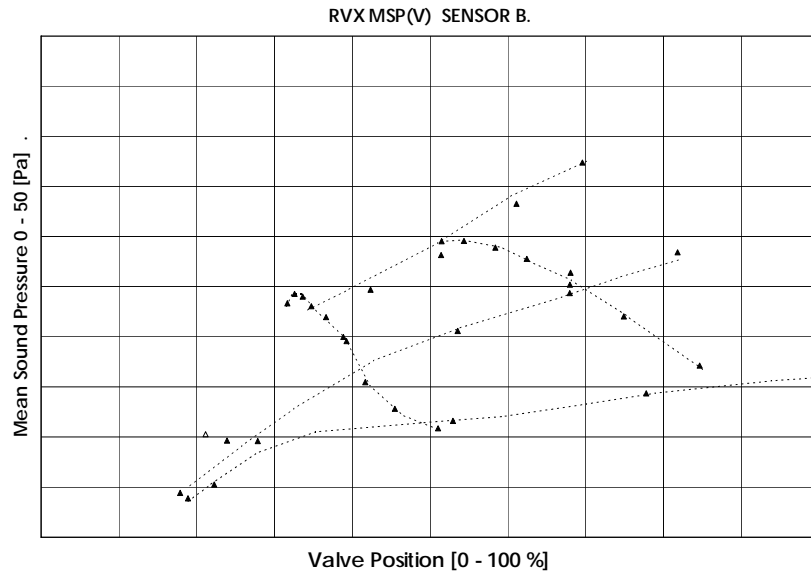
Fig. 6.12. MSP as function of valve position upstream of non-silent regulator RVX.

RVX MSP(V) SENSOR L.
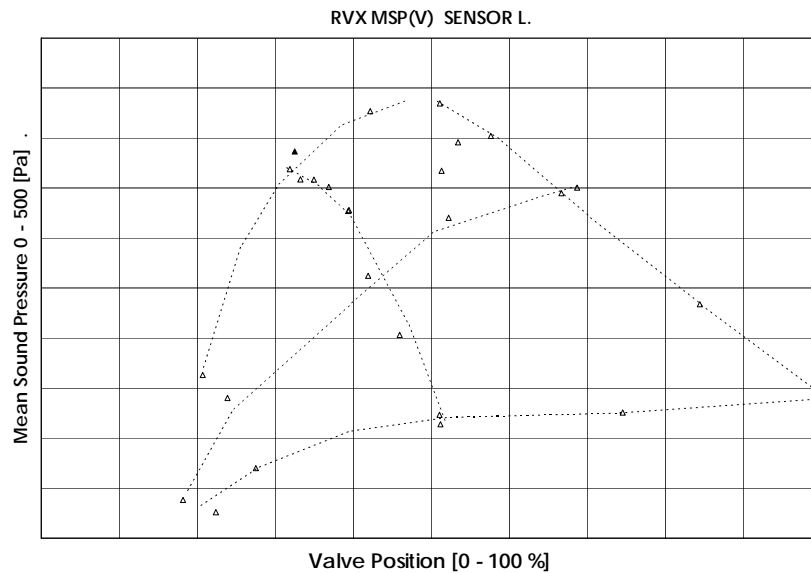
Fig. 6.13. MSP as function of valve position downstream of non-silent regulator RVX.

Figs. 6.12 and 6.13 show mean sound pressures MSP for regulator RVX, upstream and downstream of the regulator, as a function of the valve position. Only data points from the sensors closest to the

regulator, B and L respectively, are given in the figures. The other sensors show similar patterns, but at lower values.

The 5 different experiment series are clearly recognisable: three lines with fixed pressures and variable flow rates, and two lines with fixed flow rate and variable pressures. At a given flow rate, increasing valve opening means decreasing pressure difference, and accordingly decreasing sound pressure. At a given pressure difference, with increasing valve opening, flow rate and sound pressure increase. With regulator RQX similar results were obtained.

Figs. 6.14 and 6.15 show mean sound pressures for regulator RVX, upstream and downstream of the regulator. With some scatter, the mean sound pressure fits logarithmically with the product of flow rate and pressure difference Q*dP. Curve fits in the form MSP = A * ln(Q*dP) - B are drawn in the figures. Factor A decreases with increasing distance to the regulator. A has larger values with silent regulator RQX than with non-silent regulator RVX. The difference between RQX and RVX increases with increasing distance, and is larger upstream than downstream of the regulator.
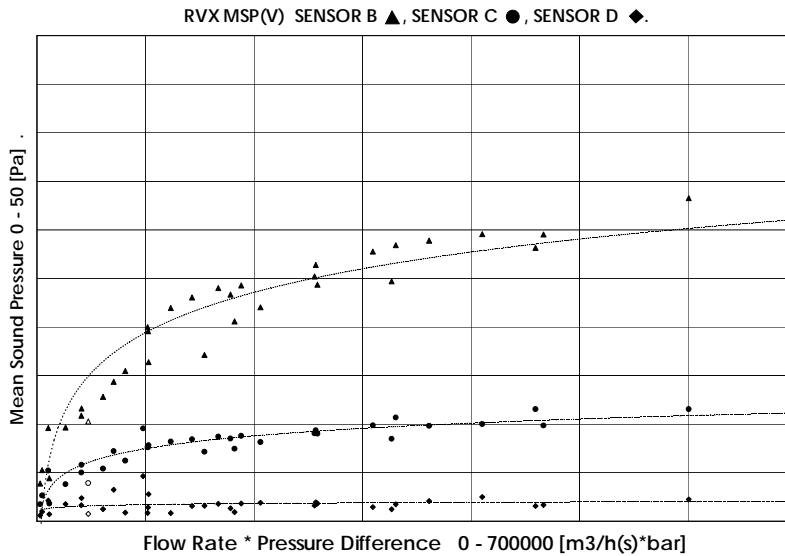
Fig. 6.14. MSP as function of Q*dP upstream of non-silent regulator RVX.
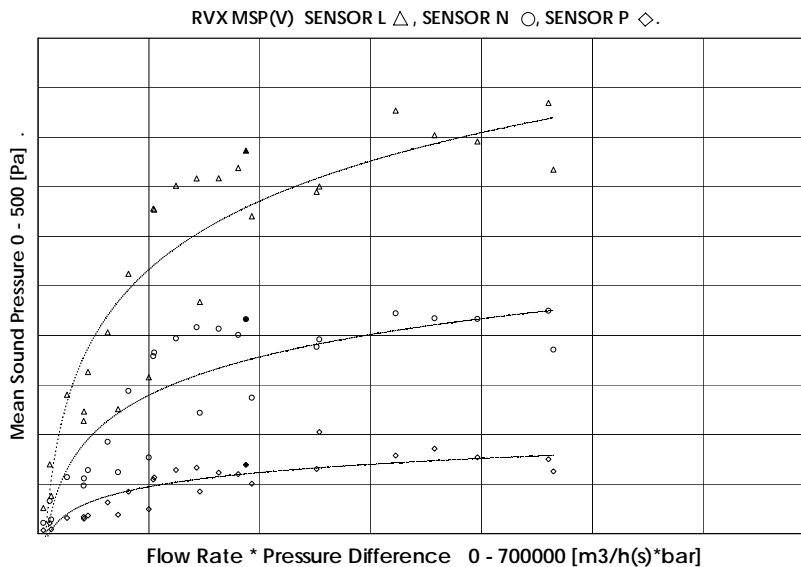
Fig. 6.15. MSP as function of Q*dP downstream of non-silent regulator RVX.

Fig. 6.16 gives MSP as a function of distance to the regulator. All results of regulator RVX (in the different set-ups, see 2.2) are drawn in the same figure. The sensors A and K are located in the short part of the test section, that is between the regulator outlet flange and the nearby downstream valve (sensor A, RVX-DN) or between the regulator inlet flange and the nearby upstream valve (sensor K, RVX-UP). The results of these sensors are given in open markers, in contrast to the results of all other sensors, given in black markers.

The results of sensors A and K are clearly very different from all other results. This shows that not only the source of the noise, the regulator is important, but also the up- and downstream pipe work and fittings. In this case, the up- and downstream valves may act as reflectors for the sound inside the pipe. When disregarding these results, the results of sensors B-D and L-P show an exponential decay with distance.

For illustration, a grid of exponential lines in the form $MSP(x) = MSP_0 * e^{-C*x}$ is drawn in the figure. The value $x = 0$ represents the middle of the regulator; the values of C and (maximum) MSP_0 are given in Table 6.1.

Table 6.1 - Exponential Decay of Mean Sound Pressure with Distance

	Upstream of regulator		Downstream of regulator	
	RVX (non-silent)	RQX (silent)	RVX (non-silent)	RQX (silent)
C	-0.00012		-0.00010	
MSP_0 (max)	32	70	480	540
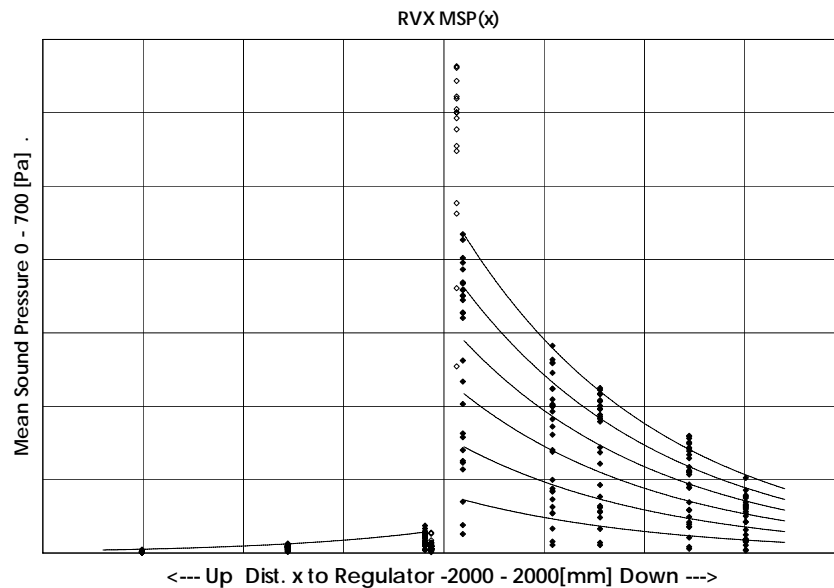
Fig. 6.16. Mean sound power in the range 50-500 kHz as a function of distance for non-silent regulator RVX.

The exponent C gives the decay rate. In the frequency range 50-500 kHz, the upstream noise decays faster (C = -0.00012) than downstream noise (C = -0.00010). From the calculations with divided frequency ranges it follows that exponent C is larger for higher frequencies than for lower frequencies: the decay goes faster for higher frequencies.

The base MSP_0, both upstream and downstream, is larger for the silent regulator RQX than for the non-silent regulator RVX. The "silent" regulator is producing more noise inside the pipe in the range of 50-500 kHz, than the "noisy" one. The ratio of noise for the two regulators RVX and RQX is not the same at the different sides of the regulator: upstream it is 0.5, downstream 0.9. These ratios change slightly with frequency.

Also, the base MSP_0 is much larger downstream than upstream for both regulators. This means that more noise is measured downstream of the regulator than upstream. The ratio downstream-upstream noise is not the same for these two regulators: 15 for regulator RVX and 7.7 for regulator RQX. These values are lower for higher frequencies, and higher for lower frequencies. Noise at lower frequencies is thus better "separated" by the regulator than noise at higher frequencies.

6.4 Results ultrasonic meters

6.4.1 Presentation of calibration results

The USM's are calibrated against the Gasunie reference flow meters during 3 times 100 s. For confidentiality reasons, the results of the calibrations of each USM in test situations with regulator are only presented as error shifts compared to the mean error of the same meter in "ideal flow": the calibration of the meter at the same pressure, when no regulator is mounted in the line. The results of these "ideal" calibrations are not presented in this paper.

A calibration of a USM under noise disturbed conditions is only sensible if the meter is functioning continuously. If one or more USM's are partially failing, one should assess its performance in another way, for example with a performance comparison method as described below.

6.4.2 A performance comparison method

As ultrasonic meters are based on a measuring principle using a beam of sound, it is likely to expect that they may be disturbed by sound in the right frequency range and/or of sufficient power. Field experience learns that this is indeed the case. When both the ultrasonic beam and noise reach the receiving sensor of the USM, it will be more difficult or even impossible to detect the right signal out of it and from that, calculate a correct gas flow velocity. The output that is shown to the user, in this case the frequency of the pulse output, depends on signal strength, signal detection, analysis techniques and often also on user-set parameters.

The following four types of behaviour and the effect on the error curves of the meter, were observed in the experiments. In brackets the number of meters that showed this behaviour is given; one meter may be in different categories.

1 The meter fails, and the pulse output frequency is set to zero Hz. If the failure is complete, a meter error E of -100 % will be found. If the meter only part of the time is failing, the error will be smaller. (4 meters).

2 The meter fails, and the pulse output frequency is set to a user specified "error-frequency", usually a frequency much higher than the maximum flow rate frequency. If the failure is complete, a high error E will be found. The value of E is dependent of the error-frequency, the frequency factor and the actual flow rate. If the meter is only partially failing, then the more it fails, the higher the meter error is. (1 meter).

3 The meter continues working but with a larger output variation. In the error curve more scatter will be observed. If the variation is on a relatively small time base, it is filtered out during the measurement time of in this case 100 s. (2 meters).

4 The meter continues working but with erroneous output. The resulting error shift is usually of several percents. The wrong output may be steady or switching between distinct values (2 meters).

For every test condition, each USM is given a "performance number" according to the scheme below. From all these performance numbers for each test set-up (USM's upstream or downstream of the regulator, the latter at two distances), a mean performance number P_i is calculated for each individual USM and P_m for all USM's together [38].

100 %	IF	USM functions correctly all the time	AND meter error E is smaller than 1 %
90 %	IF	USM functions correctly all the time	AND E lies between 1 and 5 %,
	OR	USM functions but shows some alarms	AND E is smaller than 1 %
75 %	IF	USM functions all the time	AND E lies between 5 and 20 %,
	OR	USM functions but gives regular alarms	AND E lies between 1 and 5 %
	OR	USM fails sometimes	AND E is smaller than 1 %
50 %	IF	USM fails sometimes	AND E lies between 1 and 5 %
	OR	USM functions only half of the time	AND E is smaller than 1 %
25 %	IF	USM functions only sometimes	AND E is smaller than 1 %
	OR	USM functions half of the time	AND E lies between 1 and 5 %
	OR	USM functions (almost) all the time	AND E is larger than 20 %
10 %	IF	USM functions only a few times shortly	
0 %	IF	USM is not functioning at all	

6.4.3 Results with USM's upstream of the regulator

Figs. 6.17 and 6.18 show meter error shift curves for all six USM's located near the middle of the test section, upstream of the regulator which is mounted at the downstream end of the test section (RVX-DN and RQX-DN). These are the results of the experiments with fixed upstream pressure, 15, 24 or 36 bar(a), and varying flow rate. The curves are given as error shifts relative to the meter error $E_{mean, Base}$ from the calibration of the same USM at the same pressure but in absence of the regulator (see Sections 6.2.6 and 6.4.1).

Except for the lowest flow rates, almost all error shifts are well within ±2 %. Although the noise is at relatively low level in these situations, at the lowest flow rates of less than 1.5 m/s, the shifts of some USM's are much larger: within ±15 %. As almost all USM's kept on functioning almost all the time, the mean performance numbers P_m are 94 % with the non-silent RVX regulator, and 93 % with the silent RQX regulator. All meters were in one way or another affected by the noise, th e maximum P_i was not 100 % but 98 %. For some USM's the noise from silent regulator RQX was more severe than the noise from non-silent regulator RVX: the lowest individual performance numbers P_i were 81 % (RQX) vs. 91 % (RVX).

---

[38] Note that this is a selection scheme, in which error deviation and failing time are rated as good as equal. If one would appoint more value to the reliability of the answer or to the amount of time it is failing, this scheme and the mean performace numbers P_i and P_m could be quite different.
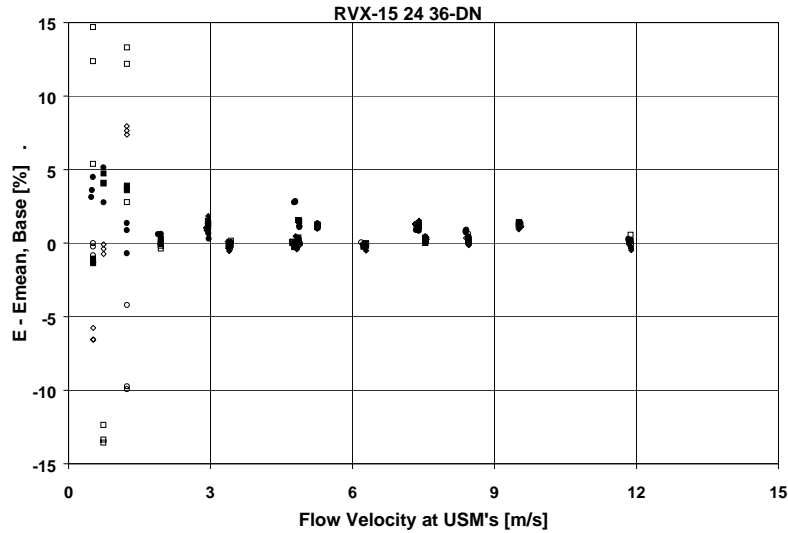
Fig. 6.17. USM's meter error shifts upstream of non-silent regulator RVX.
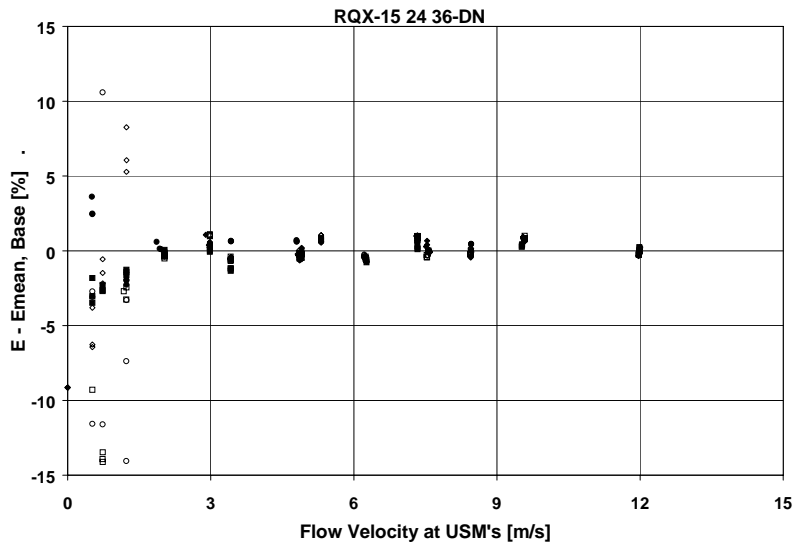
Fig. 6.18. USM's meter error shifts upstream of silent regulator RQX

6.4.4 Results with USM's downstream of the regulator

Figs. 6.19 and 6.20 show meter error shifts for all six USM's located at the end of the test section, as far as possible downstream of the at the upstream end mounted regulator (RVX-UP-L and RQX-UP-L). These situations are in two ways worse than with the USM's upstream of the regulator: downstream of the regulator the noise is considerably more than upstream, and the USM's operate at a lower pressure. The performance of the USM's is in these cases clearly much less than described above.

The figures show the 4 different meter behaviours, see Section 6.4.2:

1 USM's partially failing and, when failing, giving zero Hz output: error shifts of -50 to -100 %,

2 USM's partially failing and, when failing, giving a (high) error frequency: error shifts of more than +50 % (these may also be even more than +100 %),

3 USM's that continue working, but output shows more fluctuation: the variation in data points around the x-axis is about twice as much as in Figs. 6.17 and 6.18,

4 USM's that "jump" between modes: mean error shift gives more variation, and may become very high (open circles).
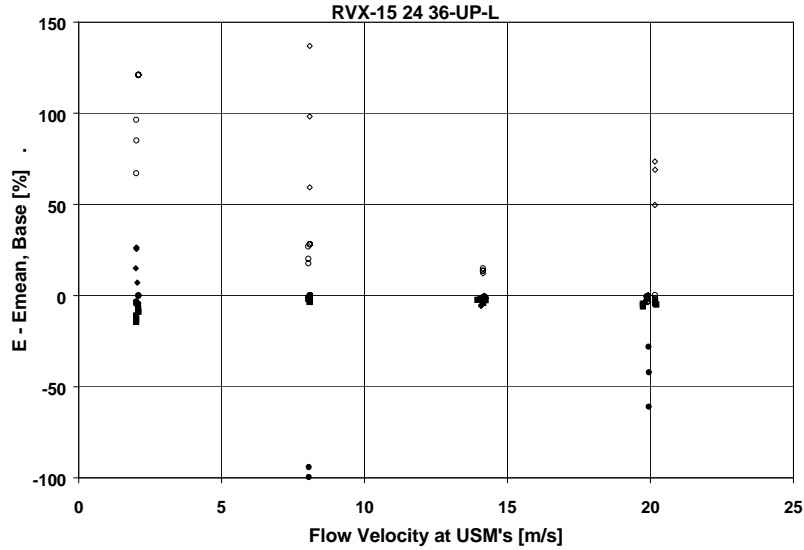
Fig. 6.19. USM's meter error shifts downstream of non-silent regulator RVX.
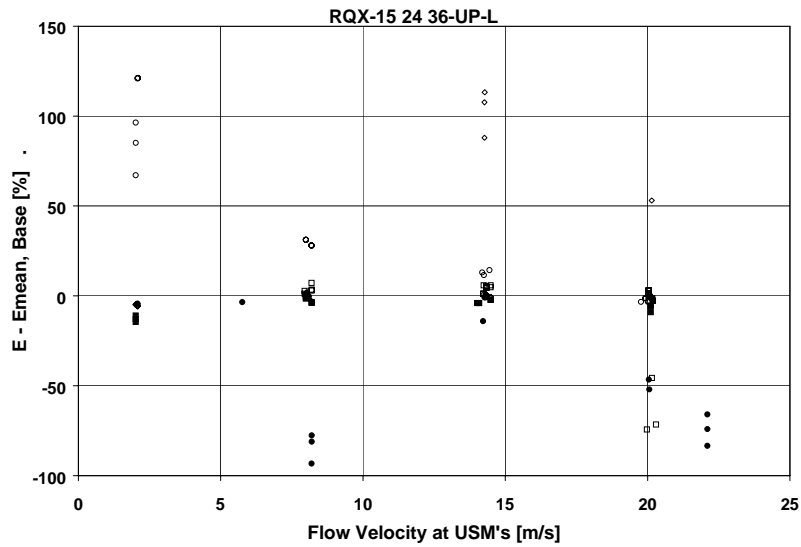
Fig. 6.20. USM's meter error shifts downstream of silent regulator RQX.

With the non-silent RVX regulator the individual performance number P_i ranges from 34 to 87, and mean performance number P_m is 64 with a standard deviation of 22, and with the silent RQX regulator P_i ranges from 25 to 83; P_m is 58 with a standard deviation of 24.

When the USM's are located near the middle of the test section, which is closer to the regulator, more meters stop functioning, or are functioning less. Mean performance numbers P_m in these cases are: 53 with the non-silent RVX regulator and 49 with the silent regulator.

6.5   Discussion

Before drawing conclusions, one should bear in mind the following:

- The situations tested here will always differ from field situations, and not only by the type and size of the regulator. For example the pipe work near the regulator (bends, valves, reducers etc.) has great influence on the noise that is measured in a certain position, due to reflection and/or absorption of noise. The pressure and flow control in the test installation (see Section 6.2.1) may influence the measured noise too. This work bears no illusion of being complete, but is more intended to make a step forward towards understanding USM's in noisy conditions.

- Immunity from noise is a subject for new developments for many meter manufacturers. In the past years, a great deal of work has been spent on this. Although this target has not been attained yet, many improvements have already been made.

- All experiments were performed with single path meters. For observing meter behaviour in noisy conditions only this is sufficient. However, for example when meter failure is not complete, the performance of a multi-path USM may be better than described in this paper.

- There is no "best meter". All meter characteristics, such as performance in pulsating flow, response times, maximum flows, error handling, and not to forget immunity from noise are a result of the specific combination of mechanical construction, path dimensions, techniques of sending and detecting of signals, signal analysis, filtering, etc. Many of these characteristics may also be influenced by a number of user-set parameters. For example: during the experiments, one meter kept on operating in almost all test conditions, albeit at the expense of large output variations; another meter was clearly indicating when it was failing, but if it was operating the output was highly reliable (no significant error shift nor variations). This makes it difficult to compare USM's, and select a "best one". A user should identify his specific conditions and needs, and select a meter accordingly.

6.6   Conclusions (for Part A)

- In-duct sound measurements near a Mokveld regulator were performed in which a "non-silent" RVX and a "silent" RQX internal cage were used. The regulator with RQX cage produces indeed considerable less audible noise outside the pipe, but more ultrasonic noise inside the pipe than with the RVX cage.

- The measured mean sound pressures of the noise fit logarithmically with the product of flow rate through and pressure difference across the regulator.

- Downstream of the regulator more noise was measured than upstream, and also relatively more low frequency noise.

- With distance the noise decays exponentially, and this decay is stronger for higher frequencies. The exponent C is larger upstream than downstream, which is a result of the frequency distribution: upstream relatively more higher frequency noise was registered.

- USM's may behave differently when subjected to noise: 4 different categories of behaviour were described. Many factors, including user-set parameters, influence the type of behaviour a meter adopts in a given situation.

- In general, a USM functions better when it is mounted upstream from the regulator, where the sound pressure is considerably less, and the operational pressure is higher. Furthermore because of the frequency distribution, the noise decays a bit faster than downstream, thus the effect of shifting the meter away from the regulator is larger.

- The mean performance of all USM's with the non-silent regulator cage RVX is better than with the silent cage RQX.

- The worst case (USM's at close distance to RQX regulator) still resulted in a mean performance number of 49 %. The best case resulted in a mean performance number of 94 %. This indicates that it is indeed possible to measure gas flows with USM's in the vicinity of a regulator. However, at this moment not with all meters and not under all circumstances.

- The work described in this paper is far from complete. In order to get a full picture of noise generated by regulators, future research could perform similar experiments under different circumstances: other pressure reducing devices, different flow and pressure regimes, varying distances to the regulator, and studying the effect of other devices such as bends and diffusers in the flow.

- Manufacturers of USM's have done a great deal of work on immunity from noise, and have already reached a number of successes. Although several meters have shown very good performances, no meter is perfect under every condition. Further development will be necessary. From the users point of view, more co-operation between the manufacturers could be a good idea.

6.7   Acknowledgements

6.8   Notation

dP	Pressure difference across regulator	[bar]
E	Meter Error $(Q_{meter} - Q_{reference})/Q_{reference} * 100$ %	[%]
$E_{mean, Base}$	Mean Meter Error in baseline calibration at the same pressure	[%]
MSP	Mean Sound Pressure	[Pa]
P_i	Performance number for individual USM, based on all test conditions	[%]
P_m	Mean performance number for all USM's, based on all test conditions	[%]
USM	UltraSonic (gas flow) Meter	[-]
Q	Flow rate	[m^3/h (s)]
V	Valve position in percentage of maximum (=open)	[%]
x	Distance to regulator	[mm]

Tests are indicated with codes in the form RRR-FF-PP-N, or parts of these., which stands for:

RRR = RVX or RQX   Regulator with standard "non-silent" cage RVX or with "silent" cage RQX
FF =   9, 15, 24 or 36   Test pressure of 9, 15, 24 or 36 bar(a), and variable flow rate
FF =   LO or HI   Flow rate is LOw or High, 6800 or 17000 m^3/h (s), pressure variable
PP =   UP or DN   Regulator at UPstream or DowNstream end of the test section
N =   M, L   USM's spool piece at Medium or Long distance from regulator

Appendix 6.A

Table 6.A.1. Indication of local gas velocities in m/s at USMs for each flow rate as a function of pressure at USMs.

Flow rate in m^3/h(s)	USM's donwstream of regulator 9 bar(a)	USM's upstream of regulator 15 bar(a)	USM's upstream of regulator 24 bar(a)	USM's upstream of regulator 26 bar(a)
27000	32	19	12	8
22000	26	15	10	6
17000	20	12	7	5
12000	14	8	5	3
6800	8	5	3	2
1700	2	1	1	1

Part B: Ultrasonic meters and noise; A theoretical approach

6.9 Model of noise attenuation

The theoretical study describes the ultrasonic disturbances present in gas networks that impair the performance of ultrasonic flowmeters. The problem lies in the range of frequencies used by the meter probes for which there is little attenuation of ultrasonic noise.

The equation used to calculate the total attenuation of a plane wave in a thermo-viscous fluid can be broken down into two phenomena: "standard" attenuation which is the sum of attenuation due to fluid viscosity and of attenuation due to the effects of thermal conduction, and attenuation due to a relaxation phenomenon which has a dispersive aspect and which modifies the speed of sound.

Hence, total attenuation can be written in the form [6.20], [6.21]:

$$\alpha_{total} = \alpha_{standard} + \alpha_{relaxation}$$

$$\alpha_{standard} = \frac{\omega^2}{2\rho C_0^3}\left[(\lambda + 2\mu) + \frac{(\gamma-1)K}{C_p}\right] \quad \text{and} \quad \alpha_{relaxation} = \frac{\pi}{2C_0}\left|\frac{(\gamma-1)^2}{\gamma}F_v\frac{\frac{f^2}{f_c}}{1+\left(\frac{f}{f_c}\right)^2}\right| \tag{6.1}$$

where : ω : pulse $= 2\pi f$ (rad/s)
         ρ : density (kg/m^3)

λ : volumetric viscosity (Pa.s)
μ : shear viscosity (Pa.s)
K : thermal conductivity (W/m.K)
C_p : specific heat at constant pressure (J/kg.k)
C_0 : speed of sound in the gas (m/s)
γ : ratio of specific heats.

From this model, the values of the attenuation depend on several thermodynamic coefficients related to the gas characteristics and also to the wave frequency.

The mathematical model developed was validated with air, in atmospheric conditions, at the University of Bordeaux laboratory, using a pair of transducers. These were installed on a special bench. They could be drawn on their axis in such a way as to change the distance between them. The values of wave attenuation obtained from the theoretical model were compared with the measurements carried out on the bench. The values were close enough to validate the mathematical model developed for the study.

Fig. 6.21 shows the results obtained from the model, at 15°C, using TROLL gas characteristics. The total attenuation remains very low for wave frequencies below 150kHz, and becomes very high for frequencies higher than 500kHz.

Using high frequencies may allow to attenuate the ultrasonic disruptive sound in gas transmission pipes even more if the noise source is far from the flow meter. Of course, the transducers must supply a good signal to noise ratio for these high frequencies.
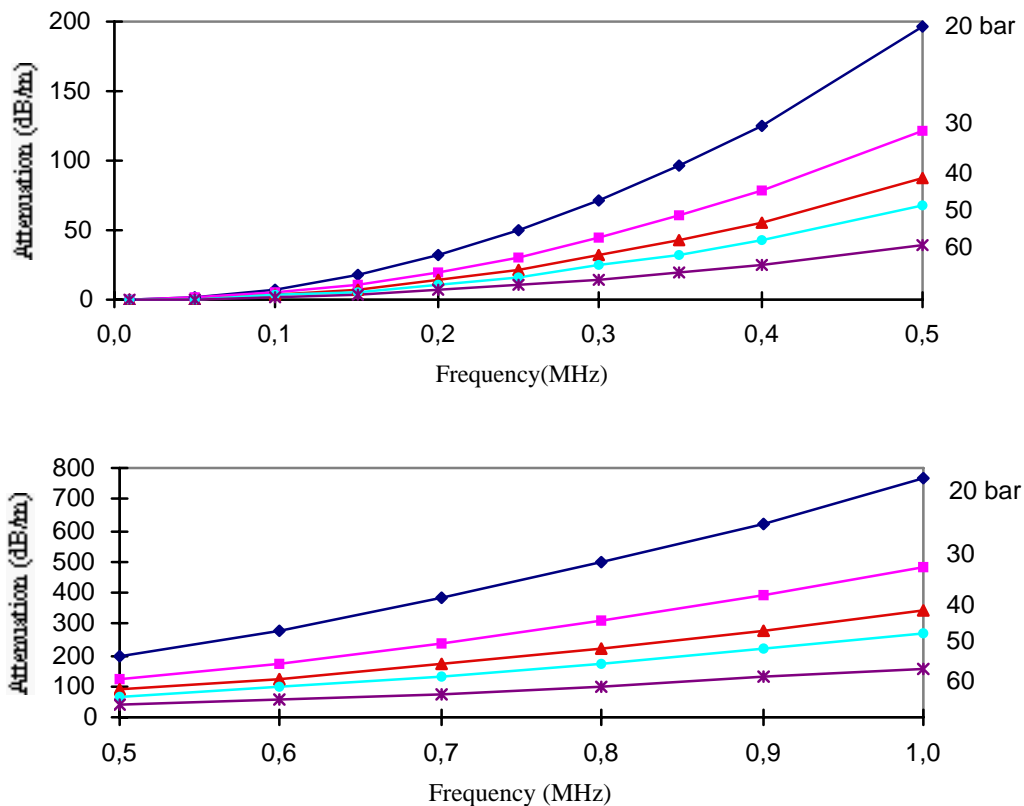
Fig. 6.21. Total attenuation in TROLL gas. (a) 0 – 0.5Mhz; (b) 0.5 - 1MHz.

6.10   Ultrasonic wave propagation along pipes

The effect of the structural vibrations is studied using the phenomenon of Lamb waves generated in pipelines walls. The starting point for the study of elastic modes of propagation in a cylinder is the integration of the equations of movement by means functions and potential vectors using a similar approach to one applied to plates [6.22], [6.23].

The dimensions of the network pipes allow approximating tubes as plates and thus applying the theory of propagation of Lamb waves in infinite plates to pipelines. The propagation of elastic vibrations in thin plates is very different from that of simple longitudinal and transverse bulk waves. The ultrasounds propagate through the plates in the form of Lamb waves which can exist in an infinite number of modes. These waves are all dispersive.

For a given frequency, several modes can exist in the structure and Fig. 6.22 shows dispersion curves of modes propagating in a 10 mm-thick steel plate placed in vacuum.
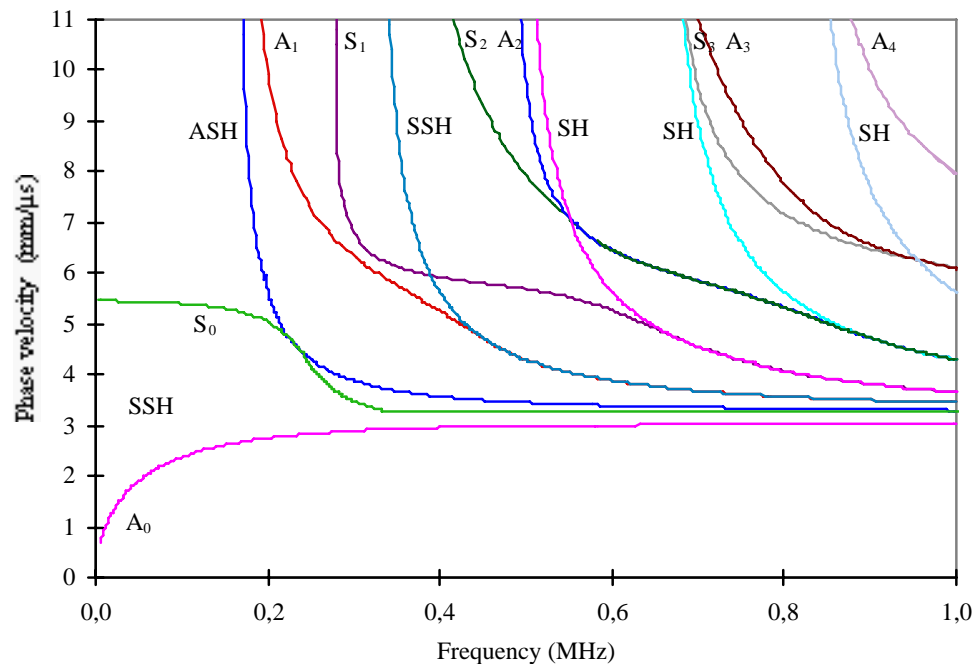
Fig. 6.22. Phase velocity of Lamb modes in a 10 mm-thick steel plate placed in vacuum.

These Lamb waves may affect the ultrasonic meters due to the structural vibrations they generate but not to the acoustic noise they create. The higher the frequency, the more the cylindrical structure of the pipeline is subjected to vibrations. To determine the displacement field of the structure reacting to a given force, a solution may be found using the finite-element method.

However, in the ultrasonic domain, the displacement field is usually in the order of few tenth of Angstrom. So the effect of the structural vibrations they generate must be negligible compared to the mechanical vibrations existing in the pipelines.

6.11   Sources of ultrasonic noise in gas transmission pipes

Very few references were found in literature to predict ultrasonic noise amplitudes and frequencies generated by pressure reducers. From previous experience, the frequency of the noise due to mechanical vibrations of the pressure governor remains at a frequency lower than 3kHz. Thus, the main source of ultrasonic waves should be gas turbulence and gas expansion.

The model developed in the reference [6.24] predicts noise level from the aerodynamic sources due to gas expansion. It was obtained from the classic acoustic energy equations and the sonic flow regime models which represents only one type of pressure reduction operating mode. The ultrasonic noise level depends on upstream (1) and downstream (2) conditions of pressure, P, and density, ρ, on the flow rate, Q_m, and on the acoustic intensity produced by the type of the regulator.

It can be expressed in the following form :

$$\text{lev (dB)} = 10 \log_{10} \left(\frac{\alpha Q_m (\kappa P)_1 \sqrt{(\kappa P \rho)_2}}{\rho_1 (\kappa_1 + 1)} \right) + 10 \log_{10} \left(\frac{K}{r^2} \right) \tag{6.2}$$

where
K : constant coefficient and $\kappa = C_p/C_v$ for real gas,
α depends on the opening, the size and the type of regulator used,
r is the distance between the noise generator and the measure.

According to the model, at the same distance the noise must increase with the flow rate and the upstream and downstream pressures. This first theoretical approach does not integrate the frequency dependence. However from previous experience, the noise seems to be deeply dependent on the frequency. Thus in a future work, it will be necessary to express a model to investigate the noise effect at the working frequency of meter probes.

Chapter 7

Uncertainty analysis of multipath
ultrasonic transit time gas flow meters

Per Lunde[*], Kjell-Eivind Frøysa[*] and Magne Vestrheim[**]

[*] *Christian Michelsen Research AS (CMR), Bergen, Norway*
[**] *University of Bergen, Dept. of Physics, Bergen, Norway*

Abstract

An uncertainty model for calculation of the relative expanded uncertainty of USMs has been developed in conformity with recommended procedures for expression of uncertainty [7.1]; [7.2]. The model has been implemented in a PC program, *GARUSO* Version 1.0. The propagation of input uncertainties of gas parameters, geometry parameters, transit time parameters and the integration technique is accounted for, including correlated and uncorrelated contributions to the USM measurement uncertainty. The program is used in an example uncertainty analysis of a 4-path 12" USM with Gauss-Jacobi quadrature and asymmetric criss-cross arrangement of paths. The present description of the uncertainty model is a condensed outline of the description given in [7.3], in which further details can be found.

7.1   Introduction

7.1.1   Background

For fiscal gas metering stations, a measured value is to be accompanied with a statement of the uncertainty of the measured value. In general, an uncertainty analysis is needed to establish the measurement uncertainty of the metering station. The uncertainty analysis is to account for the propagation of all input uncertainties which influence significantly on the uncertainty of the station. These are the uncertainty of the gas meter in question (e.g. one or several USMs), the uncertainty of the reference meter used by the flow calibration laboratory at which the gas meter was calibrated, uncertainties of additional measurements and models used (e.g. pressure and temperature measurements, Z-factor estimates), etc. In this context, the uncertainty of the gas meter (e.g. the USM) is represented by a single value, the expanded uncertainty (or relative expanded uncertainty) of the gas meter.

For the USM isolated, the measured output value of the USM is also to be accompanied with a statement of the uncertainty of the measured value. To establish the expanded uncertainty of the USM measurement, an uncertainty analysis of the USM is required, describing the propagation of input uncertainties to the USM measurement. The purpose of the uncertainty analysis is to establish the measurement uncertainty of the USM for operational use.

Until now, the calibration procedure for USMs consists of a combination of dry calibration and flow calibration.

If the USM is flow calibrated in a flow calibration facility, AGA-9 [7.4] recommends that the USM shall meet specific minimum measurement performance requirements before the application of any calibration factor adjustment. These requirements (deviation limits), which are shown in Fig. 7.1, therefore in practice represent dry calibration requirements. To further reduce a meter's measurement uncertainty, a calibration factor may be used in addition, based on the flow calibration. The amount of calibration-factor adjustment should be within the deviation limits stated by Fig. 7.1 [7.4].

If the USM is *not* flow calibrated (only dry calibrated), AGA-9 recommends that the manufacturer shall provide sufficient test data confirming that each meter shall meet the minimum performance requirements shown in Fig. 7.1.
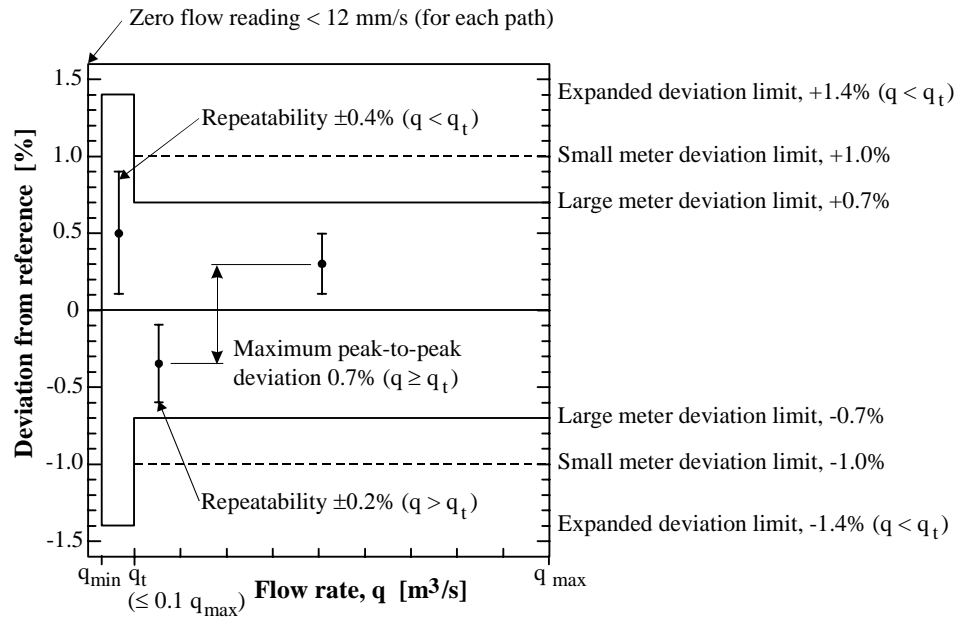
Fig. 7.1 Minimum performance requirements for USMs, as specified by AGA-9 [7.4].

The flow calibration is usually limited, for economical and practical reasons. Consequently, in the field, a number of effects may appear which have not necessarily been accounted for in the dry calibration or flow calibration. This may include installation conditions (bends, pipe roughness, flow conditioners, etc.), possible deposits at transducers and pipe wall, wear, noise effects (pressure regulation valves, etc.), possible changes in transducer time delay and electronic/cable time delay (pressure, temperature and long-time drift effects), etc. In general an uncertainty analysis will be needed to evaluate the influence of such effects on the meter's measurement uncertainty under operational conditions.

AGA-9 states that the manufacturers should provide an uncertainty analysis to demonstrate that their field verification tests[39] are sufficient to validate the meter's specified physical and electrical performance characteristics. The manufacturer should make reference to the uncertainty method used in this analysis.

---

39 For operation in the field, AGA-9 recommends that the manufacturer shall provide a written field verification test procedure to the operator that will allow the USM to be functionally tested to ensure that the meter is operating properly. These procedures may include a combination of a zero-flow verification test, sound velocity measurement analysis, individual path measurement analysis, internal inspection, dimensional verification and other mechanical or electrical tests [7.4] (Chapter 8).

It is also well-known that the USM technology has inherent potentials of being used with a dry calibration only, and that some manufacturers are already discussing the possibility of avoiding flow calibration and use dry calibration only, and claim sufficient accuracy with such a concept [7.5]. However, a possible reduced dependency of flow calibratrion in the future will necessitate the establishment of a totally new chain of traceability to international standards for the USM measurement. Today, the traceability is achieved through the accreditation of the flow calibration laboratory. With a possible reduced dependence on flow calibration, and an increased dependency on dry calibration, the traceability of the individual meter manufacturer's dry calibration procedures will become much more important and critical than today, especially for transit time dry calibration. This involves both (1) the measurement uncertainty of the dry calibration methods, (2) change of the dry calibration parameters with operational conditions (pressure, temperature, gas composition and transducer distance, relative to at dry calibration conditions), and (3) the contributions of such dry calibration uncertainties to the total USM measurement uncertainty. Today USM measurement technology is not at a level where the traceability of the dry calibration methods has been proved.

For reasons such as outlined above, it was recommended in the GERG TM 8 [7.6] that, on request, the manufacturer shall be able to supply an uncertainty analysis for a specific meter for a given installation. The uncertainty analysis shall handle the significant error contributions in the meter, and must therefore include effects of geometry measurements, electronics, transducers, transit time detection and integration technique. The applied integration technique shall be theoretically evaluated on a predetermined set of symmetrical and asymmetrical axial flow velocity profiles agreed on between the users and the manufacturers. The applied integration technique shall be evaluated for presence of non-axial (transversal) flow velocity components (e.g. swirl or cross flow), including influence of orientation of the acoustic paths relative to the axial and transversal flow profiles.

Based on the recommendations of the GERG TM 8, the participants in the GERG US meter project initiated the development of a relatively comprehensive uncertainty model for USMs, named *GARUSO* Version 1.0 [7.3].

At the time of that initiative, there was no established or accepted method available for calculation of the uncertainty of USMs. To establish an accepted method, the intention was to develop an uncertainty model which: (1) to a large degree is meter type independent, and (2) is in accordance with accepted international standards and recommendations, such as [7.1] (cf. also [7.8], [7.9], [7.10], which are documents based on [7.1] and [7.7]).

An important question relates to which "level" of input uncertainties that should be used for the uncertainty analysis. For several reasons, it may be argued that the propagation of uncertainties should be described from "the bottom" level, from the basic measurements, as explained in the following.

Firstly, in order to be able to investigate the influence of field operation effects which are not accounted for in the dry calibration or flow calibration (see above), the input uncertainties to the uncertainty model must be specified at a sufficiently "basic level" of input quantities and uncertainties. That means, at the level of gas parameters, geometry parameters and transit time contributions, cf. Chapter 3. One important reason for this is that some essential transit time contributions are uncorrelated, while others are correlated, and if such effects are not accounted for, the model may not be so relevant and useful in practice.

Secondly, the uncertainty model should be cabable of propagating the measurement uncertainties of the dry calibration method, as well as possible changes of the dry calibration parameters with operational conditions (pressure, temperature, gas composition, and transducer distance), if these are not corrected for in the USM. Consequently, input uncertainties have to be specified at the level of dry calibration parameters, i.e., geometry parameters and transit time contributions.

Thirdly, it is often of interest to use an uncertainty model in sensitivity studies, and in such applications the objective should be to model *all* input uncertainties which influence on the meter's total measurement uncertainty (also those influencing on the dry calibration result). The uncertainty model *GARUSO* has been developed along such lines.

7.1.2   Scope of Work

The scope of work for Task 2 of the GERG project was [7.3] (a) development of an uncertainty model for USMs, (b) implementation of the model in a PC program, *GARUSO* Version 1.0, and (c) to use the model in an example uncertainty analysis of a 12" USM.

To constitute a relatively general model, a meter type independent uncertainty model was to be established (preferably). Moreover, the study was restricted to USMs configured with paths in parallel planes (parallel chords, cf. Chapter 3). To avoid overlap with the work reported in Chapter 4 (Task 1), the part of Task 2 which is related to integration methods, was further restricted to studying only a fully developed turbulent flow velocity profile (power law) with no transversal flow components[40], and implementation of an option offering Gauss-Jacobi integration and a user defined integration method. Further details are given in [7.3]. Later extensions[41] relative to Version 1.0 of *GARUSO* have not been included in the present description.

7.1.3   Procedure, terminology and symbols

The procedure used here for evaluating and expressing uncertainty is basically the procedure recommended by the *Guide* [7.1], and conforms with the proposed revision of ISO 5168 [7.2]. Other reference documents used as a basis for the work include the VIM [7.7], EAL-R2 [7.8], and [7.9].

With respect to expression of uncertainties, the following notation is used: An *estimated value* of an input quantity, x, is denoted $\hat{x}$, and an *estimated value* of an output quantity, y, is denoted $\hat{y}$. The *standard uncertainty* of an input estimate, $\hat{x}$, is denoted $u(\hat{x})$; the *combined standard uncertainty* of an output estimate, $\hat{y}$, is denoted $u_c(\hat{y})$; and the *expanded uncertainty* of an output estimate, $\hat{y}$, is denoted $U(\hat{y})$, where $U(\hat{y}) = k \cdot u_c(\hat{y})$. k is the coverage factor, and $k = 2$ corresponds to a 95 % confidence level. The *relative standard uncertainty* of an input estimate, $\hat{x}$, is denoted E_x, where $E_x = u(\hat{x})/|\hat{x}|$. The *relative combined standard uncertainty* of an output estimate, $\hat{y}$, is denoted E_y, where $E_y = u_c(\hat{y})/|\hat{y}|$. The symbol E_y is used also for the *relative expanded uncertainty* of an output estimate, $\hat{y}$, i.e. $E_y = U(\hat{y})/|\hat{y}|$. The meaning of E_y in each context should be clear from the text.

---

[40] Hence, the study of asymmetric, distorted axial flow velocity profiles and transverse flow (e.g. swirl and cross-flow) were omitted from Task 2 of the GERG project on USMs (and thus from *GARUSO* Version 1.0).

   However, in a later CMR upgrade of *GARUSO* (Version 2.0), the program is being upgraded to account for all of the five uncertainty contributions $E_{Ida}, E_{I\ell a}, E_{Ids}, E_{I\ell s}$ and $E_{I\phi s}$ (cf. Section 7.2.5), i.e., to account also for the effects of asymmetric distorted flow profiles and transverse flow (e.g. swirl and cross-flow). The upgraded model uses either computational fluid dynamics (CFD) calculations of 3D flow velocity profiles as input (axial and transverse flow velocity components, at various installation conditions with pipe bends), or (optionally) analytical flow velocity profiles (mathematical expressions).

[41] Cf. Footnote 40.

7.2.   USM uncertainty model

The functional relationship for USM measurement of the volume flow rate at standard conditions, Q, is given by Eqs. (3.8)-(3.12). Similar expressions apply for the flow rate at line conditions, q, and average flow axial velocity at line conditions, $\bar{v}_A$, cf. Eq. (3.1). For measurement of q or $\bar{v}_A$, the measurement uncertainty of a USM depends on:

(1) Geometry parameters for the USM spoolpiece, and their uncertainties (pipe diameter, lateral chord positions, path inclination angles, pressure and temperature corrections),

(2) Transit time parameters and their uncertainties (time detection, cable/electronics/transducer time delay, Δt-correction, change of dry calibration values with P, T and gas, diffraction time shift, noise effects, possible transducer deposit effects, transducer cavity effects, flow velocity profile effects (sound refraction), sound velocity fluctuations due to turbulent temperature fluctuations, flow velocity fluctuations due to turbulence effects, effects of possible beam reflection at the pipe wall), and

(3) The **integration method** and its uncertainties (numerical discretisation effects (finite number of acoustic paths), uncertainties in lateral chord positions and beam inclination angles, non-parallelity of chords, as well as the capability of the integration method to integrate different (symmetric and asymmetric) flow velocity profiles (with both axial and transversal flow components), for relevant **installation conditions** (bend configurations, pipe roughness, possible flow conditioners, pressure regulation valves, etc.).

For conversion of the measured volumetric flow rate at line conditions, q, to volumetric flow rate at standard conditions, Q, additional uncertainty contributions have to be accounted for:

(4) Gas parameters and their uncertainties: pressure, temperature, Z-factor. (Gas parameters are measured/estimated externally of the USM, and do not influence on the USM reading itself.)

Within the limitations specified by the scope of work for the project (cf. Section 7.1.2), the propagation of these input uncertainty contributions to constitute the relative expanded uncertainty of the USM is described in the following, on basis of the functional relationship for the USM described in Chapter 3, Eqs. (3.8)-(3.15). For compactness in presentation, only the main expressions of the uncertainty model are given here; - for the derivation of the expressions as well as for further details and interpretation, it is referred to [7.3].

7.2.1   The relative expanded uncertainty

With reference to Eq. (3.8), the relative expanded uncertainty of the estimate $\hat{Q}$ is modelled as [7.3]

$$E_Q = k\sqrt{E_m^2 + E_I^2} \tag{7.1}$$

where E_m is the **"estimation uncertainty"** (the contribution to the *relative combined standard uncertainty* of the estimate $\hat{Q}$, due to use of *estimated* (measured) values for the input quantities), and E_I is the **"integration uncertainty"** (the contribution to the *relative combined standard uncertainty* of the

estimate $\hat{Q}$, due to use of the *finite-sum integration* formula instead of the integral). The contributions to E_m and E_I are discussed in the following.

7.2.2 Contributions to the relative "estimation uncertainty", E_m

From Eq. (3.8), it can be shown [7.3] that the relative "estimation uncertainty" E_m is approximately given by

$$E_m^2 \approx E_P^2 + E_T^2 + E_Z^2 + E_{Z0}^2 + s_R^2 E_R^2 + \sum_{i=1}^{N} \left[s_{yi}^2 E_{yi}^2 + s_{\phi i}^2 E_{\phi i}^2 \right]$$

$$+ \frac{1}{N_{ave}} \sum_{i=1}^{N} \left[s_{t1i}^2 (E_{t1i,U}^{(n,U)})^2 + s_{t2i}^2 (E_{t2i,U}^{(n,U)})^2 \right] + \sum_{i=1}^{N} \left[s_{t1i}^2 (E_{t1i,U}^{(n,C)})^2 + s_{t2i}^2 (E_{t2i,U}^{(n,C)})^2 \right] \qquad (7.2)$$

$$+ \sum_{i=1}^{N} \left[s_{t1i} E_{t1i,C}^{(n)} + s_{t2i} E_{t2i,C}^{(n)} \right]^2 .$$

Here, E_P, E_T, E_Z, E_{Z0} are the *relative standard uncertainties* of the input estimates $\hat{P}, \hat{T}, \hat{Z}, \hat{Z}_0$, respectively (gas parameters), and $E_R, E_{yi}, E_{\phi i}$ are the *relative standard uncertainties* of the input estimates $\hat{R}, \hat{y}_i, \hat{\phi}_i$, respectively, for path no. i (geometry parameters). These terms are discussed in Section 7.2.3.

$E_{t1i,U}^{(n,U)}$ and $E_{t2i,U}^{(n,U)}$ are the relative combined standard uncertainties of those contributions to the upstream and downstream transit time estimates $\hat{t}_{1i}^{(n)}$ and $\hat{t}_{2i}^{(n)}$, respectively, which are **uncorrelated** with respect to upstream and downstream propagation, and also **uncorrelated** with respect to the N_{ave} "shots" (for a given propagation direction of path no. i).

$E_{t1i,U}^{(n,C)}$ and $E_{t2i,U}^{(n,C)}$ are the relative combined standard uncertainties of those contributions to the upstream and downstream transit time estimates $\hat{t}_{1i}^{(n)}$ and $\hat{t}_{2i}^{(n)}$, respectively, which are **uncorrelated** with respect to upstream and downstream propagation, but **correlated** with respect to the N_{ave} "shots" (for a given propagation direction of path no. i).

$E_{t1i,C}^{(n)}$ and $E_{t2i,C}^{(n)}$ are the relative combined standard uncertainties of those contributions to the upstream and downstream transit time estimates $\hat{t}_{1i}^{(n)}$ and $\hat{t}_{2i}^{(n)}$, respectively, which are **correlated**. The correlated and uncorrelated uncertainty contributions related to the transit time estimates are further described in Section 7.2.4.

$s_R, s_{yi}, s_{\phi i}, s_{t1i}, s_{t2i}$ are the *relative (non-dimensional) sensitivity coefficients* for the sensitivity of the estimate $\hat{Q}$ to the input estimates $\hat{R}, \hat{y}_i, \hat{\phi}_i, \hat{t}_{1i}, \hat{t}_{2i}$, respectively, given as

$$s_R = \frac{1}{|\hat{Q}|} \sum_{i=1}^{N} \hat{Q}_i \left(2 + \frac{1}{1 - (\hat{y}_i / \hat{R})^2} \right), \qquad s_{yi} = -sgn(\hat{y}_i) \frac{\hat{Q}_i}{|\hat{Q}|} \frac{(\hat{y}_i / \hat{R})^2}{1 - (\hat{y}_i / \hat{R})^2},$$

(7.3a)

$$s_{\phi i} = -\frac{\hat{Q}_i}{|\hat{Q}|} \frac{2|\hat{\phi}_i|}{\tan 2\hat{\phi}_i}, \qquad\qquad s_{t1i} = \frac{\hat{Q}_i}{|\hat{Q}|} \frac{\hat{t}_{2i}}{\hat{t}_{1i} - \hat{t}_{2i}}, \qquad\qquad s_{t2i} = -\frac{\hat{Q}_i}{|\hat{Q}|} \frac{\hat{t}_{1i}}{\hat{t}_{1i} - \hat{t}_{2i}}, \qquad (7.3b)$$

respectively, where for convenience in notation, the definititions

$$\hat{Q} \equiv \sum_{i=1}^{N} \hat{Q}_i , \qquad\qquad \hat{Q}_i \equiv 7200\pi\hat{R}^2 \frac{\hat{P}T_0\hat{Z}_0}{P_0\hat{T}\hat{Z}} w_i \frac{\sqrt{\hat{R}^2 - \hat{y}_i^2}\,(\hat{t}_{1i} - \hat{t}_{2i})}{\hat{t}_{1i}\hat{t}_{2i}\,|\sin 2\hat{\phi}_i\,|} , \qquad (7.4)$$

have been used.

7.2.3   Contributions to the relative "geometry parameter uncertainties"

From Eqs. (3.9), it can be shown [7.3] that the relative "geometry parameter uncertainties" become

$$E_R = \sqrt{E_{KT}^2 + E_{KP}^2 + (E_{R0}^{round})^2 + (E_{R0}^{m})^2 + (E_{R}^{wax})^2} ,$$

$$E_{yi} = \sqrt{E_{KT}^2 + E_{KP}^2 + E_{yi0}^2} , \qquad\qquad (7.5)$$

$$E_{\phi i} = \sqrt{\left(\frac{\sin 2\hat{\phi}_{i0}}{2\hat{\phi}_{i0}}\right)^2 E_{KP}^2 + E_{\phi i0}^2} , \qquad\qquad i = 1, ..., N,$$

respectively. Here, E_{KT} and E_{KP} are the relative standard uncertainties of the temperature and pressure correction factor estimates, $\hat{K}_T$ and $\hat{K}_P$, respectively. E_{R0}^{m}, E_{R0}^{round} and E_{R}^{wax} are the relative standard uncertainties of the pipe radius estimate, $\hat{R}_0$ due to, respectively, measurement uncertainty in dry calibration, the pipe's out-of-roundness, and possible deposits (e.g. wax, liquid, scaling) at the pipe wall. E_{yi0} and $E_{\phi i0}$ are the relative standard uncertainties of, respectively, the lateral chord position estimate of path no. i, $\hat{y}_{i0}$, and the inclination angle estimate of path no. i, $\hat{\phi}_{i0}$, at dry calibration, due to machining and measurement uncertainties.

7.2.4   Contributions to the relative "transit time uncertainties"

For upstream propagation of path no. i (cf. Fig. (3.2)), it can be shown [7.3] that the relative combined standard uncertainty of the contributions to the upstream transit time estimate $\hat{t}_{1i}^{(n)}$ is given by

$$(E_{t1i,C}^{(n)})^2 = (E_{t1i,0}^{eltr})^2 + (E_{t1i}^{eltr})^2 + (E_{t1i}^{cavity})^2 +$$
$$\qquad\qquad (E_{t1i}^{wax})^2 + (E_{t1i}^{profile})^2 + (E_{t1i,C}^{c})^2 + (E_{t1i,C}^{v})^2 + (E_{t1i}^{refl})^2$$
(7.6a)

$$(E_{t1i,U}^{(n,U)})^2 = (E_{t1i,U}^{c})^2 + (E_{t1i,U}^{v})^2 + (E_{t1i}^{noise})^2 , \qquad\qquad (7.6b)$$

$$(E_{t1i,U}^{(n,C)})^2 = (E_{t1i}^{d})^2 . $$
(7.6c)

Similarly, for downstream propagation of path no. *i*, the relative combined standard uncertainty of the contributions to the downstream transit time estimate $\hat{t}_{2i}^{(n)}$ is given by

$$(E_{t2i,C}^{(n)})^2 = \left(\frac{\hat{t}_{1i}}{\hat{t}_{2i}} \right)^2 \left[(E_{t1i,0}^{eltr})^2 + (E_{i,0}^{\Delta tcor})^2 + (E_{t1i}^{eltr} - E_i^{\Delta tcor})^2 \right] + (E_{t2i}^{cavity})^2 +$$

$$(E_{t2i}^{wax})^2 + (E_{t2i}^{profile})^2 + (E_{t2i,C}^{c})^2 + (E_{t2i,C}^{v})^2 + (E_{t2i}^{refl})^2$$

(7.7a)

$$(E_{t2i,U}^{(n,U)})^2 = (E_{t2i,U}^{c})^2 + (E_{t2i,U}^{v})^2 + (E_{t2i}^{noise})^2 \ ,$$

(7.7b)

$$(E_{t2i,U}^{(n,C)})^2 = (E_{t2i}^{d})^2 \ \ .$$

(7.7c)

The terms appearing in Eqs. (7.6) and (7.7) are defined as follows (where subscript *i* denotes acoustic path no., *i = 1, ..., N*; and subscript *1* or *2* denotes upstream or downstream propagation of path no. *i*, respectively):

$E_{t1i,0}^{eltr}$: Relative standard uncertainty of the estimate $\hat{t}_{1i,0}^{eltr}$ (**time delay from cables, electronics, transducers and diffraction time shift** (transmit and receive)), due to measurement uncertainty of $\hat{t}_{1i,0}^{eltr}$ **at dry calibration conditions**.

E_{t1i}^{eltr} : Relative standard uncertainty of the estimate $\hat{t}_{1i,0}^{eltr}$ (**time delay from cables, electronics, transducers and diffraction time shift** (transmit and receive)), due to an unknown **change** of $\hat{t}_{1i,0}^{eltr}$ at line conditions relative to the measured dry calibration value. Such a change may be induced e.g. by pressure, gas temperature, air temperature, changed diffraction time shift (e.g. by transducer distance), ageing (drift) and wear.

$E_{i,0}^{\Delta tcorr}$: Relative standard uncertainty of the estimate $\Delta \hat{t}_{i,0}^{corr}$ (the **Δt-correction**), due to measurement uncertainty of $\Delta \hat{t}_{i,0}^{corr}$ **at dry calibration conditions**.

$E_{i}^{\Delta tcorr}$: Relative standard uncertainty of the estimate $\Delta \hat{t}_{i,0}^{corr}$ (the **Δt-correction**), due to an unknown **change** of $\Delta \hat{t}_{i,0}^{corr}$ at line conditions relative to the measured dry calibration value. Such a change may be induced e.g. by pressure, gas temperature, air temperature, changed diffraction time shift (e.g. by transducer distance), ageing (drift) and wear.

E_{t1i}^{cavity} , E_{t2i}^{cavity} : Relative combined standard uncertainty of the estimate $\hat{t}_{i}^{cavity}$ (**transducer cavity time delay**). Caused by uncertainties of the estimated cavity distance, $\hat{L}_{ci}$, and sound velocity, $\hat{c}_i$.

E_{t1i}^{wax} , E_{t2i}^{wax} : Relative standard uncertainties of the estimates $\hat{t}_{1i}^{m,n}$ and $\hat{t}_{2i}^{m,n}$ due to change in the detected transit time caused by possible **deposits** (e.g. wax, liquid, scaling) **at the two transducer front faces** (transmit and receive).

$E_{t1i}^{profile}$, $E_{t2i}^{profile}$: Relative standard uncertainty of the estimates $\hat{t}_{1i}^{m,n}$ and $\hat{t}_{2i}^{m,n}$ due to change in the detected transit time caused by refraction of sound caused by the (unknown) **curved (non-uniform) flow velocity profile** in the pipe (cf. Fig. 3.5).

$E_{t1i,C}^{v}$, $E_{t2i,C}^{v}$: Relative standard uncertainties of the estimates $\hat{t}_{1i}^{m,n}$ and $\hat{t}_{2i}^{m,n}$ due to change in the detected transit time caused by **turbulent flow velocity fluctuations (systematic effects)**.

$E_{t1i,U}^{v}$, $E_{t2i,U}^{v}$:   Relative standard uncertainties of the estimates $\hat{t}_{1i}^{m,n}$ and $\hat{t}_{2i}^{m,n}$ due to random time fluctuations in the detected signal caused by **turbulent flow velocity fluctuations (random effects)**.

$E_{t1i,C}^{c}$, $E_{t2i,C}^{c}$:   Relative standard uncertainties of the estimates $\hat{t}_{1i}^{m,n}$ and $\hat{t}_{2i}^{m,n}$ due to change in the detected transit time caused by fluctuating sound velocity (caused by **turbulent temperature fluctuations) (systematic effects)**.

$E_{t1i,U}^{c}$, $E_{t2i,U}^{c}$:   Relative standard uncertainties of the estimates $\hat{t}_{1i}^{m,n}$ and $\hat{t}_{2i}^{m,n}$ due to random time fluctuations in the detected signal caused by fluctuating sound velocity (caused by **turbulent temperature fluctuations) (random effects)**.

E_{t1i}^{noise} , E_{t2i}^{noise} :   Relative standard uncertainties of the estimates $\hat{t}_{1i}^{m,n}$ and $\hat{t}_{2i}^{m,n}$ due to random time fluctuations in the detected signal caused by **incoherent noise**.

E_{t1i}^{refl} , E_{t2i}^{refl} :   Relative standard uncertainties of the estimates $\hat{t}_{1i}^{m,n}$ and $\hat{t}_{2i}^{m,n}$ due to change in the detected transit time caused by possible **beam reflection at the pipe wall** (relevant only for reflecting-path meter types).

E_{t1i}^{d} , E_{t2i}^{d} :   Relative standard uncertainty of the estimates $\hat{t}_{1i}^{m,n}$ and $\hat{t}_{2i}^{m,n}$ due to the **time detection method**. Due to e.g. the finite clock resolution, A/D conversion (sampling frequency and finite bit resolution), and possible averaging over zero crossings in the detected signal.

For the time delay of the transducer cavities, one finds, from Eqs. (3.15),

$$(E_{t1i}^{cavity})^2 \approx (E_{t2i}^{cavity})^2 \approx \left(\frac{\hat{t}_i^{cavity}}{\hat{t}_{1i}}\right)^2 \left\{ E_{KTP}^2 + E_{ci}^2 + \left(\frac{\hat{L}_{pi0}}{\hat{L}_{ci0}}\right)^2 E_{Lpi0}^2 + \right.$$

$$\left. \left(\frac{\hat{L}_{i0}}{\hat{L}_{ci0}}\right)^2 \left[\left(\frac{\hat{\phi}_{i0}}{tan\,\hat{\phi}_{i0}}\right)^2 E_{\phi i0}^2 + \left(\frac{1}{1-\left(\hat{y}_{i0}/\hat{R}_0\right)^2}\right)^2 \left([E_{R0}^{round}]^2 + [E_{R0}^m]^2 \right) + \left(\frac{\left(\hat{y}_{i0}/\hat{R}_0\right)^2}{1-\left(\hat{y}_{i0}/\hat{R}_0\right)^2}\right)^2 E_{yi0}^2 \right] \right\}$$

(7.8)

where E_{KTP} , E_{ci} and E_{Lpi0} are the relative standard uncertainties of the pressure and temperature corection factor estimate, $\hat{K}_{TP}^*$, the sound velocity estimate, $\hat{c}_i$, and the transducer distance estimate, $\hat{L}_{Pi0}$, respectively. Note that in the case of no cavity correction (transducers mounted with their front face centre point "flush" with the pipe wall), E_{t1i}^{cavity} and E_{t2i}^{cavity} will still be different from zero, since they still include contributions from the relative input uncertainties E_{Lpi0} , E_{yi0} , $E_{\phi i0}$, E_{R0}^{round} and E_{R0}^m , as discussed in Section 3.9

Expressions for $E_{t1i}^{profile}$ and $E_{t2i}^{profile}$ (flow velocity profile effects, causing sound refraction) are given in [7.3], for a fully developed turbulent axial flow velocity profile (power law, cf. Fig. 3.5b). For this profile, the effect is relatively small, but may be larger for other profiles, cf. Figs. 3.5c and d. Expressions for $E_{t1i,C}^{v}, E_{t2i,C}^{v}, E_{t1i,U}^{v}$ and $E_{t2i,U}^{v}$ (representing turbulent temperature fluctuations); and $E_{t1i,C}^{c}, E_{t2i,C}^{c}, E_{t1i,U}^{c}$ and $E_{t2i,U}^{c}$ (representing turbulent flow velocity fluctuation) are also given in [7.3]. These expressions are all relatively complex, and have therefore not been included in the present Monograph. (However they are all accounted for in the program *GARUSO*.)

7.2.5   Contributions to the relative "integration uncertainty", E_I

From Eq. (3.8) it can be shown [7.3] that the "integration uncertainty" E_I is given by

$$E_I^2 = E_{Ida}^2 + E_{I\ell a}^2 + E_{Ids}^2 + E_{I\ell s}^2 + E_{I\phi s}^2 \qquad (7.9)$$

where, for the **axial flow:**

E_{Ida} :   Relative standard uncertainty of the estimate $\hat{Q}$ due to the *numerical discretization* of the axial volume flow rate integral, Eq. (3.2), for *ideal (nominal) positioning of the acoustic paths (as specified) and no transversal flow components* (cf. Fig. 7.2a),

$E_{I\ell a}$:   Relative combined standard uncertainty of the estimate $\hat{Q}$ due to the *standard uncertainties of the lateral chord positions (y_i)*, and the *standard uncertainties of the parallelity of the chords* (cf. Fig. 7.2c and d),

and, for the **transversal flow:**

E_{Ids} :   Relative standard uncertainty of the estimate $\hat{Q}$ due to *incomplete compensation of transversal flow (e.g. swirl and cross flow)*, when assuming *ideal positioning of the acoustic paths* (cf. Fig. 7.2a),

$E_{I\ell s}$:   Relative combined standard uncertainty of the estimate $\hat{Q}$ due to *incomplete compensation of transversal flow (e.g. swirl and cross flow)*, caused by the *standard uncertainties of the lateral chord positions (y_i)*, and the *standard uncertainties of the parallelity of the chords* (cf. Fig. 7.2c and d),

$E_{I\phi s}$:   Relative combined standard uncertainty of the estimate $\hat{Q}$ due to *incomplete compensation of transversal flow (e.g. swirl and cross flow)*, caused by the *standard uncertainties of the inclination angles (ϕ_i)* (cf. Fig. 7.2e)

In general, each of the five uncertainty contributions $E_{Ida}, E_{I\ell a}, E_{Ids}, E_{I\ell s}$ and $E_{I\phi s}$ are to account for the influences of:

(1) the integration method used (the use of a finite number of paths);

(2) a wide selection of axial flow velocity profiles (such as the uniform profile, fully developed turbulent flow profile, and asymmetric disturbed profiles of relevant installation conditions (bends, etc.)); and

(3) the orientation of the USM relative to the axial flow velocity profile (meter rotation 0-360°).

7.3   Program *GARUSO*, Version 1.0

The uncertainty model outlined in Section 7.2 has been implemented in a PC program, *GARUSO* Version 1.0 (*GA*s *R*ate *U*ncertainty ultra*SO*nic) [7.3]. Input parameters to the program are (cf. Chapter 3 and Section 7.2): the gas parameters (P, T, Z, Z_0, c_i); the geometry parameters ($R_0, y_i, \phi_i, L_{ci}, i = 1, ..., N$); the integration technique (w_i, no. of paths (N), and type of method); the standard uncertainties of the gas parameter estimates, geometry parameter estimates and transit time contributions; the number of averagings in the time averaging interval (N_{ave}), and the coverage factor (k).
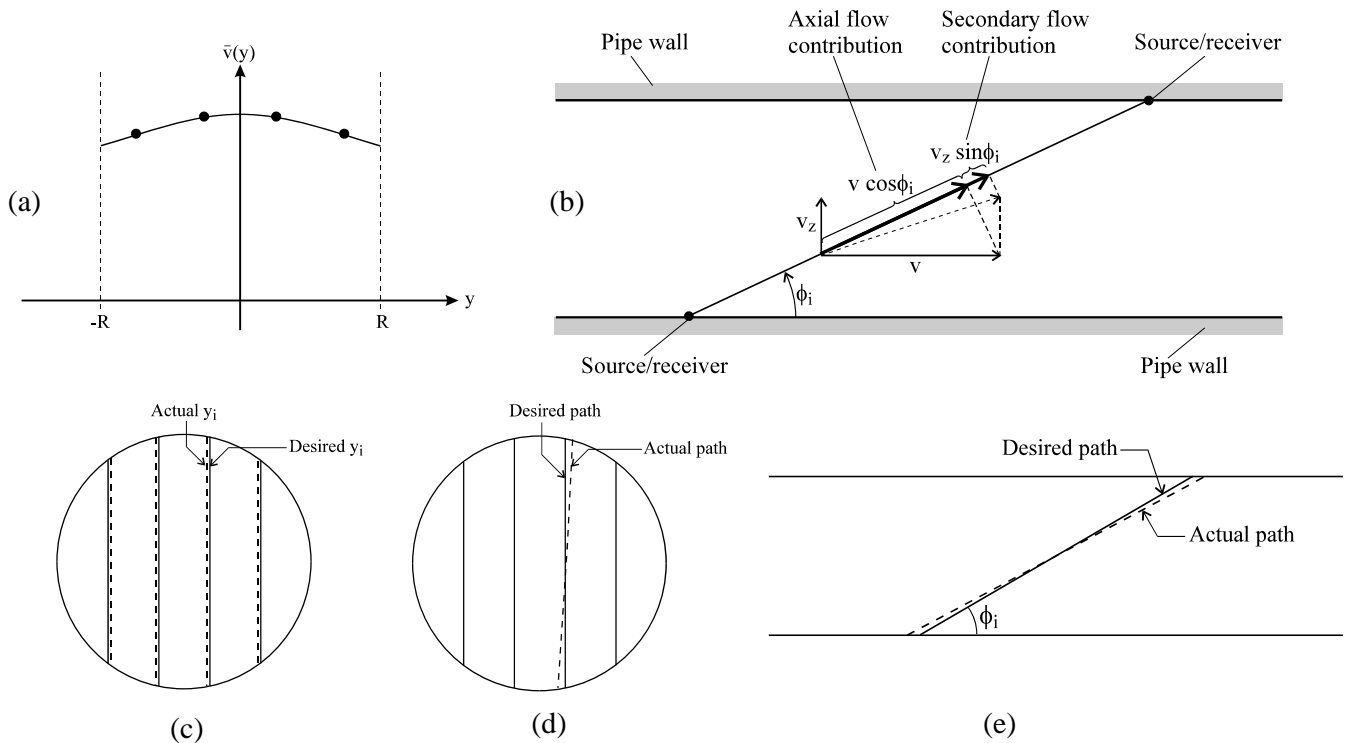
Fig. 7.2. Illustration of effects which influence on the integration uncertainty, E_I: (a) spatial sampling of $\overline{v}_A$ (4-path USM example); (b) transversal flow (illustrated for the simplified example of a uniform axial flow velocity profile, cf. Fig. 3.5a); (c) uncertaintiy of the lateral position estimate , $\hat{y}_i$; (d) non-parallellity of chords; and (e) uncertainty of the inclination angle estimate, $\hat{\phi}_i$, $i = 1, ..., N$.

The program calculates the relative expanded uncertainty of (1), the axial flow velocity at line conditions ($\overline{v}_A$), (2) the axial volume flow rate at line conditions (q), or (3) the axial volume flow rate at standard reference conditions (Q). Uncertainty calculations can be performed for one gas flow velocity (or rate) or for a range of velocities (or rates) (i.e., for a range of $\overline{v}_A$, q or Q).

In accordance with the scope of work for Task 2 (cf. Section 7.1.2), all effects of transversal flow on the integration uncertainty have been omitted here, so that in the uncertainty analysis and Version 1.0 of the program *GARUSO*, the simplifying approach $E_{Ids} = E_{I\ell s} = E_{I\phi s} = 0$ has been used, cf. Section 7.2.5. Moreover, for the effects of axial flow profiles on the integration uncertainty, the terms E_{Ida} and $E_{I\ell a}$ are limited to accounting for a fully developed turbulent flow profile (the power law profile) only, so that effects of asymmetric distorted flow profiles have been omitted from *GARUSO* Version 1.0 [42].

The following integration methods have been built into this first version of *GARUSO*: Gauss-Jacobi integration, and a user defined integration. At present the model describes parallel chords; however, a generalisation to non-parallel chords is straightforward, provided the integration weights used in the meter are known.

7.4   Uncertainty analysis for a 12" USM

---

[42] However, in a later CMR upgrade of *GARUSO* (Version 2.0), such limitations are being removed, cf. Footnote 40.

Table 7.1 shows an example of an uncertainty analysis of an artificial 12" USM with four paths arranged in an "asymmetric criss-cross" configuration, using a Gauss-Jacobi integration method [7.3].

Part (a) of Table 7.1 gives the input estimates, the standard uncertainties of the input estimates, and the calculated contribution to E_Q of Eq. (7.1) from each input uncertainty considered isolated[43] (calculated at three flow velocities, $\hat{\bar{v}}_A$ = 0.4, 1 and 20 m/s)[44].

Part (b) of the table gives the calculated "estimation uncertainties" $E_{m\bar{v}A}$, E_{mq} and E_{mQ} (i.e., E_m of Eq. (7.2) calculated for $\hat{\bar{v}}_A$, $\hat{q}$ and $\hat{Q}$, respectively), and the "integration uncertainty" E_I (from Eq. (7.9)). (Note that E_I is relatively small in this example, since only a fully developed turbulent flow profile is considered, and effects of transversal flow are omitted.)

Part (c) of Table 7.1 gives the calculated relative expanded uncertainties $E_{\bar{v}A}$, E_q and E_Q (i.e., Eq. (7.1) calculated for $\hat{\bar{v}}_A$, $\hat{q}$ and $\hat{Q}$, respectively), at a 95 % confidence level ($k = 2$). Fig. 7.3 gives the same $E_{\bar{v}A}$, E_q and E_Q calculated as a function of flow velocity, $\hat{\bar{v}}_A$, in the range 0.4 to 20 m/s.

For a dicussion of the results, it is referred to [7.3].
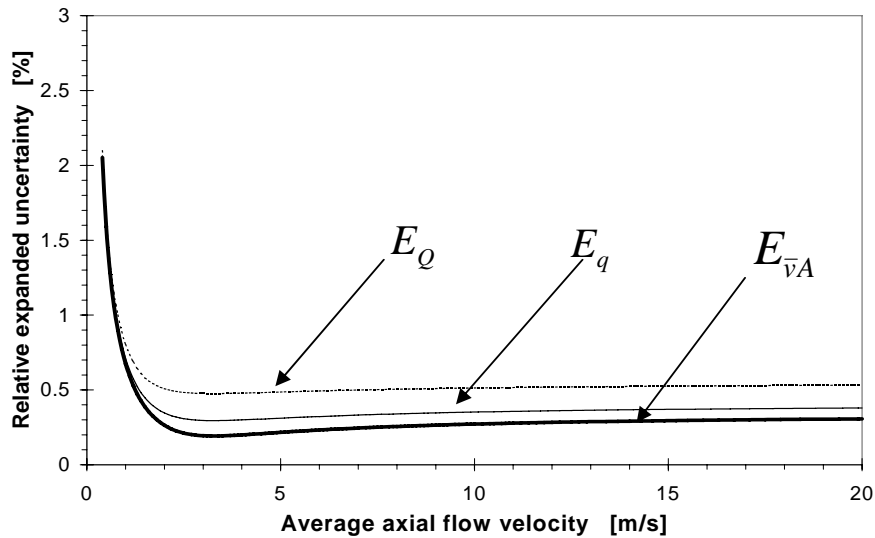
Fig. 7.3 Example of output generated by the *GARUSO* program, for a 12" USM configured with four paths arranged in an "asymmetric criss-cross" configuration, using a Gauss-Jacobi quadrature. The figure shows the relative expanded uncertainties of (a) the average axial flow velocity (lower curve, thick solid line), $E_{\bar{v}A}$, (b) the axial volume flow rate at pipe conditions (mid curve, thin solid line), E_q, and (c) the axial volume flow rate at standard reference conditions (upper curve, dotted line), E_Q.

---

[43] Note that when the contribution to E_Q from each input uncertainty is considered *isolated* (as in Table 7.1a), cancellation effects in the propagation of uncertainties due to systematic effects (correlated uncertainties) are not accounted for. However, this is accounted for in Table 7.1b and c.

[44] With respect to the technical basis for the examples of input estimates and input uncertainties used here, it is referred to [7.3].

Table 7.1. Uncertainty analysis of an artificial 12" USM with four paths arranged in an "asymmetric criss-cross" configuration and with a Gauss-Jacobi quadrature.

(a)		Estimate (or quantity)		Std. uncertainty (or rel. std. uncertainty)			Output — Isolated contribution to E_Q (rel. combined std. uncertainty) (k=1)		
		Symbol	Value	Symbol	Value	Type	0.4 m/s	1 m/s	20 m/s
Input	Gas parameters	$\hat{P}$	200 bar	$u(\hat{P})$	0.09 bar	B	0.05 %	0.05 %	0.05 %
		$\hat{T}$	50 °C	$u(\hat{T})$	0.06 °C	B	0.02 %	0.02 %	0.02 %
		$\hat{Z}$	0.796	E_Z	0.17 %	B	0.17 %	0.17 %	0.17 %
		$\hat{Z}_0$	0.997	E_{Z0}	0.06 %	B	0.06 %	0.06 %	0.06 %
		$\hat{c}_i$	477 m/s	$u(\hat{c}_i)$	1 m/s	B	0.01 %	0.01 %	0.01 %
	Geometry parameters	$\hat{D}_0$	26 cm	$u(\hat{D}_0^m)$	0.007 mm	B	0.01 %	0.01 %	0.01 %
				$u(\hat{D}_0^{round})$	0.075 mm	B	0.11 %	0.11 %	0.11 %
				E_{KT}	0.016 %	B	0.06 %	0.06 %	0.06 %
				E_{KP}	0.011 %	B	0.04 %	0.04 %	0.04 %
				E_{KTP2}	0.02 %	B	0.001 %	0.001 %	0.001 %
		$\hat{y}_{10}/\hat{R}_0$	- 0.8090	$u(\hat{y}_{10})$	0.012 mm	B			
		$\hat{y}_{20}/\hat{R}_0$	- 0.3090	$u(\hat{y}_{20})$	"	B			
		$\hat{y}_{30}/\hat{R}_0$	0.3090	$u(\hat{y}_{30})$	"	B	0.01 %	0.01 %	0.01 %
		$\hat{y}_{40}/\hat{R}_0$	0.8090	$u(\hat{y}_{40})$	"	B			
		$\hat{\phi}_{10}$	- 45°	$u(\hat{\phi}_{10})$	0.058 °	B			
		$\hat{\phi}_{20}$	45°	$u(\hat{\phi}_{20})$	"	B			
		$\hat{\phi}_{30}$	- 45°	$u(\hat{\phi}_{30})$	"	B	0.11 %	0.11 %	0.11 %
		$\hat{\phi}_{40}$	45°	$u(\hat{\phi}_{40})$	"	B			
		$\hat{L}_{c10}$	20 mm						
		$\hat{L}_{c20}$	20 mm						
		$\hat{L}_{c30}$	20 mm						
		$\hat{L}_{c40}$	20 mm						
				$u(\hat{L}_{p10})$	0.012 mm	B			
				$u(\hat{L}_{p20})$	"	B			
				$u(\hat{L}_{p30})$	"	B	0.004 %	0.004 %	0.004 %
				$u(\hat{L}_{p40})$	"	B			
		w_1	0.1382						
		w_2	0.3618						
		w_3	0.3618						
		w_4	0.1382						
	Transit time parameters	$\hat{t}_{1i,0}^{eltr}$		$u(\hat{t}_{1i,0}^{eltr})$	140 ns	B			
		$\hat{t}_{1i}^{eltr}$		$u(\hat{t}_{1i}^{eltr})$	520 ns	B			
		$\Delta\hat{t}_{i,0}^{corr}$		$u(\Delta\hat{t}_{i,0}^{corr})$	12 ns	B	1.84 %	0.68 %	0.05 %
		$\Delta\hat{t}_i^{corr}$		$u(\Delta\hat{t}_i^{corr})$	29 ns	B			
				$u(\hat{t}_{1i}^{wax})$	0 ns	B	0 %	0 %	0 %
				$u(\hat{t}_{2i}^{wax})$					

Parameter	Value	Symbol	Value	Type	0.4 m/s	1 m/s	20 m/s
			0 ns	B			
		$u(\hat{t}_{1i}^{refl})$	0 ns	B	0 %	0 %	0 %
		$u(\hat{t}_{2i}^{refl})$	0 ns	B			
		$u(\hat{t}_{1i}^{d})$	3 ns	B	0.29 %	0.12 %	0.006 %
		$u(\hat{t}_{2i}^{d})$	3 ns	B			
		$u(\hat{t}_{1i}^{profile})$			≈ 0 %	≈ 0 %	0.001 %
		$u(\hat{t}_{2i}^{profile})$					
N_{ave}	200						
		E_v^{fluct}	1 %	B	0.005 %	0.005 %	0.005 %
		$u(\hat{T}_{fluct})$	0.01 °C	B	0.01 %	0.005 %	0.001 %
		$u(\hat{t}_{1i}^{noise})$	11 ns	A	0.08 %	0.03 %	0.002 %
		$u(\hat{t}_{2i}^{noise})$	11 ns	A			
Integration method	Fully developed turbulent axial flow velocity profile, no transversal flow	E_{Ida}		B			
		$E_{I\ell a}$		B			
		E_{Ids}		B	0 %	0 %	0 %
		$E_{I\ell s}$		B	0 %	0 %	0 %
		$E_{I\phi s}$		B	0 %	0 %	0 %

(b)

Output		Symbol	Symbol	Rel. combined std. uncertainty (k=1)		
				0.4 m/s	1 m/s	20 m/s
Output	Flow velocity	$\hat{\bar{v}}_A$	$E_{m\bar{v}A}$	1.02 %	0.33 %	0.14 %
	Volume flow rate (line cond)	$\hat{q}$	E_{mq}	1.03 %	0.35 %	0.18 %
	Volume flow rate (std. cond.)	$\hat{Q}$	E_{mQ}	1.05 %	0.40 %	0.26 %
	Integration		E_I	0.06 %	0.06 %	0.06 %

(c)

Output		Symbol	Symbol	Relative expanded uncertainty (k=2, 95 % c.l.)		
				0.4 m/s	1 m/s	20 m/s
Output	Flow velocity	$\hat{\bar{v}}_A$	$E_{\bar{v}A} = k\sqrt{E_{m\bar{v}A}^2 + E_I^2}$	2.05 %	0.67 %	0.31 %
	Volume flow rate (line cond)	$\hat{q}$	$E_q = k\sqrt{E_{mq}^2 + E_I^2}$	2.06 %	0.71 %	0.38 %
	Volume flow rate (std. cond.)	$\hat{Q}$	$E_Q = k\sqrt{E_{mQ}^2 + E_I^2}$	2.10 %	0.80 %	0.53 %

7.5 Conclusions and perspectives

An uncertainty model has been developed for calculation of the relative expanded uncertainty of USMs configured with parallel chords. The procedure for evaluation of uncertainty recommended by the *Guide* [7.1] has been used as the primary basis for the model, in conformity with the proposed revision of ISO 5168 [7.2]. The uncertainty model has been implemented in a PC program, *GARUSO* - Version 1.0. The propagation of input uncertainties of gas parameters, geometry parameters, transit time parameters and the integration technique is accounted for, including correlated and uncorrelated contributions to the USM measurement uncertainty.

Using this program, a simplified and limited uncertainty analysis has been carried out for a 12" 4-path USM. Examples of estimated input uncertainties have been used to examine the relative expanded uncertainty of the meter. By "simplified uncertainty analysis" is meant that a sufficiently complete investigation regarding input values for all the uncertainty terms appearing in the uncertainty model has not been made here. The present analysis therefore serves more as an example on use of the uncertainty model.

The uncertainty model and the program *GARUSO* are considered to serve as useful tools in several applications:

- Analysis of the influence on the USM measurement uncertainty of field operation effects which are not accounted for in the dry calibration or the flow calibration (cf. Section 7.1).

- In possible future calibration scenarios based on a reduced dependence on flow calibration and increased dependence on dry calibration, a reliable and accepted method for describing the propagation of the uncertainties related to the dry calibration measurements will be necessary, to achieve traceability of the USM measurement. This involves both the measurement uncertainties of the dry calibration method(s) in use, and the change of the dry calibration parameters with environmental conditions (P, T, gas composition, transducer distance). The present uncertainty model accounts for the propagtion of such input uncertainties.

- Identification of critical factors in USMs, and to investigate the propagation of input uncertainties for selected quantities of specific interest, either isolated or in a combined manner. The program may thus be used for sensitivity analyses.

However, at the time of the present study the knowledge on important details of ultrasonic flow metering systems does not seem to be sufficiently developed to be able to carry out such investigations to the required level of accuracy. In particular this concerns traceability and measurement uncertainty issues of the dry calibration methods. The measurement uncertainty of dry calibration methods needs to be addressed in further work. Further experience with and work on meters of this type, combined with use of the uncertainty model presented here, is expected to yield an improved basis in this respect.

The uncertainty model developed here is based on present-day "state of the art of knowledge" for meters of this type, and is not expected to be complete with respect to description of effects influencing on such meters. In particular, some issues of importance for further development and improvement of the uncertainty model include:

- The systematic effects of axial flow velocity profiles (symmetric and asymmetric) on the *measured transit times* should be investigated more closely, cf. Fig. 3.5. Only fully developed turbulent flow velocity profiles are accounted for in the uncertainty model at present. For distorted profiles and high velocities, such systematic effects may be significant (cf. footnote 5).

- The systematic effects of transversal flow on the measured transit times should be investigated more closely, cf. Section 3.4.1. The traditional functional relationship for USMs, Eq. (3.8), does not account for transversal flow.

- The influence of turbulent flow velocity fluctuations and turbulent temperature fluctuations on the measured transit times is described in the uncertainty model. However, better information on the order of magnitude of these turbulence terms is needed to evaluated whether they are significant to the USM uncertainty or not.

- Present-day USM technology is based on a simplifying (high-frequency) ray-tracing approximation, cf. Chapter 3.4.1. In practice, the acoustic beam does not propagate as a ray, or as a "bundle of rays". The systematic effects of a *finite* acoustic *beam* on the measured *transit times* should be investigated, using more accurate wave-theory descriptions of acoustic propagation in flow.

- At present, the uncertainty model assumes no net flow in the transducer cavities, which represents an approximation. The effects of flow in the cavities should be further investigated and accounted for by the uncertainty model.

In spite of such limiting factors, the present uncertainty model does account for a number of the important factors which influence on the uncertainty for meters of this type. With exception for the installation effect contributions to the "integration uncertainty" (transversal flow and disturbed axial flow velocity profiles, which were omitted from this part of the project (cf. section 7.1.2), but which are being included in a later version of *GARUSO*[45]), it is expected that the most important uncertainty contributions have been accounted for. Analysis of the effects of these factors on the meter uncertainty should be possible with the uncertainty model and the PC program developed here.

As an important conclusion from the work one may state that, in spite of the numerous factors which may potentially contribute to the uncertainty of USMs, the uncertainty model predicts a relative expanded uncertainty at a level which gives additional basis and support for today's tendency of increasingly taking USMs into use for fiscal metering of natural gas.

In connection with future work on the uncertainty model, two factors are mentioned here, in addition to the above discussion. A better basis for estimating realistic values for the input uncertainties is needed in order to estimate a realistic relative expanded uncertainty for the meter. This concerns in particular transit time parameters, such as the dry calibration parameters used for transit time correction. In addition, the uncertainty model has to be used and tested critically, preferably in combination with controlled experiments, in order to investigate the capabilities of the model to describe the propagation of input uncertainties in a realistic and relevant way, for the types of USM considered here. Such testing work may also turn out to be valuable as a basis for obtaining realistic estimates for the important input uncertainties.

---

[45] Cf. Footnote 40.

Chapter 8

Closing remarks

Gert H. Sloet[*] , Reidar Sakariassen[**] and Per Lunde[***]

[*] *N. V. Nederlandse Gasunie, Groeningen, The Netherlands*
[**] *Statoil K-Lab, Haugesund, Norway*
[***] *Christian Michelsen Research AS, Bergen, Norway*

Phase II of the "GERG project on Ultrasonic Meters" which is summarized in the present Monograph, represents a continuation of Phase I of the project, which was reported in the GERG TM 8 [8.1]. In that Monograph, a number of actions were identified and recommended to close the gap between the status of USM technology at that time (1995) and the industrial functional requirements. The recommended actions were grouped in "Flow testing" and "Technology" tasks, including (listed in arbitrary order):

(A) Flow testing:

- Testing of small and large meters (less than 6", larger than 24"),
- Wet gas effects (pilot installation, flow testing),
- P & T effects (10-150 bar, 20 to 55 $^{\circ}$C),
- Temperature difference effects (flowing gas - to - surrounding air),
- High flow rates of large meters,
- Reproducibility tests / long term effects,
- Influence of noise generated by pressure regulation valves (PRV),
- Effects of bends on meter sizes,
- Electronics and transducer exchange testing,
- "Plug-and-play" test.

(B) Technology:

- Measurement of acoustic parameters of natural gases (absorption, sound velocity, density),
- Effect of high CO_2 concentrations (absorption),
- Wet gas effects (theoretical and experimental investigations),
- Effects of deposits (transducers, pipe wall),
- Terminology and procedures for specification of USM uncertainty,
- Uncertainty model / analysis,
- Integration methods (standardised theoretical test of USM integration methods),
- Characterization and influence of PRV noise,
- Ultrasonic transducers (vibration and noise tests, (de)pressurization and heating/cooling tests, charactersation measurements over operational $P\&T$ range, linearity and reciprocity test, long time performance, specifications)
- Dry calibration (recommended procedure, stability of dry calibration over operational $P\&T$ range, possibility for reducing the need for flow calibration).

Among this relatively extensive list of recommended actions, four tasks were agreed on amongst the nine GERG companies participating in Phase II, for continued work under Phase II:

(1) A numerical investigation into the effect of non-ideal flow on the meter error,
(2) Uncertainty analysis of multipath ultrasonic transit time gas flow meters,
(3) The development of methods for characterization and testing of USM transducers under pressure,
(4) An experimental and theoretical investigation into the effect of noise on ultrasonic meters.

The reason for selecting these tasks was to increase the general knowledge about the concept of multipath ultrasonic meters. The four tasks are complementary. They address different contributions to the USM uncertainty, and provide improved knowledge on factors which influence on the USM uncertainty.

Under Task 1 (cf. Chapter 4), a numerical model, *Kalibra*, has been developed for numerical investigation of USM integration methods, and effects of non-ideal flow on the meter error. That means, the meter error of the flow rate Q due to numerical discretisation of the axial volume flow rate integral, Eq. (3.2) (i.e. the use of a finite number of discrete acoustic paths). In the context of the uncertainty model, this concerns the "integration uncertainty" contribution to the total USM uncertainty, E_I, cf. Chapter 7. Two of the contributions to E_I have been addressed here, namely the terms E_{ida} and E_{Ids}, defined in Section 7.2.5. For these two contributions, the effects of installation conditions (bends), and effects of orientation of the meter relative to the flow profile, are considered.

Under Task 2 (cf. Chapter 7), an uncertainty model has been developed for calculation of the relative expanded uncertainty of USMs when performing a dry calibration, in conformity with recommended ISO procedures for expression of uncertainty in measurement, and the proposed revision of ISO 5168. The model has been implemented in a PC program, *GARUSO* (Version 1.0). With this model the propagation of input uncertainties of gas parameters, geometry parameters, transit time parameters and the integration method can be simulated, accounting for correlated and uncorrelated input quantities. The model has been used in an example uncertainty analysis of a 4-path 12" USM configured with parallel paths in an asymmetric criss-cross arrangement, using the Gauss-Jacobi integration method.

Under Task 3 (cf. Chapter 5), methods for characterization and testing of USM transducers at elevated pressures, and over a temperature range, have been developed and used. The work addresses two types of transducer characteristics: (1) characteristics which are used for correction of transit times (dry calibration parameters), and (2) characteristics which are not used directly for correction of transit times, but which are still very important for the functionality and performance of the meter, including correction of transit times (should be in accordance with "expected normal behaviour" for the transducer type in question). These latter characteristics may also influence on the transit time corrections. Three transducers types from two USM manufacturers were characterised; up to 100 bar, at 15 and 50/60 °C.

Under Task 4 (cf. Chapter 6), en experimental and theoretical investigation into the effects of ultrasonic noise on ultrasonic flow meters, and propagation of noise along the pipe, is carried out. The effects of incoherent (non-synchronous) ultrasonic noise produced by pressure regulation valves (PRVs) are addressed. Transducers from six USM manufacturers was investigated in flow tests. The work shows that all ultrasonic meters are affected by ultrasonic noise and that increasing the distance between noise source and meter will reduce the problem.

The four tasks summarised in this Technical Monograph have undoubtly increased the general knowledge on certain important aspects and effects attributed to USMs, and pointed out directions to follow to increase the reliability and confidence on the use of USMs.

There are however areas related to these tasks which do require even more research, such as:

In relation to *Task 1* (USM integration method / installation effects):

- Introduction of the weight factors into the model will increase the confidence in such a model.

- The manufacturers are encouraged to provide more experimental data for a variety of installation conditions and a variety of meter dimensions.

- The manufacturers are also encouraged to be more open on the algoritms they have implemented for the integration and weighing of path velocities in order to be able to make better judgements on uncertainty effects caused by phenomena like wall roughness influences and non-ideal flow profiles.

- In Chapter 4, the contributions to the "integration uncertainty" E_I from numerical discretization of the flow integral have been addressed, represented in the uncertainty model of Chapter 7 by the relative uncertainty terms E_{Ida} and E_{Ids} (cf. Eq. (7.9)). The description of Chapter 4 should be extended to also cover the contributions to E_I from the uncertainties in lateral chord positions and inclination angles, $E_{I\ell a}$, $E_{I\ell s}$ and $E_{I\phi s}$. These may contribute significantly to the USM uncertainty[46].

- The effect of a *finite* acoustic *beam* on the *integration method* should also be investigated (spatial averaging).

In relation to *Task 2* (USM uncertainty model/analysis):

- At present the basis for estimating the input uncertainties to the uncertainty model is not sufficiently developed to provide a sufficiently reliable estimate of the USM measurement uncertainty. In particular, this concerns the uncertainties of the transit time parameters, e.g. related to dry calibration methods.

- Present-day USM technology is based on a simplifying (high-frequency) ray-tracing approximation, cf. Chapter 3.4.1. In practice, the acoustic beam does not propagate as a ray, or as a "bundle of rays". The systematic effects of a *finite* acoustic *beam* on the measured *transit times* should be investigated, using more accurate wave-theory descriptions of acoustic propagation in flow.

- Other factors related to further development of the uncertainty model are discussed in Section 7.5.

In relation to *Task 3* (Transducer characterization under pressure):

- A question of major importance relates to the traceability of the USM measurement to international standards. In possible future USM calibration scenarios based on a reduced dependence of flow calibration, the traceability of the dry calibration measurements becomes a far more important and critacal issue than for today's typical scenario, based on both dry calibration and flow

---

46 Modelling of these effects are available from other work, cf. Footnote 40.

calibration. This concerns the geometrical measurements as well as the time measurements of the dry calibration. In the dry calibration, the quantities $t_{1i,0}^{eltr}$ and $\Delta t_{i,0}^{corr}$ (or equivalent time corrections, cf. Section 3.8) are determined experimentally. Thus measurement uncertainties are associated with these estimates. If the USM is only calibrated "dry", the dry calibration measurements should be traceable, with a statement of measurement uncertainty. It seems as relatively little has been done in this field up to now, and this issue will need to be addressed in future development of USM technology for fiscal metering of gas.

- At present, the characterization measurements of Task 3 have been made up to 100 bar, and at 15 and 50/60 ^{o}C. These characterization measurements should be extended to cover a larger part of the operational *P&T* range; 10-200 bar, -25 to 55 ^{o}C.

- The measurements should also be extended to cover additional transducer characteristics, cf. Section 5.5.

In relation to *Task 4* (USM sensitivity to PRV noise):

- The measurements should be extended to similar experiments under different circumstances: other pressure reducing devices, different flow and pressure regimes, varying distances to the regulator, and studying the effect of other devices such as bends and diffusers in the flow.

In general, work will be needed also on other areas than those discussed above. It is important for the users of the technology also to encourage the manufacturer to increase the number of experimental data to reduce the lack of data mentioned above. This will undoubtfully increase the confidence in USMs for even more applications.

However, the users (i.e. the GERG group) feels that the most important matter now is to combine the current knowledge in such a way that engineering guidelines are developed also in those areas where there is largest uncertainty in the effect on USM and where existing standards and regulation are rather vague. This will most likely be the objective of a potential Phase 3 in USM investigation by the GERG group.

A collaborative project such as the "GERG Project on Ultrasonic Gas Flow Meters" reported here provides an excellent opportunity to advance this technology and to share the cost of doing so. It is not always easy for all parties to agree on the content of the research programmes, as inevitably each company has it's own priorities and expertise. However, the negotiation and compromises that are necessary to find agreement amongst the parties assists in directing the work towards the most important issues. It is important that work such as this, and information from actual operating experience be it good or bad, is shared amongst the industry so that suitable and unsuitable applications are identified.

Appendix

GERG Technical Monographs

TM 1   A.E. Humphreys: *Some Thermophysical Constants of Components of Natural Gas and Cognate Fluids*, TPC/1, 1986

TM 2   M. Jaeschke, S.Audibert, P. van Caneghem, A.E. Humphreys, R. Janssen-van Rosmalen, Q. Pellei, J.P.J. Michels, J.A. Schouten, C.A. ten Seldam: *High Accuracy Compressibility Factor Calculation for Natural Gases and Similar Mixtures by Use of a Truncated Virial Equation*, 1988

TM 3   M. Jaeschke, P. van Caneghem, M. Fauveau, A.E. Humphreys, R. Janssen-van Rosmalen, Q. Pellei: *GERG Round-Robin Test of Z-Meters, Burnett Apparatus and an Interferometric Device for pVT Measurements, 1989*

TM 4   M. Jaeschke, A.E. Humphreys: *The GERG Databank of High Accuracy Compressibility Factor Measurements*, 1990

TM 5   M. Jaeschke, A.E. Humphreys: *Standard GERG Virial Equation for Field Use. Simplification of the Input Data Requirements for the GERG Virial Equation – an Alternative Means of Compressibility Factor Calculation for Natural Gases and Similar Mixtures*, 1991

TM 6   M. Diritti, M. Arietti, H. Bellinga, M. Cannizzo, F.J. Delhez, F. Deneuve, D. Donat, W. Frankvoort., B. Harbrink, P.M.A. van der Kam, W. Kerkmann, R. Norman, P. Rombouts*: Intercomparison Exercise of High Pressure Test Facilities within GERG*, 1993

TM 7   M. Jaeschke and H.M. Hinze: *Supplement to the GERG databank of High-Accuracy Compression Factor Measurements*, 1996

TM 8   A. Lygre, P. Lunde, K.-E. Frøysa: *Present Status and Future Research on Multi-path Ultrasonic Gas Flow Meters*, 1995

TM 9   B. Harbrink, W. Kerkmann, J.L. De Schutter, D. Bawin, M. Tedeschi, V.M. Cannizzo, D. King, C. Tremel, V. De Laharpe, P.M.A. Van Der Kam, G.J. De Nobel, G.H. Sloet: *Perturbation Tests on Turbine Meters; Part 1: Meter Tests*, 1998

TM 10 B. Harbrink, W. Kerkmann, D. Vieth, J.L. De Schutter, D. Bawin, M. Tedeschi, V.M. Cannizzo, D. King, C. Tremel, V. De Laharpe, P.M.A. Van Der Kam, G.J. De Nobel, G.H. Sloet: *Perturbation Tests on Turbine Meters; Part 2: Profile Measurements*, 2000

References

Chapter 1:

[1.1] **Sakariassen, R.,** "Gas measurement by use of ultrasonic flowmeters". 19th World Gas Conference, Milan, 20-23 June 1994. International Gas Union, Round Table Committee C, Measurement Accuracy (IGU/RC7-94), 1994.

[1.2] **Bloemendaal, K. van, and Kam, P. M. A. van der:** "Installation effects on multi-path ultrasonic flow meters: the Ultraflow Project". Proc. of *The 12th North Sea Flow Measurement Workshop, Scotland, October 1994.*

[1.3] **Vulovic, F., Harbrink, B., and Bloemendaal, K. van:** "Installation effects on a multipath ultrasonic flow meter designed for profile disturbances". Proc. of *The 13th North Sea Flow Measurement Workshop*, *Lillehammer, Norway, October 23-26, 1995.*

[1.4] **Sakariassen, R.,** "Why we use ultrasonic gas flow meters". Proc. of *The 13th North Sea Flow Measurement Workshop, Lillehammer, Norway, October 23-26, 1995.*

[1.5] **Robbins, P.,** "Ultrasonic metering on an offshore gas platform". Proc. of *The 14th North Sea Flow Measurement Workshop, Peebles, Scotland, October 28-31, 1996.*

[1.6] **de Nobel, G. J. and Sloet, G. H.,** "Experience with ultrasonic flow meter at the Gasunie Export Stations". Proc. of *The 15th The North Sea Flow Measurement Workshop, Kristiansand, Norway, October 27-30, 1997.*

[1.7] **Agricola, J. B.,** "Gas well flowline measurement by ultrasonic flow meter (UFM)". Proc. of *The 15th North Sea Flow Measurement Workshop, Kristiansand, Norway, October 27-30, 1997.*

[1.8] **Coughlan, L., Colley, A., Jamieson, A. W.,** "Operational experience of multipath ultrasonic meters for fiscal gas service". Proc. of *The 16th North Sea Flow Measurement Workshop, Perthshire, Scotland, October 26-29, 1998.*

[1.9] **Folkestad, T.,** "Experience from Oseberg C with prototype 6" multi-path ultrasonic gas flowmeter in well developed flow, swirl flow and flow straigthened conditions, compared to an orifice gas flowmeter". Proc. of *The 16th North Sea Flow Measurement Workshop, Perthshire, Scotland, October 26-29, 1998.*

[1.10] **Sloet, G. H.,** "Bi-directional fiscal metering by means of ultrasonic meters". Proc. of *The 17th North Sea Flow Measurement Workshop, Oslo, Norway, October 25-28, 1999.*

[1.11] **Lygre, A., Lunde, P. and Frøysa, K.-E.** "Present status and future research on multi-path ultrasonic gas flow meters". GERG Tecnical Monograph No. 8, Groupe Européen de Recherches Gazières, Groeningen, The Netherlands (1995). Also issued as: CMR Report no. CMR-95-A10037, Christian Michelsen Research AS, Bergen (December 1995).

[1.12] **ISO,** "Measurement of fluid flow in closed cirquits - Methods using transit time ultrasonic flowmeters". ISO Technical Report ISO/TR 12765:1997, International Organization for Standardization, Genéve, Switzerland (1997).

[1.13]   **AGA-9**, "Measurement of gas by ultrasonic meters", A.G.A. Report no. 9, American Gas Association, Transmission Measurement Committee (June 1998).

[1.14]   **Daniel**, "The Daniel SeniorSonic gas flow meter", Sales brochure, Daniel Flow Products, USA (1999)

[1.15]   **KOS**, "The MPU 1200 ultrasonic gas flow meter", Sales brochure, Kongsberg Offshore AS, Norway (1999).

[1.16]   **Instromet**, "Ultrasonic gas flow meters", Sales brochure, Instromet International N.V., Belgium (1999).

[1.17]   **Lunde, P., Frøysa, K.-E., Fossdal, J. B. and Heistad, T.:** "Functional enhancements within ultrasonic gas flow measurement". Proc. of *The 17th North Sea Flow Measurement Workshop, Oslo, Norway, 25-28 October 1999.*

[1.18]   **NPD**, "Regulations relating to fiscal measurement of oil and gas etc.", Norwegian Petroleum Directorate, Stavanger, Norway (January 20, 1997).

[1.19]   **Lygre, A., Lunde, P. and Frøysa, K.-E.** "GERG project on ultrasonic flow meters", CMR Report no. CMR-95-F10026, Christian Michelsen Research AS, Bergen (October 1995). (Confidential.) (Extended version of [1.11].)

[1.20]   **van der Kam, P. M. A.:** "Present European Status and Future Research Plans for Multipath Ultrasonic Gas Flow Meters", AGA 1996 Operations Conference, May 19 - 22, 1996, Queen Elizabeth Hotel, Montreal, Quebec, Canada.

[1.21]   **Sloet, G. H.:** "Developments in multi-path ultrasonic gas flow meters". Proc. of *Practical Developments in Gas Flow Metering*, One day seminar, 7 April 1998, National Engineering Laboratory, East Kilbride, Scotland (1998).

[1.22]   **Wild, K.:** "A European collaboration to evaluate the application of multi-path ultrasonic gas flow meters", Proc. of *The 4th International Symposium on Fluid Flow Measurement, Denver, Colorado, USA, June 27-30, 1999.*

[1.23]   **Hüwener, T.:** "Numerical determination of measurement uncertainties for ultrasonic flow-meters under disturbed flow conditions", RG-report of project no. 990.400.4.1.30, Ruhrgas AG, Dorsten, Germany (1997).

[1.24]   **Lunde, P., Frøysa, K.-E. and Vestrheim, M.:** "*GARUSO* Version 1.0. Uncertainty model for multipath ultrasonic transit time gas flow meters", CMR Report no. CMR-97-A10014, Christian Michelsen Research AS, Bergen (September 1997).

[1.25]   **Lunde, P., Bø, R., Andersen, M., Vestrheim, M. and Lied, G.:** "GERG project on ultrasonic flow meters. Phase II - Transducer testing. Part 1: Measurement methods. Part 2: KOS transducers. Part 3: Daniel transducers", CMR Report no. CMR-99-F10018, Christian Michelsen Research AS, Bergen (April 1999). (Confidential.)

[1.26]   **Bloemendaal, K. v.:** "Ultrasonic meters and Noise Task 4 of the Second GERG Project on Ultrasonic Meters. Part I: General: Introduction, Test Set-Up, Conclusions. Part II: Results

sound measurements. Part III: Results US-meters", Gasunie Report, N. V. Nederlandse Gasunie, Groeningen, The Netherlands (1998).

[1.27]   **Brassier, P., Hosten, B., Castaings, M., and Vulovic, F.: "**Study of Ultrasonic Disturbances in Gas Pipelines", Université de Bordeaux and Gaz de France (December 1997).

[1.28]   **Hilgenstock, A., Hüwener, T. and Nath, B.:** "Kalibra$^{®}$ - A fast numerical method for determining installation effects in ultrasonic flowmeters", Proc., of *The 9th International Conference on Flow Measurement, FLOMEKO '98, Lund, Sweden.*

[1.29]   **Bloemendaal, K. and Sloet, G.:** "Ultrasonic meters and noise". Proc. of *The 16th North Sea Flow Measurement Workshop, Pertshire, Scotland, 26-29 October 1998.*

Chapter 2:

[2.1]   **AGA-9**, "Measurement of gas by ultrasonic meters", A.G.A. Report no. 9, American Gas Association, Transmission Measurement Committee (June 1998).

[2.2]   **Abromowitz, M. and Stegun, I.A.:** *Handbook of mathematical functions*, Applied Mathematics Series, Vol. 55 (National Bureau of Standards, Washington D.C., 1964). Reprinted by Dover Publications, Inc., New York, May 1968.

[2.3]   **ISO,** "Guide to the expression of uncertainty in measurement. First edition". International Organization for Standardization, Genéve, Switzerland (1995).

Chapter 3:

[3.1]   **Lunde, P., Frøysa, K.-E., and Vestrheim, M.:** "GARUSO version 1.0. Uncertainty model for multipath ultrasonic transit time gas flow meters", CMR report no. CMR-97-A10014, Christian Michelsen Research, Bergen, Norway (September 1997).

[3.2]   **ISO,** "Measurement of fluid flow in closed cirquits - Methods using transit time ultrasonic flowmeters". ISO Technical Report ISO/TR 12765:1997, International Organization for Standardization, Genéve, Switzerland (1997).

[3.3]   **AGA**, "Ultrasonic flow measurement for natural gas applications". Engineering Technical Note M-96-2-3, American Gas Association (A.G.A.), The Ultrasonic Metering Task Group of the Operating Section Transmission Measurement Committee (March 1996). (Also included as an Appendix in [AGA, 1998].)

[3.4]   **AGA-9**, "Measurement of gas by ultrasonic meters", A.G.A. Report no. 9, American Gas Association, Transmission Measurement Committee (June 1998).

[3.5]   **Daniel**, "The Daniel SeniorSonic gas flow meter", Sales brochure, Daniel Flow Products, USA (1999)

[3.6]   **KOS**, "The MPU 1200 ultrasonic gas flow meter", Sales brochure, Kongsberg Offshore AS, Norway (1999).

[3.7]   **Instromet**, "Ultrasonic gas flow meters", Sales brochure, Instromet International N.V., Belgium (1999).

[3.8] **Hallanger, A. and Johnsen, F.:** "CFD simulations of turbulent gas flow in pipes with bends", CMR Report no. CMR-99-F10085, Christian Michelsen Research AS, Bergen (December 1999). (Confidential.)

[3.9] **McCartney, M.L., Mudd, C.P. and Livengood, R.D**.: "A corrected ray theory for acoustic velocimetry". J. Acoust. Soc. Amer., **65**(1), 50-55 (January 1979).

[3.10] **Hemp, J.:** "Theory of transit time ultrasonic flowmeters", J. Sound Vib., **84**(1), 133-147 (1982).

[3.11] **Lunde, P., Frøysa, K.-E., Fossdal, J. B. and Heistad, T.:** "Functional enhancements within ultrasonic gas flow measurement". Proc. of *The 17th North Sea Flow Measurement Workshop, Oslo, Norway, October 25-28, 1999.*

[3.12] **Lighthill, J.:** *Waves in Fluids* (Cambridge University Press, 1978).

[3.13] **Løland, T., Sætran, L., Olsen, R., Gran, I. and Sakariassen, R.:** "Cavity flow correction for the ultrasonic flowmeter". Proc. of *Flomeko '98, Lund, Sweden (1998).*

[3.14] **Kinsler, L. E., Frey, A. R., Coppens, A. B. and Sanders, J. V.:** *Fundamentals of Acoustics*, Third edition (John Wiley & Sons, New York, 1982).

[3.15] **Stepanishen, P. R.:** "Transient radiation from pistons in an infinite plane baffle", J. Acoust. Soc. Amer., **49**, 1629-1638 (1971).

[3.16] **ISO,** "Guide to the expression of uncertainty in measurement. First edition". International Organization for Standardization, Genéve, Switzerland (1995).

[3.17] **Sattary, J.:**, "Uncertainty in gas flow measurements", Proc. of *Practical Developments in Gas Flow Metering*, One day seminar, 7 April 1998, National Engineering Laboratory, East Kilbride, Scotland (1998).

Chapter 4:

[4.1] Fluent V4.2, Fluent Incorporated, Centerra Resource Park, 10 Cavendish Court, Lebanon, NH 03766, USA.

[4.2] **Mickan, B., Wendt, G., Kramer, R., Dopheide, D.:** "Systematic investigation of pipe flows and installation effects using Laser Doppler Anemometry", Flow Measurement and Instrumentation, **7**(3/4) (1996).

[4.3] **Hilgenstock, A. and Ernst, R.:** "Analysis of installation effects by means of computational fluid dynamics - CFD versus experiments?", Flow Measurement and Instrumentation, **7**(3/4) (1996).

[4.4] **Hilgenstock, A., Heinz, M. and Nath B.: "N**umerical flow simulation as a tool for developing and calibrating ultrasonic flowmeters", 8th International Conference on Flow Measurement, FLOMEKO`96, Oct. 20-24, 1996 Beijing, China.

[4.5] **Hüwener, T.:** "Numerical determination of measurement uncertainties for ultrasonic flowmeters under disturbed flow conditions", RG-report of Project No. 990.400.4.1.30, Ruhrgas AG, Dorsten (1997).

Chapter 5:

[5.1]   **Lunde, P., Bø, R., Andersen, M., Vestrheim, M. and Lied, G.:** "GERG project on ultra-sonic flow meters. Phase II - Transducer testing. Part 1: Measurement methods. Part 2: KOS transducers. Part 3: Daniel transducers", CMR Report no. CMR-99-F10018, Christian Michelsen Research AS, Bergen (April 1999). (Confidential.)

[5.2]   **Lunde, P., Bø, R. and Isaksen, Ø.:** "GERG project on ultrasonic flow meters, Phase II - Transducer testing. Revision 2". CMR proposal no. CMR-M-10-97/11, Christian Michelsen Research AS, Bergen (December 1997). (Confidential.)

[5.3]   **Hemp, J.:** "Theory of transit time ultrasonic flowmeters", J. Sound Vib., **84**(1), 133-147 (1982).

[5.4]   **Nygaard, G. H.:** "TransLog. Datastøttet system for logging av impedans, admittans, strålingsmønster og lydtrykk for en ultralydtransduser", CMR Report No. 89:10970-1, Christian Michelsen Research AS, Bergen (August 1989). (In Norwegian.)

[5.5]   **Andersen, M. I. and Lied, G.:** "TRANSLOG 3.0, Fluenta Versjon", CMR Technical Note CMR-TN99-A10012, Christian Michelsen Research AS, Bergen (April 1999). (In Norwe-gian.)

[5.6]   **Kinsler, L. E., Frey, A. R., Coppens, A. B. and Sanders, J. V.:** *Fundamentals of Acous-tics*, Third edition (John Wiley & Sons, New York, 1982).

[5.7]   **Williams, A. O. Jr.:** "The piston source at high frequencies", J. Acoust. Soc. Am., **23**(1), 1-6 (January 1951).

[5.8]   **AGA-9**, "Measurement of gas by ultrasonic meters", A.G.A. Report no. 9, American Gas Association, Transmission Measurement Committee (June 1998).

Chapter 6:

[6.1]   **Lygre, A., Lunde, P., and Frøysa, K.-E.:** "Present status and future research on multi-path ultrasonic gas flow meters", GERG Technical Monograph No. 8, Groupe Européen de Re-cherches Gazières, Groeningen, The Netherlands (1995).

[6.2]   **Hilgenstock, A., Hüwener, T., and Nath, B.:** "Kalibra® - A fast numerical method for de-termining installation effects in ultrasonic flowmeters", Proc. of *The 9th International Con-ference on Flow Measurement FLOMEKO '98*. Lund, Sweden (1998).

[6.3]   **Lunde, P., Frøysa, K.-E., and Vestrheim, M.:** "GARUSO version 1.0. Uncertainty model for multipath ultrasonic transit time gas flow meters", CMR report no. CMR-97-A10014, Christian Michelsen Research, Bergen, Norway (September 1997).

[6.4]   **Lunde, P., Bø, R., Andersen, M., Vestrheim, M. and Lied, G.:** "GERG project on ultra-sonic flow meters. Phase II - Transducer testing. Part 1: Measurement methods. Part 2: KOS transducers. Part 3: Daniel transducers", CMR Report no. CMR-99-F10018, Christian Michelsen Research AS, Bergen (April 1999). (Confidential.)

[6.5]   **Brassier, P., Hosten, B., Castaings, M., and Vulovic, F.:** "Study of Ultrasonic Disturbances in Gas Pipelines", Université de Bordeaux and Gaz de France, France (December 1997).

[6.6]   **Rogi, M.J., Williamson, I.D., and McBrien, R.K.:** "Single path ultrasonic meters, performance evaluation and operational experience" *A.G.A. Op. Conf. 1996*, Montreal, Canada (1996).

[6.7]   **Smits, T.C.L.:** "Acoustic noise investigation GASSONIC ® - 400 Ruhrgas Winterswijk", Stork Servex Report 014853.TST.001 (August 1994).

[6.8]   **Agricola, J.B.:** "Gas well flowline measurement by ultrasonic flow meter (UFM)". Proc. of *The 15th North Sea Flow Measurement Workshop, Kristiansand, Norway, October 27-30, 1997.*

[6.9]   **AGA**, "Ultrasonic flow measurement for natural gas applications". Engineering Technical Note M-96-2-3, American Gas Association (A.G.A.), The Ultrasonic Metering Task Group of the Operating Section Transmission Measurement Committee (March 1996).

[6.10]   **Kristensen, B.D., Lofseik, C., Frøysa, K.-E.:** "Testing of noise suppression system for multipath ultrasonic gas flow meters". Proc. of *The 15th North Sea Flow Measurement Workshop, Kristiansand, Norway, October 27-30, 1997.*

[6.11]   **Bloemendaal, K. van, and Kam, P. M. A. van der:** "Installation effects on multi-path ultrasonic flow meters: the Ultraflow Project". Proc. of *The 12th North Sea Flow Measurement Workshop, Scotland, October 1994.*

[6.12]   **Vulovic, F., Harbrink, B., and Bloemendaal, K. van:** "Installation effects on a multipath ultrasonic flow meter designed for profile disturbances", Proc. of *The 13th North Sea Flow Measurement Workshop, Lillehammer, Norway, October 23-26, 1995.*

[6.13]   **Bruggeman, J.C., Hopmans, L.J.M., Looijmnas, K.H.N.:** "Sound power radiated into pipes by control valves", TNO report TPD-HAG-RPT-960041 (April 1996).

[6.14]   **Frøysa, K.-E., Lunde, P., Sakariassen, R., Grendstad, J., and Norheim, R.:** "Operations of multipath ultrasonic gas flow meters in noisy environments". Proc. of *The 14th North Sea Flow Measurement Workshop, Scotland, October 28-31, 1996.*

[6.15]   "Control valves", Commercial brochure, Mokveld Valves B.V., Gouda, The Netherlands.

[6.16]   "Series 132A30 & A40. ICP® Microsensor for high frequency and dynamic pressure measurement", Commercial brochure, PCB Piezotronics Inc., Depew, NY, USA.

[6.17]   **Norton, M.P.:** *Fundamentals of Noise and Vibration Analysis for engineers* (Cambridge University Press, 1989).

[6.18]   **Bloemendaal, K. and Sloet, G.:** "Ultrasonic meters and noise". Proc. of *The 16th North Sea Flow Measurement Workshop, Perthshire, Scotland, October 26-29, 1998.*

[6.19]   **Bloemendaal, K. v.:** "Ultrasonic meters and Noise Task 4 of the Second GERG Project on Ultrasonic Meters. Part I: General: Introduction, Test Set-Up, Conclusions. Part II: Results sound measurements. Part III: Results US-meters", Gasunie Report, N. V. Nederlandse Gasunie, Groeningen, The Netherlands (1998).

[6.20]   **Etcharren, M. E.:** "Etude de faisabilité d'un débitmètre ultrasonore adapté au transport industriel de gaz naturel" Ph.D. thesis, University of Bordeaux I, n° 371 (1989)

[6.21]   **Audibert, S.:** "Banc de mesure de vitesse du son dans les gaz naturels -Cavités sphériques - Etude théorique", Internal G.D.F. report, M. CERSTA (1989)

[6.22]   **Meeker, T. R. and Meitzler, A. H.:** "Guided wave propagation in elongated cylinders and plates", Physical Acoustics, Vol. I, Part A (Academic Press, New York, 1964).

[6.23]   **Gazis, D.C.:** "Three-dimensional investigation of the propagation of waves in hollow circular cylinders", J. Acoust. Soc. Amer., **31**(5) (1959).

[6.24]   **Ducousset, R.:** "Estimation du niveau de bruit d'une vanne installée sur une conduite industrielle", Revue d'Acoustique, **31** (1974).

Chapter 7:

[7.1]   **ISO,** "Guide to the expression of uncertainty in measurement. First edition". International Organization for Standardization, Genéve, Switzerland (1995).

[7.2]   **Sattary, J.:**, "Uncertainty in gas flow measurements", Proc. of *Practical Developments in Gas Flow Metering*, One day seminar, 7 April 1998, National Engineering Laboratory, East Kilbride, Scotland (1998).

[7.3]   **Lunde, P., Frøysa, K.-E. and Vestrheim, M.:** "*GARUSO* Version 1.0. Uncertainty model for multipath ultrasonic transit time gas flow meters", CMR Report no. CMR-97-A10014, Christian Michelsen Research AS, Bergen (September 1997).

[7.4]   **AGA-9**, "Measurement of gas by ultrasonic meters", A.G.A. Report no. 9, American Gas Association, Transmission Measurement Committee (June 1998).

[7.5]   **de Boer, G.:**, "Dry calibration of ultrasonic gas flow meters", Proc. of *One-day Seminar Practical Developments in Gas Flow Metering*, National Engineering Laboratory, East Kilbride, Glasgow, June 24, 1999.

[7.6]   **Lygre, A., Lunde, P. and Frøysa, K.-E.** "Present status and future research on multi-path ultrasonic gas flow meters". GERG Tecnical Monograph No. 8, Groupe Européen de Recherches Gazières, Groeningen, The Netherlands (1995).

[7.7]   **VIM,** "International vocabulary of basic and general terms in metrology (VIM), Second edition", International Organization for Standardization, Genéve, Switzerland (1993).

[7.8]   **EAL-R2**, "Expression of the uncertainty of measurement in calibration", European Cooperation for Accreditation of Laboratories (EAL) (April 1997).

[7.9]   **Taylor, B.N. and Kuyatt, C.E.**, "Guidelines for evaluating and expressing the uncertainty of NIST measurement results", NIST Technical Note 1297, 1994 Edition, Physics Laboratory, National Institute of Standards and Technology, MD, USA (September 1994).

[7.10] **NIS 3003,** "The expression of uncertainty and confidence in measurement for calibrations", NAMAS executive, National Physical Laboratory, Teddington, England (Edition 8, May 1995).

Chapter 8:

[8.1] **Lygre, A., Lunde, P., and Frøysa, K.-E.:** "Present status and future research on multi-path ultrasonic gas flow meters", GERG Technical Monograph No. 8, Groupe Européen de Recherches Gazières, Groeningen, The Netherlands (1995).